

NIST  
PUBLICATIONS

A11104 433938



United States Department of Commerce  
Technology Administration  
National Institute of Standards and Technology

## ***NIST Technical Note 1408***

---

# ***Summary Report of NIST's Industry-Government Consortium Research Program on Flowmeter Installation Effects: The 45 Degree Elbow***

***T. T. Yeh and G. E. Mattingly***

---

QC  
100  
.U5753  
NO.1408  
1994

**T**he National Institute of Standards and Technology was established in 1988 by Congress to “assist industry in the development of technology . . . needed to improve product quality, to modernize manufacturing processes, to ensure product reliability . . . and to facilitate rapid commercialization . . . of products based on new scientific discoveries.”

NIST, originally founded as the National Bureau of Standards in 1901, works to strengthen U.S. industry’s competitiveness; advance science and engineering; and improve public health, safety, and the environment. One of the agency’s basic functions is to develop, maintain, and retain custody of the national standards of measurement, and provide the means and methods for comparing standards used in science, engineering, manufacturing, commerce, industry, and education with the standards adopted or recognized by the Federal Government.

As an agency of the U.S. Commerce Department’s Technology Administration, NIST conducts basic and applied research in the physical sciences and engineering and performs related services. The Institute does generic and precompetitive work on new and advanced technologies. NIST’s research facilities are located at Gaithersburg, MD 20899, and at Boulder, CO 80303. Major technical operating units and their principal activities are listed below. For more information contact the Public Inquiries Desk, 301-975-3058.

---

### **Technology Services**

- Manufacturing Technology Centers Program
- Standards Services
- Technology Commercialization
- Measurement Services
- Technology Evaluation and Assessment
- Information Services

### **Electronics and Electrical Engineering Laboratory**

- Microelectronics
- Law Enforcement Standards
- Electricity
- Semiconductor Electronics
- Electromagnetic Fields<sup>1</sup>
- Electromagnetic Technology<sup>1</sup>

### **Chemical Science and Technology Laboratory**

- Biotechnology
- Chemical Engineering<sup>1</sup>
- Chemical Kinetics and Thermodynamics
- Inorganic Analytical Research
- Organic Analytical Research
- Process Measurements
- Surface and Microanalysis Science
- Thermophysics<sup>2</sup>

### **Physics Laboratory**

- Electron and Optical Physics
- Atomic Physics
- Molecular Physics
- Radiometric Physics
- Quantum Metrology
- Ionizing Radiation
- Time and Frequency<sup>1</sup>
- Quantum Physics<sup>1</sup>

### **Manufacturing Engineering Laboratory**

- Precision Engineering
- Automated Production Technology
- Robot Systems
- Factory Automation
- Fabrication Technology

### **Materials Science and Engineering Laboratory**

- Intelligent Processing of Materials
- Ceramics
- Materials Reliability<sup>1</sup>
- Polymers
- Metallurgy
- Reactor Radiation

### **Building and Fire Research Laboratory**

- Structures
- Building Materials
- Building Environment
- Fire Science and Engineering
- Fire Measurement and Research

### **Computer Systems Laboratory**

- Information Systems Engineering
- Systems and Software Technology
- Computer Security
- Systems and Network Architecture
- Advanced Systems

### **Computing and Applied Mathematics Laboratory**

- Applied and Computational Mathematics<sup>2</sup>
- Statistical Engineering<sup>2</sup>
- Scientific Computing Environments<sup>2</sup>
- Computer Services<sup>2</sup>
- Computer Systems and Communications<sup>2</sup>
- Information Systems

---

<sup>1</sup>At Boulder, CO 80303.

<sup>2</sup>Some elements at Boulder, CO 80303.

***Summary Report of NIST's Industry-Government Consortium Research Program on Flowmeter Installation Effects: The 45 Degree Elbow***

---

T. T. Yeh and G. E. Mattingly

Chemical Science and Technology Laboratory  
National Institute of Standards and Technology  
Gaithersburg, MD 20899-0001

September 1994



**U.S. Department of Commerce**

Ronald H. Brown, Secretary

**Technology Administration**

Mary L. Good, Under Secretary for Technology

**National Institute of Standards and Technology**

Arati Prabhakar, Director

---

National Institute of Standards  
and Technology  
Technical Note 1408  
Natl. Inst. Stand. Technol.  
Tech. Note 1408  
97 pages (September 1994)  
CODEN: NTNOEF

U.S. Government Printing Office  
Washington: 1994

For sale by the Superintendent of  
Documents  
U.S. Government Printing Office  
Washington, DC 20402

## PREFACE

The research results reported in this document were produced with the support of a National Institute of Standards and Technology (NIST) initiated industry-government consortium. This is an established cooperative research effort on generic technical issues to produce industry needed flow metering improvements. In this mode of operation, there is a high degree of interaction between the representatives of the consortium member companies and the NIST researchers. These interactions include: (1) the planning of the specific focus of the NIST research efforts, (2) the discussions and analyses of the results obtained, and (3) the conclusions drawn for the particular phase of the work. For this reason, it is pertinent to acknowledge both the support given to this phase of the research program and the technical contributions made by the representatives of the consortium members.

The current consortium as of November 1992 is, alphabetically:

1. Chevron Oil
2. Controlotron
3. Daniel Industries
4. Dow Chemical Co.
5. E.I. Dupont de Nemours
6. Ford Motor Co.
7. Gas Research Institute\*
8. Gas Unie (The Netherlands)
9. Instrument Testing Assoc.
10. Ketema-McCrometer
11. Kimmon Mfg. Ltd. (Japan)
12. NOVA Husky (Canada)
13. Pacific Gas & Electric Co.
14. Rosemount
15. Institute for Paper Science and Technology
16. Consolidated Edison

\*The Gas Research Institute (GRI) in Chicago, IL is the major sponsor of this flowmetering research effort and this support is gratefully acknowledged. Central to this support is GRI staff member Mr. John G. Gregor whose involvements and efforts in this program are specifically acknowledged.





## TABLE OF CONTENTS

	<u>Page</u>
PREFACE .....	iii
ABSTRACT .....	1
INTRODUCTION .....	1
PREVIOUS RESULTS .....	4
TEST CONFIGURATION: THE 45° ELBOW .....	5
EXPERIMENTAL RESULTS .....	6
A) LDV Velocity Measurements .....	6
1. Downstream of the 45 Degree Elbow .....	6
2. Downstream of the 45 Degree Elbow and 19-Tube Tube Bundle .....	9
3. Comparisons Among Different Configurations .....	11
a. Without Flow Conditioner .....	11
b. With 19-Tube Tube Bundle Flow Conditioner .....	12
B) Results of Meter Performance .....	14
1. Reference Values of Orifice Meters .....	15
2. Orifice Meter Performance For Conventional and Scaled Pressure Ports .....	19
a. Downstream of the 45 Degree Elbow .....	20
b. Downstream of the 45 Degree Elbow and Tube Bundles .....	23
3. Effects of Pressure Tap Orientation on Orifice Meter Performance .....	26
a. Downstream of the 45 Degree Elbow .....	26
b. Downstream of the 45 Degree Elbow and Tube Bundles .....	28
4. Turbine Meter Performance .....	30
CONCLUSIONS .....	31
REFERENCES .....	35





**Summary Report of NIST's Industry-Government Consortium Research  
Program on Flowmeter Installation Effects:  
The 45 Degree Elbow**

**T.T. Yeh  
G.E. Mattingly**

**Fluid Flow Group  
Process Measurements Division  
Chemical Science and Technology Laboratory  
National Institute of Standards and Technology  
Gaithersburg, Maryland 20899**

**ABSTRACT**

This report presents recent results obtained in a consortium-sponsored research program on flowmeter installation effects being conducted at NIST-Gaithersburg, MD. This project is supported by an industry-government consortium and has been underway for several years. This report contains the recent results presented at the meeting of consortium participants at NIST-Gaithersburg, MD. in November 1992.

The piping element tested and reported here is the conventional 45° elbow; the conventional 19-and 7-tube concentric tube bundle flow conditioners were also tested. The LDV velocity measurements are reported for the pipeflows produced downstream of the 45° elbow with and without the 19-tube tube bundles. The performance characteristics of a range of orifice meters with various pressure tap geometries and a specific turbine meter are obtained downstream of the 45° elbow with and without the 19- and 7-tube tube bundle flow conditioners.

**INTRODUCTION**

The increasing scarcity of fluid resources and the rising value of fluid products are placing new emphases on improved flow measurements. Improvements are sought from many starting points. In many cases, meters are being retrofitted into fluid systems that were not designed for them. This invariably means the flowmeters are being inserted into "non-ideal" installation conditions where the upstream piping conditions produce pipeflow distributions that differ from those associated with "ideal" installations. "Ideal" installation conditions are where the meter location is

preceded by sufficiently long, straight lengths of constant diameter piping that the meter's performance is not affected by the meter installation position. Pipeflows in ideal installation conditions have mean and turbulent velocity profiles which conform to those for fully developed, equilibrated pipe flows established for the pertinent flow conditions.

The prevalent concern in the flow measurement community is for increased metering accuracy levels. These levels are desired for existing meter systems - either by upgrading the flow conditions that enter the installed meter or by replacing the device itself or its auxiliary components so that accuracy levels are increased. Flow conditioning devices of one geometry or another are frequently recommended in metering standards for improving flowmeter performance when installation conditions are not ideal. However, the pipeflows generated by these devices have to be considered with respect to the flowmeter installed downstream of the specific piping configuration, the pipeflows entering it, and the factors that influence the performance of the particular meter. It has been shown previously [1-4]<sup>1</sup> that certain flow conditioner installations can produce serious deviations from the performance of specific meters in ideal installation conditions.

The NIST-formed, industry-government consortium research program on flowmeter installation effects is designed to help improve fluid metering performance when installation conditions are not ideal. This program has the main objective of producing a basic understanding of the flow phenomena that are produced in prevalently encountered, non-ideal installation conditions and to quantify these phenomena relative to reference fluid dynamic conditions, i.e., the pipeflow in ideal installation conditions. When these phenomena and their quantified characteristics are correlated with the performance of specific types of meters, it is considered feasible to predict and achieve satisfactory measurements in non-ideal meter installations. The success of this approach has been demonstrated using several different types of flowmeters installed downstream of several different pipe elbow configurations, [1-6]. This approach is being incorporated into the new standards on methods for establishing flowmeter installation effects, [7].

This research effort has also included experimental studies of the flow into and out

---

<sup>1</sup> Square bracketed integers refer to references given below.



of several tube bundle flow conditioners. These results have produced detailed descriptions of the effects these devices have on swirling pipe flows. The performances of both orifice and turbine meters have also been determined for different installation locations downstream of selected pipeline elements, both without and with tube bundles.

The experimental flow metering research program underway at NIST is based upon the measurements of pipe flows from selected piping configurations using laser Doppler velocimetry (LDV). The program is intended to use the basic experimental research tools available to the fluid dynamicist to measure, understand, and parameterize the salient features of the pipeflow phenomena produced by pipeline configurations. The successive phase of the program is to evaluate quantitatively how these phenomena influence fluid meters and how to handle these effects. Selections of piping configurations and pipeline elements such as flow conditioners are done by the consortium members.

It is expected that improved flowmeter performance will be significant and wide spread over a broad range of conditions. Assuredly, it will enhance the custody transfer of valuable fluid resources and the optimization of industrial processes involving costly fluid products through better control produced by better fluid flow measurements.

In the present study, the fluid is water and the piping is 52.5 mm (2 in diameter), smooth, stainless steel. Water temperature is controlled using a heat exchanger to maintain a set temperature of 21°C. The relative roughness of this pipe has been measured with a profilometer to indicate a value of 0.006% based on interior pipe diameter. Diametral Reynolds numbers range from  $10^4$  to  $10^5$  using bulk average velocity. According to the concepts of dynamic similitude, the results of the present research program should predict a range of other flows - both liquids and gases - in geometrically scaled piping configurations when pertinent parameters match those in our experiments. The pertinent parameters considered important in the current experiments are Reynolds numbers, and pipe relative roughness. All pertinent reference conditions regarding pipeflows are completely documented according to basic fluid flow principles. When all these conditions occur in other, geometrically scaled pipe systems, in liquids or gases, the flows should be appropriately scaled versions of our results.

It is suggested here that both flowmeter manufacturers and users can also use this approach to achieve improved performance for meters that are different from the orifice and turbine meter geometries used in this program. They can, for example, duplicate the piping geometry and Reynolds number conditions that have been investigated at NIST and use dimensional similitude concepts to conclude that similar flow phenomena prevail in the duplicate system. In this way, the time and expense needed to conduct duplicate LDV surveys can be saved. When meter performance is then produced in these non-ideal installation conditions, analogous prediction schemes can be produced for the respective meters. As in the NIST program, the success of the prediction scheme can be tested in laboratory tests. In this way, the NIST LDV results can be used simultaneously by numerous investigators for their benefit and for performance standards that are critically needed.

## **PREVIOUS RESULTS**

Previous phases of this research program have produced LDV measurements of the pipeflows in the downstream piping from the configurations of single elbow, double elbows out of plane, the tee used as elbow and the concentric reducer. Conventional, long-radius elbows are used in all of these studies; the radius of the centerline through these elbows is 1.5 pipe diameters. Detailed results of these studies are given in [1-6]; summary descriptions are given in [8-10].

Previous phases of this research program have also produced data for the performance of orifice and turbine meters installed downstream of the selected configurations. Additionally, the demonstration of the success of the above-described prediction scheme for attaining accurate flowmeter performance for these types of meters installed downstream of these elbow configurations is demonstrated in [4-6].

Earlier phases of this research program determined the effects on orifice and turbine meters of several types of tube bundles installed downstream of selected configurations. As well, different tube bundle installation positions were investigated both with LDV and with respect to orifice and turbine calibration results.



The results obtained for the conditions tested to date show that while the conventional 19-tube tube bundle successfully removes swirl from these pipeflows it apparently produces other effects in the streamwise velocity profiles that cause several different types of perturbations on orifice meter performance. The effects on the specific design of turbine meter selected for these tests were less varied than those for orifice meters [10].

## **TEST CONFIGURATION: THE 45° ELBOW**

Figure 1 shows a sketch of the 45° elbow piping arrangement and the coordinate system used in the test. A right handed coordinate system is used which has the origin in the exit plane of the elbow on the pipe centerline. That is, the coordinate Z has its origin in the exit plane of the elbow and aligns with the pipe centerline, the coordinate Y is upward and is in the exit plane of the elbow, and the X coordinate which is not shown in the figure is normal to the Y-Z plane. The positive Z direction is downstream; the positive Y direction is upward; the positive X direction is therefore to the right looking upstream. The mean velocities in the X, Y, and Z directions are U, V, and W respectively; and the corresponding turbulence velocities are  $u'$ ,  $v'$ , and  $w'$ , respectively. In this study only two velocity components, the axial velocity, W and the vertical velocity, V are measured. The horizontal component, U is not measured. In all of the results that follow, unless otherwise specified, non-dimensional quantities will be used. Lengths and velocities are normalized using the pipe diameter, D and average-bulk velocity  $W_b$ , respectively. Meter performances are given via orifice discharge coefficients and Strouhal numbers, respectively, for the selected orifice and turbine meters. In this report, the uncertainty on the LDV measurement is estimated to be  $\pm 0.01\%$ . The position uncertainty is  $\pm 0.01\%$  in X/D and Y/D, and  $\pm 0.1\%$  in Z/D. The measurement uncertainty on meter constant is estimated to be  $\pm 0.5\%$  for orifice meters, and  $\pm 0.2\%$  for turbine flowmeter.

To study the effect of the selected piping configuration, efforts have been made to ensure a fully developed pipe flow that is free from other disturbances, such as anomalous turbulence effects, flow pulsations, etc., enters the 45° elbow configuration being studied. The upstream piping was arranged so that over 70 pipe diameters of straight, constant diameter piping preceded the 45° elbow. Upstream of this straight length of piping, the inlet flow was arranged, as shown

in figure 1, to have a special, radial inlet so that no axial vorticity was produced by this entrance condition. This inlet pipe section was a single piece of standard piping to assure a concentric constant diameter along the entire section without any misalignment that could result from joints. When LDV measurements were made of the profiles exiting this 70 diameter pipe length, they were found to be fully developed, equilibrated pipeflows. With these reference profiles entering the 45° elbow, the exiting pipeflows can be interpreted, for this conventional piping configuration, to be due solely to this single piping element. The tube bundle designs tested in this program are installed downstream of the piping configurations as shown in figure 1. The distance between the meter position and the exit plane of the conditioner is denoted by length C, in diameters.

The tube bundles used were the conventional 19 tube concentric design and the 7 tube arrangement. Figure 2 shows these tube bundles with dimensions given in millimeters. These units are either identical to the practically used units (7 tube) for 50 mm diameters, or geometrically scaled versions of the prevalent unit (19 tube) used in large pipe sizes according to orifice meter technology [11]. The 19-tube tube bundle shown in figure 2(a) is comprised of tubes having a diameter of 9.5 mm, wall thickness of 0.4 mm, and tube length of 101.6 mm. It is approximately 2D in length. The 7-tube tube bundle, shown in figure 3(b) has tubes of diameter 11.8 mm, 2.4 mm wall thickness, and length of 152.4 mm or about 3D.

## EXPERIMENTAL RESULTS

### A) LDV Velocity Measurements

#### 1. Downstream of the 45 Degree Elbow

Figure 3 shows LDV measurements of the mean axial velocity profiles,  $W/W_b$ , versus horizontal radial position,  $X/D$ , at successive downstream locations,  $Z/D$ , from the 45° elbow for Reynolds number,  $Re=100000$ . For these results and all of the LDV data that follows, the imprecision is estimated to be at the 1% level. The solid curve in is the fully developed, equilibrated pipeflow distribution put forth by Bogue and Metzner [12]. The data clearly indicate that the 45° elbow significantly



modifies the axial velocity profile as the fluid passed through the elbow. These axial velocity profiles are symmetric about the pipe centerline along the horizontal diameter. In the region near the pipe center the flow is slower than the fully developed pipe flow, while near the pipe wall the flows are faster compared to the fully developed pipe flow. The centerline deviation from the ideal profile at the most upstream location of  $Z/D=2.7$  is about 40% of the bulk velocity. Near the wall the deviations are about 20% in excess of the bulk velocity. These deviations decrease with downstream distance. However, even up to  $Z/D=18.3$ , the profile is very flat over about 80% of the center core yet lies significantly below the ideal curve. At this location, the centerline velocity is about 8% slower than the ideal velocity.

Figure 4 presents the mean axial velocity profile,  $W/W_b$ , versus the vertical radial position,  $Y/D$ , at successive downstream locations,  $Z/D$ , from the 45° Elbow for  $Re=10^5$ . The solid curve is the fully developed, equilibrated pipeflow distribution of Bogue and Metzner. This traverse in the plane of the 45° elbow shows high speed flow toward the outside of the elbow turn. Near the inside portion of the turn, the data show that a region of slow flow is present. These velocity profiles are quite different from those along the horizontal diameter and quite different from the ideal distribution. Near the elbow exit, the flow is much slower than the ideal profile in the upper half of pipe and much faster in the bottom quarter of the pipe. The fast layers of the flow near the bottom of the pipe exceed the bulk flow by about 25% and the slow layers at the upper region are about 40% of bulk flow slower than the ideal profile. These velocity profiles are skewed toward the bottom of the pipe at all stations measured. With downstream distance, these deviations decrease so that at  $Z/D=18.3$ , the central core flow is only about 10% of the bulk velocity slower than the ideal values. At this location, the profile is still skewed toward the bottom of this pipe and is flatter or more smoothly varying as compared to the fully developed distribution.

Both figures 3 and 4 also indicate that, for these conditions, these axial mean velocity profiles do not conform well to the fully developed distribution even eighteen 18 diameters from the 45° elbow.

Figure 5 presents vertical mean velocity profiles,  $V/W_b$ , versus horizontal radial position,  $X/D$  at successive downstream positions from the 45° elbow for  $Re=10^5$ .

Here, the ideal fully developed pipeflow is zero as shown by the solid line. As expected, the velocity profiles are symmetric about the pipe centerline along the horizontal diameter which is normal to the plane of the elbow. These distributions indicate that at the nearest location of  $Z/D=2.7$  the upward vertical velocities near the pipewalls are about 18% of the bulk velocity, while at the centerline, the downward velocity is about 10% of the bulk velocity. With downstream distance these deviations diminish so that at  $Z/D=18.3$  the upward velocity is about 4% of the bulk velocity near the wall and is about 3% downward near the pipe centerline. These vertical mean velocity profiles indicate that a dual eddy swirl distribution is generated by the turning action of this  $45^\circ$  elbow. This dual eddy flow is very similar to those of the single elbow and the tee used as an elbow [1,5]. Looking upstream, the secondary axial vorticity on the left portion of the pipeflow is rotating clockwise; on the right, the rotation is counterclockwise. The dissipation of this dual eddy flow is slower than those observed both for the single elbow and tee used as a single elbow.

Figure 6 shows the vertical mean velocity profiles versus the vertical radial position at successive downstream locations from the  $45^\circ$  elbow for  $Re = 100000$ . Again, the solid line shows the ideal flow distribution. These profiles show all the flow is downward, and is more pronounced in the upper part of the pipe or near the inner bend of the elbow. These skewed profiles indicate that at  $Z/D=2.7$ , the downward velocity reaches about 25% of the bulk velocity at  $Y/D=0.25$ .

Figures 7 and 8 present, respectively, the root-mean-square (r.m.s.) value of the axial component of the turbulent velocity,  $w'/W_b$ , versus horizontal and vertical radial positions from the pipe centerline for  $Re=100000$ . Figure 9 presents profiles of the r.m.s. values of the vertical component of the turbulent velocity,  $v'/W_b$ , along horizontal radial positions for  $Re = 100000$ . These measurements for different downstream distances from the  $45^\circ$  elbow are plotted with the results measured by Laufer as shown via the solid curve for  $Re=41000$  [13]. These results indicate that the turbulent intensity profiles are symmetric about the pipe centerline along the horizontal diameter which is perpendicular to the plane of the elbow and are slightly asymmetric along the vertical diameter, which is in the plane of the elbow. At the nearest position of  $Z/D=2.7$ , there are two regions of high axial turbulence of about 14% of the bulk velocity at  $X/D = \pm 0.2$  along the X axis as shown in figure 7, and there is a region of high turbulence of about 13% near the



pipe centerline along the Y axis as shown in figure 8. These regions of intense turbulence coincide with the regions where high velocity gradients exist as shown in figures 3 and 4. These are regions where turbulence generation is high.

Figure 9 indicates that the single peak value of the vertical component of the turbulent velocity is about 12% of the bulk velocity and occurs at the pipe centerline where a large downward velocity exists. The data also indicates that the measured turbulence is much higher than that measured by Laufer, [13]. These enhanced turbulence levels are interpreted to be due to the abrupt turning action of this elbow. With downstream distance, the turbulence levels decrease. At  $Z/D=18.3$  the intensities of the turbulence are close to the ideal values of Laufer, however the distributions are still quite different from the ideal case. The measured profile is smoothly varying and intensities near the pipe walls are lower than the levels measured by Laufer but are higher near the pipe center. These data are similar to those of the  $90^\circ$  elbow and the tee used as a elbow as reported previously except with a slightly lower level of turbulence [1,5]. Both the mean and turbulence velocity profiles indicate that the pipe flow is still in the developing stage 18D downstream of the  $45^\circ$  elbow.

## 2. Downstream of the 45 Degree Elbow and 19-Tube Tube Bundle

Figures 10 and 11 present, respectively, profiles of the time-averaged, streamwise velocity components along diameters perpendicular to and in the plane of the  $45^\circ$  elbow for  $Re=100000$ . The solid curve is the fully developed, equilibrated pipeflow distribution put forth by Bogue and Metzner [12]. The 19-tube tube bundle shown in figure 2(a) is installed as shown in figure 1 at the position  $Z-C=5.7D$  and the velocity profiles are measured at several axial distances,  $C$ , downstream of this tube bundle. These results show, just downstream from the 19-tube tube bundle, at  $C/D = 1.5$ , the jetting effects of the flows from the individual tubes. These jetting effects diminish very quickly so they can not be seen at  $C/D=4.0$ . The results show that this tube bundle does not completely suppress the characteristics of the streamwise velocity profile which exits the elbow as shown in figures 3 and 4. Figure 10 confirms that the streamwise velocity profile is essentially symmetric about the center plane (Y-Z) of the elbow and preserves this feature with downstream distance from the tube bundle exit as the distribution

approaches that of the Bogue and Metzner profile. Figure 11 similarly shows the high speed flow occurring at the outside portion (negative Y) of the turn through the elbow and the slow flow near the inside (positive Y) of the turn. The effect of the tube bundle seems to make the axial velocity profiles more smoothly varying, however some of the skewness can still be seen. Within 13D from the exit of the 19-tube tube bundle the profile is still significantly skewed relative to the fully developed distribution. These profiles are clearly not fully developed. The profiles downstream of the 19-tube tube bundle show more smoothly varying velocity distributions in which the major portion of the center core of the pipeflow is quite slow in comparison with the fully developed distributions. With downstream distance, these deviations decrease. However, the profiles in the center of the pipeflow are found to be lower than the fully developed distribution and having no "over-shoot" condition as was found in some other conditions up to  $C/D=13.0$  [1,2]. At this  $C/D=13.0$  position the centerline velocities show differences of about 8% from the fully developed distributions. These profiles are more smoothly varying than the fully developed profile along the horizontal diameter, and they continue to show faster flow near the outside of the elbow turn.

Figure 12 presents measurement results of the vertical component of the time-averaged velocity profile along the X and Y diameters downstream of the 45° elbow and 19-tube tube bundle for  $Re = 100000$ . These show that the 19-tube tube bundle is very effective in reducing the transverse velocities and that these velocities are below the 2% level at all stations measured. Figure 12 shows that the energetic, dual eddy flow generated by the elbow and clearly visible via the vertical velocity component along the X axis as shown in figure 5 is reduced by this tube bundle to 2% or less just downstream of the tube bundle exit. Further downstream, the vertical velocities are below 1% of the bulk velocity.

Figures 13 - 16 present r.m.s. distributions of the streamwise and vertical components of the turbulent velocity measured downstream of the 45° elbow and 19-tube tube bundle along the X and Y diameters. The profiles measured nearest the tube bundle exit show via the peaks in these distributions the effects of the interactions between the jetting flows from the individual tubes. The turbulence intensity at the pipe centerline does not decay monotonically toward the fully developed value. This ideal distribution is shown by the solid line. The decay continues so that the centerline turbulence intensity is very close to the ideal values



for  $C/D$  between 6.5 and 9.5 and is lower than the ideal value at  $C/D=13.0$ . Also, these measured profiles are more smoothly varying across the pipe and the turbulence intensity near the wall is lower than the ideal. These data indicate the turbulence distribution is still dominated by the effects of the multi-jets mixing flow and the pipeflow is still developing downstream of the 19-tube tube bundle at  $C/D=13$ .

### 3. Comparisons Among Different Configurations

#### a.) Without Flow Conditioner

In this section the velocity profiles produced by the  $45^\circ$  elbow, L45, are compared with those from a  $90^\circ$  elbow, L90, and from the tee used as an elbow, Tee. The data are compared at two closely similar locations; one near the exit of  $Z/D=2.7$  and the other further downstream at about  $Z/D=19$ .

Figure 17 shows the comparisons of the axial velocity profiles along the horizontal radial position at two axial locations downstream from different piping configurations for  $Re = 100000$ . Figure 18 shows a similar comparison along the vertical radial position. In both figures, the upper figure (a) is taken at  $Z/D=2.7$  and the lower figure (b) is at about  $Z/D=19$ . The solid curve is the fully developed, equilibrated pipeflow by Bogue and Metzner, [12]. Although there are some differences in the quantitative details of the profiles, all three configurations basically produce qualitatively similar axial mean velocity profiles. As compared to the fully developed profile, the velocities near the pipe center are much slower and those near the pipe walls are faster along X, the diameter normal to the plane of the elbows, as shown in figure 17. In the plane of the elbow, Y, as shown in figure 18, all three configurations produce skewed distributions. These profiles show high speed flow in the outside region (-Y) of the turn and a region of slow flow near the inside (+Y) of the turn. Near the exit, the fast layers of the flow near the bottom of the pipe are about 20-25% of the bulk flow faster than the ideal profile and the slow layers in the upper portion are about 35-40% of bulk flow slower than the ideal profile.

Figures 19 and 20 show the comparisons of the vertical velocity profiles at two

axial locations downstream from the three piping configurations for  $Re = 100000$ . Figure 19 presents results along X, the diameter normal to the elbows, while figure 20 shows measurements along Y, the diameter in the plane of the elbows. Also, the upper figure (a) is taken at  $Z/D=2.7$  and the bottom figure (b) is for  $Z/D$  about 19. Here, the vertical velocity distribution for the fully developed pipeflow is zero.

The data indicate again that three configurations produce a qualitatively similar vertical velocity profiles. The profiles shown in figure 19 are symmetric about the pipe centerline along X, the horizontal diameter. Figure 20 shows that the negative velocity profiles are skewed to the part of the pipe which is the inside part (+Y) of the turn. The distributions in figure 19 all show that there are upward vertical velocities near the pipewall and downward velocities at the centerline and thus indicate that a dual eddy swirl distribution is generated by the turning action of these elbows. Looking upstream, the secondary axial vorticity on the left portion of the pipeflow is rotating clockwise, while on the right, the rotation is counterclockwise. The data also show that although the initial intensity of the dual eddy swirl for the  $45^\circ$  elbow is not as high as that of the  $90^\circ$  elbow, it is the highest among all three configurations at the downstream location of about  $Z/D=19$ . These results seem to indicate that the dual eddy produced by the  $45^\circ$  elbow is much more stable and organized and thus the dissipation is slower than those observed for both the single elbow and the tee used as an elbow.

Figures 21 and 22 show the comparison of the profiles of the turbulent velocities along the horizontal diameter at two axial locations downstream from the three different piping configurations for  $Re = 100000$ . The solid curves are the results measured by Laufer [13]. The data indicate that, among the three configurations, the  $45^\circ$  elbow flow has least turbulence and the tee flow has highest turbulence. All three flows have more smoothly varying turbulence distributions across the pipe and thus indicate that all these flows are still in developing stages at the most distant locations measured.

#### b.) With 19-Tube Tube Bundle Flow Conditioner

In this section the velocity profiles downstream of the 19-tube tube bundle in three different piping configurations are compared. The three configurations are the  $45^\circ$  elbow (L45), the  $90^\circ$  elbow (L90) and the double elbows out-of-plane (2Ls). The 19-tube tube bundle was installed at the fixed location of  $Z-C=5.7D$  downstream



of the elbow exits as shown for the 45° elbow in figure 1. The data at two extreme axial locations are chosen for the comparisons. The near locations are around  $C/D=1.5\sim2.5$  ( $Z/D=7.2\sim8.2$ ) and the further downstream locations are around  $C/D=13.0\sim18.9$  ( $Z/D=18.7\sim24.6$ ).

Figure 23 presents the comparisons of the axial mean velocity profiles downstream of the 19-tube tube bundle along the horizontal radial position for three different piping configurations and  $Re = 100000$ . The solid curves are the fully developed pipeflow distributions given by Bogue and Metzner. The upper figure (a) is for the data just downstream from the exit plane of the tube bundle, while the bottom figure (b) is for the data at the further downstream locations. At the near locations, all profiles are fairly similar and are quite smoothly varying as compared to the Bogue and Metzner profile. These results show that the axial mean velocity profiles just downstream of the 19-tube tube bundle are dominated by the effects of the tube bundle. The velocity profiles are somehow insensitive to the upstream flow conditions or the tube bundle has effectively removed most of the upstream flow disturbance. All these distributions show the jetting effects of the flows from the individual tubes. Although all three profiles at the further downstream location approach the ideal pipeflow profile, as shown in figure (b), some of the upstream disturbance effects still seem evident. The profiles for both the 45° and 90° elbows are very similar and have a region of smoothly varying flow velocities near the pipe centerline, while the profile for the double elbows out-of-plane configuration is more peaked than the ideal profile and has velocities that exceed ideal values.

Figure 24 shows the comparison of the vertical mean velocity profiles along the X axes for two axial locations downstream of the 19-tube tube bundle and the three piping configurations for  $Re = 100000$ . These data show that the 19-tube tube bundle is very effective in reducing transverse swirl velocities and that the vertical mean velocity profiles just downstream of the tube bundle are very insensitive to the upstream flow disturbance. These downstream velocities are primarily the result of the tube bundles. These vertical velocities are below the 2% level just downstream of the tube bundle for all three configurations, and they are below 1% of the bulk velocity further downstream. The energetic single or dual eddy flow generated by the elbows shown in figure 19 and in early reports [1,3,5,6] have essentially disappeared.

Figures 25 and 26 present, respectively, the comparisons of the profiles of the r.m.s. values for the axial and vertical components of the turbulent velocity along the X axes at two axial locations downstream of the 19-tube tube bundles in the three piping configurations for  $Re = 100000$ . The solid curves are the results measured by Laufer. These data show that the turbulence velocities downstream of the 19-tube tube bundle are dominated by the effects of the tube bundles. At the near positions, as shown in the upper figure (a), the turbulence intensities for all three cases are much higher than that of ideal case with the highest turbulence from the case of the double elbows out of plane configuration. At the further downstream locations all the turbulence velocities have decayed to below the ideal levels and the profiles are more smoothly varying than the ideal. These indicate that these pipeflows are still in decaying processes at these locations downstream of the tube bundle which appears to be analogous to the multi-jet turbulence. The viscous effects of the pipe wall boundary layer have not completely traversed the entire pipe cross section and equilibrated these flows. Thus, it is concluded that these pipeflows are still in developing processes.

## B) Results of Meter Performance

The performances of selected flowmeters downstream of the  $45^\circ$  elbow and the two tube bundles were obtained. Furthermore, two additional tasks were performed and results are reported below. First, orifice meter performance for both conventional flange taps and scaled flange taps were obtained. Second, the effects of pressure tap orientations on orifice meter performance were determined. To produce these results, two new orifice plate holders were designed and fabricated.

Figure 27 shows a sketch of the pressure ports and the orifice plate holders for flange taps. The dimensions for conventional pressure ports for flange taps are given for both 10 cm (4") and 5 cm (2") diameter meters. The scaled ports on the 5 cm (2") pipe is the scaled down ( half scale ) version of the 10 cm (4") meter. The API standard [14,15] indicates that meter tubes using flange taps shall have the center of the upstream pressure tap hole placed 2.54 cm (1") from the upstream face of the orifice plate. The center of the downstream pressure tap hole shall be 2.54 cm (1") from the downstream face of the orifice plate. The tap hole diameter should be within 6.4 mm ~ 9.5 mm (0.25"~ 0.375") for 5 cm (2") meter, and within



6.4 mm ~ 12.7 mm (0.25"~0.5") for 10 cm (4") meter and larger.

Figure 28 shows the sketch of the two-port orifice plate holder. There are two sets of pressure taps, one conventional flange tap set and one scaled flange tap set in this holder. The centers of the conventional pressure taps are respectively 2.54 cm (1") from the upstream and downstream faces of the orifice plate. For the scaled taps this distance is 1.27 cm (0.5"). These two pressure tap sets are located 180° apart. In this report, the holder was installed in an orientation so that both ports were in the horizontal plane. When looking upstream, the conventional ports were at 3 o'clock (90°), i.e., the positive X position, and the scaled ports were at 9 o'clock (270°), i.e., the negative X position. The second special orifice plate holder is shown in figure 29. It is a holder with four sets of ports scaled to be similar to the conventional flange tap arrangement for a 10 cm (4 in.) diameter meter; this is intended to give results similar to those from other tests [16]. For the test results reported, the holder was mounted in an orientation so that two sets (0° and 180°) were in the vertical plane and the other two (90° and 270°) were in the horizontal plane. These orifice plate holders, which are similar to conventional orifice flanges, use three dowel pins to align the flanges properly and centering pins to hold the plate in position while bolting the flanges. In order to match better with the data obtained by other test facilities, a new set of orifice plates were selected to match the beta ratios used in these facilities. The nominal values of the beta ratio selected were 0.4, 0.6, and 0.75.

## 1. Reference Values of Orifice Meters

Before examining flowmeter installation effects one needs to know the reference values of the specific flowmeter. Here, the reference values of the test meters were measured in a fully developed pipe flow downstream of about 200 diameters of constant diameter, straight pipe. A transfer standard which was calibrated gravimetrically before these tests was used for all flowmeter performance tests. However, during the course of these tests of flowmeter installation effects, all conditions were established and maintained to be the same as those for the reference case, In this way, the actual effects due to any installation condition can be accurately determined.

Figure 30 presents the variations of the reference discharge coefficients obtained

from the different sets of pressure ports for  $\beta=0.75$ . The imprecision of the discharge coefficients and those that follow is estimated to be  $\pm 0.3\%$  or better. In figure 30, all data are normalized by the discharge coefficients obtained from the  $90^\circ$  ports of the 4-port scaled holder. These data show that the variations are normally very small and within about  $\pm 0.1\%$  which is considered within the uncertainty of the experiments. The discharge coefficients obtained from the conventional pressure taps are about .6% higher than those from the scaled pressure taps. The variations for the two smaller  $\beta$  ratios are smaller. These data indicate that the reference values for all five sets of scaled ports (four from the 4-port holder and one from the 2-port holder) are practically the same. Although the averaged value from these five references could be chosen as a common reference value in determining the amount of the installation effect for all pressure ports, the individual reference from the same set of the test ports was used as the reference for that set of ports. This is intended to keep the uncertainty due unknown factors as small as possible.

As expected, the data show different reference discharge coefficients for the conventional ports and the scaled ports. Because of the variations of the wall pressure along the pipe, the differential pressure and thus the discharge coefficients obtained from the different pressure tap locations can be different. The effect of pressure tap separation on the discharge coefficients had been documented in various references [15,17,18]. In 1990, the American National Standard Institute adopted a new empirical equation, known as RG equation, for determining discharge coefficients [15]. The RG equation has included the effects of the tap location on the empirical coefficient of discharge equation for orifice meters. Based on the RG equation, the variation of the discharge coefficients as functions of the pressure tap separation,  $e/D$ , for  $\beta=0.4$ , 0.6, and 0.75, and for  $Re=55000$  is shown on figure 31. Figure 31(a) shows the values of the discharge coefficients,  $C_d$ ; while in figure 31(b) the  $C_d$  values were normalized by the  $C_d$  value obtained for the conventional tap separation of  $e=2.54$  cm (1 in.). The present test data are also included in figure 31(b) for comparison. The results indicate that the test data are very consistent with the values predicted by the RG equation. The  $C_d$ s for the scaled ports are smaller than those of the conventional ports for  $\beta$ s of 0.6 and 0.75 and is essentially the same for  $\beta=0.4$ . The RG prediction curves indicate that, for  $D=5.26$  cm (2.07 in.), and  $\beta \geq 0.6$ , the  $C_d$ s for scaled-down cases ( $e/D < 0.49$ ) are smaller than those for conventional ports, and



are larger for scaled-up cases ( $e/D > 0.49$ ). For  $\beta = 0.4$  the  $C_d$  value is practically the same for different tap separations although the RG equation seems to indicate a larger  $C_d$  for smaller tap separations.

The wall pressure distributions along the pipe near orifice plates have been studied by many investigators, [15,18-20]. All published data show that the wall pressure on the upstream side close to the orifice plate increases to a maximum at the plate. On the downstream side, the pressure continues to decrease until a minimum is reached somewhere between about  $1/4 D$  and  $1 D$  and then increases as distance increases. The location of minimum wall pressure is nearly independent of the flow rate and is a function of the beta ratio,  $\beta$ , of the plate. The location is closer to the plate as the value of  $\beta$  becomes larger. The effect of the pressure distribution on discharge coefficients has been included in the RG equation as the "Tap Term" [15]. The new equation was developed from a significantly larger data base (the API/GPA Data Base and the EC Data Base) than was previously used for the discharge coefficient equation development. Here, we concentrate on the "Tap Term" and attempt to infer the wall pressure distribution from the RG equation. RG equation states that the discharge coefficient,  $C_d(e_u, e_d)$  is a function of the upstream and downstream tap locations,  $e_u$  and  $e_d$  for a given condition. From the relationship of the  $C_d$  and the upstream and downstream tap pressures,  $P_u$  and  $P_d$ , we have

$$C_d(e_u, e_d) \sim 1/\sqrt{P_u - P_d}$$

$$\frac{C_d(e_u, e_d)}{C_{d,c}} = \sqrt{\frac{DP_c}{P_u - P_d}}$$

$$\frac{P_u - P_d}{DP_c} = \left( \frac{C_{d,c}}{C_d(e_u, e_d)} \right)^2$$

where  $C_{d,c}$  is the discharge coefficient for conventional ports, and  $DP_c = P_{uc} - P_{dc}$ , the differential pressure between the upstream pressure,  $P_{uc}$ , and downstream pressure,  $P_{dc}$ , of the conventional ports. The above equations give the differential pressure between any upstream location,  $e_u$ , and the downstream location,  $e_d$ . Here it is more convenient to describe the pressure with respect to that of the

conventional port. Thus we have

$$\frac{P_u - P_{dc}}{DP_c} = \left( \frac{C_{d,c}}{C_d(e_u, e_{dc})} \right)^2$$

$$\frac{P_d - P_{dc}}{DP_c} = 1 - \left( \frac{C_{d,c}}{C_d(e_{uc}, e_d)} \right)^2$$

where  $e_{uc}$  and  $e_{dc}$  are the conventional upstream and downstream port locations, respectively.

The wall pressure distributions near orifice plates based on the above equations are thus calculated and shown on figure 32(a) for  $\beta=0.4, 0.6$ , and  $0.75$  and  $Re=55000$ . The pressure distributions obtained from two other sources are also included for comparison. One is from a numerical modeling given by Davis and Mattingly [19] for  $\beta=0.4$  and  $0.75$  and  $Re=400000$  and the other is from a test given by Morrison [20] for  $\beta=0.75$  and  $Re=54700$  and  $91000$ . In the figure the locations of the conventional ports and the scaled ports are indicated by  $c$  and  $s$ , respectively. To expose the variation more clearly, the pressure distribution is replotted on the figure 32(b) in a slightly different form. The upstream pressure is plotted with respect to the pressure at the upstream conventional port, and the downstream pressure is plotted with respect to the pressure at the downstream conventional port. The data show the upstream pressures increase to a maximum at the upstream face of the plate and the agreement among the data are fairly good. However, the variations on the downstream pressures are much larger. Since the wake flow downstream of the plate is a very complex turbulent mixing flow, the prediction of the downstream pressure is much more difficult. Both the data given by Davis & Mattingly and Morrison show large pressure variation on the downstream side of the plate. The downstream pressures from the RG equation show only a moderate variation. The downstream pressure distributions seem strongly dependent on the recirculation flow formed downstream of the plate. The plate dam height,  $h=(1-\beta)/2$ , produces these variations. These wall pressure distributions



indicate that the location of the downstream tap is more critical than the upstream tap in determining the pressure difference. Depending on the beta ratio, the minimum wall pressure location will be different. A larger  $\beta$  means a smaller dam height,  $h$  and a smaller recirculation region and thus the minimum wall pressure location will be closer to the plate. The minimum wall pressure location for smaller beta ratio will occur further away from the plate.

The data show the upstream scaled pressure is larger than the upstream conventional pressure and the downstream scaled pressure is either smaller or only slightly larger than the downstream conventional pressure so that the differential pressures for the scaled ports are larger than those of the conventional ports. Consequently, the measured pressure differences are larger and the discharge coefficients are smaller for these scaled ports. This is true for  $\beta = 0.6$ , and  $0.75$  and the differences between scaled and conventional ports for  $\beta = 0.4$  and smaller are negligibly small.

Figure 33 presents the ratio of the discharge coefficients for the scaled ports and the conventional ports as functions of Reynolds number for  $\beta = 0.4$ ,  $0.6$ , and  $0.75$ . These results span a turndown of 2.5 for each of these beta ratios and the entire Reynolds number range is from 20000 to 100000. The measurement results are compared with the predictions of the RG equations. In general, the data are fairly consistent with the predictions in the sense that the  $C_d$  from the scaled ports are smaller than those for the conventional ports for large beta ratio and little difference is found for  $\beta = 0.4$ .

## 2. Orifice Meter Performance for Conventional and Scaled Pressure Ports

The two-port plate holder was used to measure orifice meter performances downstream of the  $45^\circ$  elbow without and with tube bundles. At each test condition the discharge coefficients for both the scaled and the conventional ports were measured. The scaled taps of the 5 cm (2") meter are meant to be scaled to conventional 10 cm (4") diameter meters. This metering arrangement is expected to lead to precedents for larger meter tests. These precedents could be that larger meter results may be able to be successfully predicted using smaller meters tested in quicker, cheaper tests. The range of Reynolds number spanned is 20000 to

100000; the beta ratio range is 0.40 to 0.75 and each meter is tested over a 2.5 to 1 turndown.

a. Downstream of the 45 Degree Elbow

Figure 34 shows the discharge coefficients obtained from the scaled and conventional ports as functions of Reynolds number for  $\beta=0.75$ , at a location of  $Z/D=3.93$  downstream of a  $45^\circ$  elbow. The range of Reynolds number is spanned over 40000 to 100000 (a turndown of about 2.5). The upper figure (a) is for discharge coefficients and the lower figure (b) is for the ratio of the discharge coefficients. The discharge coefficient ratio from the RG equation prediction are also included in figure 34(b). Similar to the ideal condition, the data show that the discharge coefficients for the scaled ports are lower than those for the conventional ports. However, the ratio of the two is slightly different from that of the long straight pipe, reference case. In the  $45^\circ$  elbow case, the measured ratio of the  $C_d$  coefficients are lower than the RG predictions, while it is little difference in the straight long pipe case. This indicates that the  $45^\circ$  elbow installation does affect the tapping separation effect and the tapping correction term should not be the same for the straight pipe case and the  $45^\circ$  elbow installation conditions.

Figure 35 presents the percentage change in discharge coefficient for a  $\beta = 0.75$  orifice meter installed at different downstream positions from a  $45^\circ$  elbow for a range of Reynolds numbers between 40000 and 100000. The upper figure (a) is for the conventional ports at the  $90^\circ$  position and the lower figure (b) is for from the scaled ports at the  $270^\circ$  position. The ordinate in each of these figures is the percentage shift, at each flowrate, in discharge coefficient relative to that obtained for the reference condition. The data from both cases show very similar installation effects for the  $45^\circ$  elbow. Near the elbow the discharge coefficient is reduced and the reduction decreases as the downstream distance from the elbow increases and the reduction is zero at about  $Z/D=30$ . Further downstream at  $Z/D=53.3$  the discharge coefficient is larger than the reference value. For the scaled ports, the corresponding reduction is slightly larger. The value of the maximum reduction is about -3.2% for the conventional ports and about -3.7% for the scaled ports. The similarity between the general relationship for the change in discharge coefficient and the distance downstream of the  $45^\circ$  elbow for the conventional ports and scaled ports can be seen more clearly on figure 36. Figure 36 shows the percentage



change in discharge coefficient for a  $\beta=0.75$  orifice meter versus the location downstream from a  $45^\circ$  elbow for (a)  $Re = 55000$  and (b)  $99000$ . The open circles show results for the conventional ports and the solid circles are for the scaled ports. These data show that the differences in the change of discharge coefficients between conventional and scaled ports are small with the scaled ports producing a slightly lower change in discharge coefficients for  $Z/D < 15$  and slightly larger change in discharge coefficients for  $Z/D > 20$ . These  $C_d$  versus  $Z/D$  curves also show that the  $45^\circ$  elbow produces negative shifts in discharge coefficient for  $Z/D < 30$ , a zero crossing point near  $Z/D = 33$ , and an overshoot condition at  $Z/D = 53$ . The maximum negative shift of about  $-3.5\%$  is found at the measured position closest to the elbow at  $Z/D = 3.9$ . It is noted that, although the shift is small, the positively shifted orifice discharge coefficient condition prevails for extended lengths downstream of the zero crossing point. Under these conditions, the orifice meter requires more than 50 diameters of downstream distance before discharge coefficients attain values equal to those for the fully developed pipeflow conditions.

Each orifice meter has been tested in a different range of Reynolds numbers over a 2.5 to 1 turndown and all three beta ratios have been tested at  $Re = 55000$ . Figure 37 presents the percentage change in discharge coefficient for all three orifice meters at different downstream installation positions from a  $45^\circ$  elbow for  $Re = 55000$ . The upper figure (a) is for the conventional ports located at  $90^\circ$  angular location and the lower figure (b) is for the scaled ports located at  $270^\circ$  location. As noted previously, discharge coefficient shifts are negative for installation positions near the  $45^\circ$  elbow with largest shifts for largest beta ratios. For meter installations more distant away from this elbow, the negative shifts diminish, become zero, and proceed to shift positively. These show sizeable differences that depend upon beta ratio. The amount of negative shift ranges from about  $-0.6\%$  for the small beta of 0.4 to  $-4\%$  for the largest beta of 0.75. When the orifice meter to elbow exit distance is increased, these negative shifts diminish and become zero around the downstream position of  $35D$  from the  $45^\circ$  elbow. However, with increased downstream distance, orifice discharge coefficients are shifted positively relative to reference values. The maximum measured value was found at  $53D$  downstream from the elbow, the furthest measured position. These maxima also appear to be dependent upon beta ratio with the smallest shift of less than  $+0.1\%$  for  $\beta = 0.4$  and the largest of about  $+0.4\%$  for  $\beta = 0.75$ . For orifice meters installed further than  $20D$  downstream of the elbow, the results show that the

deviations from reference condition values are essentially less than 0.1% for  $\beta=0.4$ . As usual, the larger  $\beta$  ratio produces a larger coefficient shift. It is also noted that, although the shift is small, the positively shifted orifice discharge coefficient condition prevails for extended lengths downstream of the  $45^\circ$  elbow. For test conditions of  $Re = 55000$  and  $\beta=0.75$ , orifice meter requires more than 50 diameters of downstream distance before discharge coefficients could attain values equal to those pertinent to the fully developed pipeflow condition. These meters indicate that the "cross-over" position where discharge coefficient shifts change sign from negative to positive is about  $35D$  from the exit of the  $45^\circ$  elbow. Beyond this location where the discharge coefficients become positive, the largest  $\beta$  ratio has the largest shift reaching a maximum of  $+0.5\%$  at the  $50D$  location.

For a given tolerance on the discharge coefficient about the ideal values, a set of required minimal upstream lengths, in diameters, between the exit plane of the elbow and the orifice can be found. If the  $\pm 0.25\%$  tolerance level was chosen as the criteria, the set of the minimal lengths were 10, 25, and 28 for the  $\beta$  ratios of 0.4, 0.6, and 0.75 respectively. Here the overshoot data for  $\beta=0.75$  at  $Z/D=53.3$  was not considered. These minimal diameter lengths are compared with those for other configurations in Table 1.

Figure 38 presents the comparison on the percentage change in discharge coefficient for a  $\beta = 0.75$  orifice meter installed downstream of different elbow configurations for  $Re=99000$ . For  $45^\circ$  elbow case, data for both from the scaled ports and the conventional ports are included. These results show that for all configurations, when the orifice meter is installed near the elbow, the discharge coefficient is shifted negatively with respect to the reference values. The downshifts are larger for the  $45^\circ$  and  $90^\circ$  elbows than for the tee-used-as-an-elbow and the double elbows-out-of-plane. Except for the double elbows out of plane, for meter installations more distant from the elbow, the negative shifts diminish, become zero, and proceed to shift positively. The amounts of these shifts differs slightly among different configurations. At positions near the elbows, both the  $45^\circ$  and  $90^\circ$  elbows produce larger downshifts in discharge coefficient than the tee-used-as-an-elbow. The zero crossing points for both the  $45^\circ$  and  $90^\circ$  elbows are at near  $Z/D=30$ . However beyond the cross-over point, the discharge coefficients for the  $45^\circ$  elbow has the largest shift reaching a maximum of  $+0.5\%$  at the  $53D$  location, while the shifts for both the  $90^\circ$  elbow and tee used as an elbow are less



than 0.2%. For 45° elbow orifice meter of  $\beta=0.75$  requires more than 50 diameters of downstream distance before discharge coefficients could attain values equal to those pertinent to the fully developed pipeflow condition. The discharge coefficients for double elbows-out-of-plane exhibit some oscillations along the axial position near the elbows.

TABLE 1. INSTALLATION LENGTHS (IN DIAMETERS) FOR THE RESPECTIVE TEST CONDITIONS AT  $Re=55000$ . CRITERIA IS  $\pm 0.25\%$  OF IDEAL VALUES.

Configuration	Beta Ratio				
	.363	.40	.50	.60	.75
45° Elbow	--	10	--	25	28, 53 <sup>*</sup>
90° Elbow	7	--	14	--	22
Tee used as Elbow	7	--	15	--	30
Two Elbows out of plane	35	--	45	--	58, 90 <sup>*</sup>
3-2 Reducer	2	--	7	--	9, 20 <sup>*</sup>

Superscript \* denotes a maximum value of  $C_d$  detected at this location, but this location was not considered in determining the minimum pipe length.

#### b. Downstream of the 45 Degree Elbow and Tube Bundles

The orifice meter performance downstream of the 45° elbow and tube bundles are reported in this section. In all cases here, the orifice meters were located at a fixed position of  $Z/D=17.95$ . Two tube bundles, 7-tube and 19-tube, were tested. For all tests, both data from the conventional and scaled ports were obtained. The pipe run between the elbow and the meter section consist three special pipe sections, having lengths of 2.87, 4.44, and 6.71D each. These three sections together with the 2.72D meter section and the 1.2D flange section just downstream of the elbow

make the total length of the meter run  $17.95D$ . Both tube bundles are the flange mount type. All three pipe sections have been machined to accept the tube bundle flange. A dummy flange (or ring) is used when no tube bundle is installed in the tube section. By arranging the installation positions among the three pipe sections and the tube bundle installation, various tube bundle positions for the fixed meter location can be achieved. This arrangement provided a test condition similar to the sliding vane test preformed at other institutions [16].

Figure 39 shows the discharge coefficients for a  $\beta=0.75$  orifice meter located at a fixed location of  $17.95D$  downstream of a  $45^\circ$  elbow and a 19-tube bundle located at  $C/D=7.16$ . The upper figure (a) is for discharge coefficients for both the conventional and scaled ports and the lower figure (b) is the ratio of the two discharge coefficients. Similar to previous results without tube bundles, the scaled ports have lower  $C_d$  than those for conventional ports. However, the measured ratio of the two  $C_d$ s with the 19-tube tube bundle is higher than the ideal RG equation prediction. A similar result is found for the 7-tube tube bundle case. The difference attributed to the tapping separation correction for cases without and with the tube bundle indicates again that the tapping separation correction should also have the installation effect.

Figures 40 and 41 present the percentage change in discharge coefficient for orifice meters located at a fix location of  $17.95D$  downstream of a  $45^\circ$  elbow with a 19-tube tube bundle. The tube bundle was located at the three different positions of  $C/D=7.16$ ,  $10.03$ , and  $13.87$ . The upper figure (a) is for conventional ports at the  $90^\circ$  position and the lower figure (b) is for scaled ports at the  $270^\circ$  position. Figure 40 presents results for a  $\beta=0.75$  orifice meter showing percentage change in  $C_D$  plotted against Reynolds number in the range of  $40000$  and  $100000$ . The reference discharge coefficients are also shown; by definition, the percentage change for these discharge coefficients are zero. Figure 41 presents results for three  $\beta$  ratios of  $0.4$ ,  $0.6$ ,  $0.75$  and shows percentage change in  $C_d$  plotted against the tube bundle locations,  $C/D$ , upstream of the meter for  $Re=55000$ . The error bars denote one standard deviation of the five repeated readings about the mean value. These results show more clearly than in figure 40 the dependence of the orifice characteristics for the three meters at the same flowrate. Significant negative shifts in discharge coefficient are noted especially for the larger  $\beta$  ratios; the magnitudes of these shifts diminish with increasing axial separation,  $C$



between the orifice plate and the tube bundle exit. The different beta ratio meters achieve slightly different zero shift positions. The  $\beta = 0.6$  meter attains a zero shift at position of about  $C = 14D$  and the  $\beta = 0.75$  meter attains a zero shift position at about  $C=12D$ . If one places a tolerance of  $\pm 0.25\%$  about the reference orifice discharge coefficients, the meter performance for  $\beta=0.4$  is acceptable for all the tube bundle locations tested and the performances for  $\beta=0.6$  and  $0.75$  are only acceptable when the 19-tube tube bundle is located at a  $C/D$  within the range of 11~14 with the cross over point at about  $C/D=13$ .

The similar results for 7-tube tube bundle case are presented in figures 42 and 43. Figure 42 shows the percentage change in the discharge coefficient as a function of the Reynolds number for a  $\beta = 0.75$  orifice meter and figure 43 shows results for the three beta ratios is plotted against the tube bundle locations for Reynolds number 55000. The upper figure (a) is for the conventional ports located at the  $90^\circ$  position and the lower figure (b) is for the scaled ports at the  $270^\circ$  position. The data show all the discharge coefficients are shifted negatively and no cross-over point occurs for these cases. The maximum negative value of the shift is about  $-2.2\%$  for  $\beta=0.75$  when the 7-tube tube bundle is installed at  $C/D=7.16$ . These data indicate that the 7-tube tube bundle produces larger negative shifts in the meter performance than the 19-tube tube bundle. This result is different from the result found previously for the case of tee-used-as-an-elbow where the 7-tube tube bundle produced better meter performance [3].

Figure 44 shows the comparison of the change in discharge coefficients for a  $\beta = 0.75$  orifice meter downstream of a  $45^\circ$  elbow and two tube bundle conditioners. Data for both scaled and conventional ports are shown. The data for 19-tube bundle reported by SwRI [16] are also given for comparison. These data show the agreement between the NIST and SwRI results is considered very good. The agreement seems to be better for the scaled ports than for the conventional ports. These data also show that the 19-tube bundle is a better flow condition than the 7-tube bundle for these installations. This result is different from the case of tee used-as-an-elbow where the 7-tube tube bundle seemed to produce better meter performance, [2].

### 3. Effects of Pressure Tap Orientation on Orifice Meter Performance

In this section the angular orientation of the orifice meter pressure taps relative to the plane of symmetry of the elbow was studied. The four-port plate holder was used to measure the orifice meter performance downstream of the  $45^\circ$  elbow without and with tube bundles. At each position tested the discharge coefficients from the pressure ports at the four angular orientations ( $0^\circ$ ,  $90^\circ$ ,  $180^\circ$ , and  $270^\circ$ ) were measured. The pressure taps are those scaled to conventional 10 cm (4") diameter meters.

#### a. Downstream of the 45 Degree Elbow

Figure 45 presents the change in discharge coefficient for a  $\beta=0.75$  orifice meter versus the meter locations downstream from a  $45^\circ$  elbow for four angular pressure tap locations. The upper figure, figure 45(a), is for a flowrate of  $Re = 55000$  and the lower figure, figure 45(b), is for  $Re=99000$ . The data indicate that, qualitatively, the relationships of  $C_d$  versus  $Z/D$  for all four tap locations are very similar. There are some quantitative differences for different tap locations, however. These differences are much smaller than the change due to the  $45^\circ$  elbow itself. The effects due to the tap location are of the order of .5% of the reference discharge coefficient, while the change in discharge coefficient due to the elbow could be as much as 4%. At small axial distances, i.e.,  $Z/D < 8$ , the negative shift in the discharge coefficient is most negative for the tap location at  $0^\circ$ , downstream of the inside of the bend of the elbow. This result is interesting and somewhat surprising since the axial velocity at the inner bend of the elbow is minimum along the circumferential position. This result indicates the axial velocity alone is not sufficient to determine the value of the discharge coefficient. At large axial distances, e.g.,  $Z/D > 15$  the largest discharge coefficient is found at the  $0^\circ$  orientation, where the axial velocity is minimum among the circumferential position.

To show the details of the effects of the tap orientation, different plots are used as shown in what follows. Figure 46 presents pressure tap orientation effects on the discharge coefficient for a  $\beta=0.75$  orifice meter for three Reynolds numbers of 45000, 72000, and 99000. The upper figure (a) is for the orifice meter located at  $Z/D=3.93$  downstream from a  $45^\circ$  elbow and the lower figure (b) is for  $Z/D=18.42$ .



The later position is an arrangement close to the condition of the usual 17D meter section. The ordinate in each of these figures is the percentage change in discharge coefficient with respect to that obtained at the  $0^\circ$  location for each case. At  $Z/D=3.93$ , the  $C_d$  at the  $0^\circ$  location is found to be the smallest. The result is somewhat surprising since the axial velocity at the inner bent of the elbow is minimum along the circumferential position. This result indicates that the discharge coefficient is not uniquely determined by a single axial velocity condition. The results in figure 46(a) also show that the difference between  $C_d$ s at  $90^\circ$  and  $270^\circ$  is about 0.2%. Because of symmetry, the  $C_d$  values at  $90^\circ$  and  $270^\circ$  should be the same. At the further downstream location of  $Z/D=18.42$ , the variation in the discharge coefficients is closer to what is expected as shown in figure 46(b). That is, the  $C_d$  value has a maximum at  $0^\circ$ , a minimum at  $180^\circ$ , and medium and symmetric values at  $90^\circ$  and  $270^\circ$ .

The value of discharge coefficient is determined from the measured differential pressure across the orifice plate. Both the upstream and downstream wall pressures can affect the outcome of the differential pressure and thus the discharge coefficient. To investigate the wall pressure distribution along the circumferential positions, the four-port plate holder was used to measure these pressure distributions. A differential pressure gage used for the orifice meter was used to measure the pressure differentials across the different pairs of taps. Data from these differential pressures were then used to construct the pressure distributions along the circumferential positions both upstream and downstream of the plate. Figure 47 presents the angular distributions of the measured pressures and the discharge coefficient for a  $\beta=0.75$  orifice meter located at  $Z/D=3.93$  downstream from a  $45^\circ$  elbow for  $Re=99000$ . Figure 47(a) shows the individual tap pressure, relative to the pressure obtained at the  $0^\circ$  tap. In these tests, the differential pressure at  $0^\circ$  was measured twice (one  $P_u-P_d$ , one  $P_d-P_u$ ) and the values obtained from the setup for  $DP_o=P_d-P_u$  were used for reference. This is why the relative upstream pressure at  $0^\circ$  shown in figure 47(a) is not equal to zero. The difference is due to the uncertainty of the pressure measurement. Figure 47(b) shows the angular distributions of the differential pressure from two different methods. The open circles show results for the differential pressure measured directly from the differential pressure gage, which is used to calculate the discharge coefficient and the solid circles show results obtained from the difference of the pressure distributions in figure (a). The data show that the two methods produce fairly



similar results. Figure 47(c) shows the variation of the discharge coefficient. These data indicate that the pressure distributions are showing the expected results - the lower axial velocity region at  $0^\circ$  having lower pressure and the higher axial velocity region at  $180^\circ$  having higher pressure. Also, the pressures at the two symmetric locations of  $90^\circ$  and  $270^\circ$  were fairly similar. However, the pressure difference and thus the discharge coefficient are not necessarily the same as that for the individual pressure distributions. The effect of tap orientation on the discharge coefficient could be as large as 0.4%. Some of this variation could be due to the small uncertainty of the measurement system.

Figure 48 presents the analogous data to those shown in figure 47, except at a different location of  $Z/D=18.42$  downstream from the  $45^\circ$  elbow. At this location, the variation on the pressure distribution and the discharge coefficient indicate what is expected. That is, that both the pressure and pressure difference have minima and the  $C_d$  value has a maximum at  $0^\circ$ , and the pressure and pressure difference both have maxima and the  $C_d$  value has a minimum at  $180^\circ$ , and that medium and symmetric values occur at  $90^\circ$  and  $270^\circ$  for pressure, pressure difference and discharge coefficient.

#### b. Downstream of the 45 Degree Elbow and Tube Bundles

The effects of tap orientation on orifice meter performance were also tested downstream of the  $45^\circ$  elbow and these tube bundles. As described above, the orifice meters were located at a fixed position of  $Z/D=17.95$ . Two tube bundles, 7-tube and 19-tube, were tested. For all tests, four sets of pressure taps were used. The pipe run between the elbow and the meter section consisted of three special pipe sections of lengths 2.87, 4.44, and 6.71D. The tube bundles could be installed in any one of the three pipe sections. By selecting different arrangements of the pipe sections, various tube bundle installation positions for the fixed meter location can be arranged. This arrangement provided a test condition similar to the sliding vane test performed at other institutions [16].

Figure 49 presents the change in discharge coefficient versus tube bundle positions for a  $\beta=0.75$  orifice meter located 17.95D downstream from a  $45^\circ$  elbow for four pressure tap locations and  $Re = 99000$ . Figure 49(a) is for the 7-tube bundle, while figure 49(b) is for the 19-tube bundle. The variation of the change in discharge

coefficient is about 0.5% of the reference discharge coefficient; this is smaller than the previously described effects attributed to the piping configurations. The maximum  $C_d$  value among the four orientations occurs at the inner bend of the elbow, the  $0^\circ$  orientation, where the axial velocity downstream of the elbow is a minimum.

Presentations of tap orientation effects similar to those of figure 47 are given next for the elbow and tube bundles. Figure 50 presents the angular distributions of the measured pressures and the discharge coefficient for a  $\beta=0.75$  orifice meter located  $Z/D=17.95$  downstream from a  $45^\circ$  elbow and the 19-tube bundle at  $C/D=10.03$  for  $Re=99000$ . Figure 50(a) shows the individual tap pressure, relative to that obtained at the  $0^\circ$  position. Figure 50(b) shows the angular distributions of the differential pressure using two different methods. The open circle data show differential pressure measured directly from the differential pressure gage, which was used to calculate the discharge coefficient; the solid circle data show the results obtained from the difference of the pressure distributions in figure (a) above.

Figure 50(c) shows the variation of the discharge coefficient with a maximum  $C_d$  at  $0^\circ$  and a minimum  $C_d$  at  $90^\circ$ . Although the data show there are some variations in the pressure and discharge coefficient for the different tap orientations, these variations seem to occur in an arbitrary manner. This variation could be partially due to small imperfections in the tube bundle or its installation. To test some of these effects, the tube bundle was removed and reinstalled after being rotated  $180^\circ$ . Figure 51 presents plots identical to those of figure 50 after the  $180^\circ$  rotation of the tube bundle. With the tube bundle rotated, the distribution of the discharge coefficient seems also rotated. In figure 50 the differential pressure at the  $90^\circ$  angular location is larger than that at  $270^\circ$  and the discharge coefficient at the  $90^\circ$  angular location is lower than that at  $270^\circ$ . In figure 51 the results of the pressure and discharge coefficient at the two angular locations are reversed. These data indicate that the effects of the pressure tap orientation are primarily due to uncertainties produced by tube bundle details. This tube bundle is a flange mounted type. The data seems to indicate that the mounting flange is not perfectly normal to the tube bundles, especially in the  $90^\circ$  - $270^\circ$  direction. A change of the tube bundle orientation could cause a change in the effect of tap orientation on the discharge coefficient up to about 0.6%. Figure 52 shows results for a 7-tube tube bundle at  $C/D=10.03$ . The minimum pressure occurs downstream of the inner bent of the elbow ( $0^\circ$  angular location). The  $C_d$  has a maximum value at  $0^\circ$  and a



minimum at  $180^\circ$  with the variation of the order of 0.35%.

#### 4. Turbine Meter Performance

As for the orifice meter tests, the turbine meter performance test was also assessed in the two types of arrangements. For the case of the  $45^\circ$  elbow without the tube bundle, the turbine meter performance was determined at various locations downstream of the elbow. For the case of the  $45^\circ$  elbow with tube bundles, the turbine meter was located at a fixed location of  $Z/D=16.81$  downstream of the  $45^\circ$  elbow and tube bundle was installed at different locations. The tube bundle test was arranged to be similar to the sliding vane test used at SwRI [16].

Figure 53 presents the percentage change in Strouhal number,  $St=fD/W_b$ , for a turbine meter at different downstream installation positions from a  $45^\circ$  elbow. The ordinate is the percentage shift in meter factor at each flowrate taken relative to the reference condition. Here the reference Strouhal number of the turbine meter was measured in a fully developed pipe flow downstream of about 200 diameters of constant diameter, straight pipe. The transfer standard was used for all these flowmeter performance tests. This appears justified since the primary objective of these tests is to study installation effects on the meter performance relative to that for the ideal installation. If absolute values for the meter were the test objective, primary flow standards should be used. Figure 53(a) shows results over the Reynolds number range from 40000 to 100000. Figure 53(b) shows results for different distances downstream from the elbow for two Reynold numbers 45000 and 99000. The difference between the two Reynolds numbers is considered small. The meter factor shift is -0.45% for the installation position 2.8D downstream of the  $45^\circ$  elbow. For further downstream positions, this shift approaches and reaches zero for the position about 18D downstream. Beyond this position, the meter factor attains positive shifts which reach a maximum of +0.04% at the 28D position downstream. At and beyond the 40D position, this meter shows no further shift relative to the reference value. If one places a tolerance of  $\pm 0.25\%$  about the reference meter constant, the minimal pipe length required to ensure an acceptable meter performance for the turbine meter is about 7 pipe diameters.

When the turbine meter is tested downstream of the elbow and the 19-tube tube bundle, results are as given in figure 54. Again, the ordinate is the percentage



shift in meter factor at each flowrate taken relative to the reference condition. Figure 54(a) shows the results over the Reynolds number range from 40000 to 100000. For the case of the 45° elbow with tube bundles, the arrangement was similar to the previously mentioned sliding vane case so that the turbine meter was located at a fixed location of  $Z/D=16.81$  downstream of the 45° elbow and tube bundle was installed at different locations. Figure 53(b) shows the percentage change in Strouhal number versus the tube bundle position,  $C/D$ , upstream from the turbine meter for two Reynolds numbers. The data show the meter factor shift is less than 0.04% for all installation positions of the 19-tube bundle. Figure 55 presents turbine meter characteristics analogous to those of figure 54 except the 7-tube bundle is used. The figure shows similar results for meter performance for the turbine meter downstream of the 45° elbow and the 7-tube bundle.

These results indicate that the turbine meter factor is within  $\pm 0.25\%$  of the reference value for all tube bundle installation positions tested. That is, this turbine meter is not affected by the pipeflows exiting from the combination of the 45° elbow and the 19- or 7-tube bundle. It is, therefore, concluded that the geometry of this turbine design is capable of successfully averaging over the flow patterns presented in figures 10-13 and producing a meter factor that is essentially the reference value in these installation conditions.

## CONCLUSIONS

The velocity profile measurements made downstream from the 45° elbow for the selected fluid and flow conditions indicate that the secondary flow produced by the elbow is very similar to those of the 90° elbow and the tee-used-as-an-elbow. As compared to the fully developed pipe profile, the velocities near the pipe center are much slower, and those near the pipe walls are higher along the diameter normal to the plane of the 45° elbow. In the symmetry plane of the elbow the results show high speed flow in the outside region of the turn and a region of slow flow near the inside of the elbow turn. At the location of  $18D$  downstream from the elbow, the profile is fairly flat over most of the center core, but it is skewed toward the outside of the elbow turn.

A dual eddy swirl distribution is generated by the turning action of this 45° elbow. The result indicates that the dual eddy produced by the 45° elbow is relatively

stable and organized and the dissipation is slower than those observed for both the 90° elbow and the tee-used-as-an-elbow. Additionally, these flows are accompanied by levels of turbulence that are slightly lower than those from the 90° elbow and much lower than those from the tee-used-as-an-elbow. The net results are that the flow effects from the 45° elbow dissipate more slowly than those from the 90° elbow and tee used as an elbow. Data for the conditions tested show that the dual-eddy swirl patterns produced by the 45° elbow persist to beyond 18 diameters from the exit of the elbow. All three flows i.e., the 45° and 90° elbows and the Tee used-as-an-elbow, have smoothly varying turbulence distributions across the pipe 18D downstream and thus indicate that all these flows are still developing toward a fully developed pipeflow condition.

Just downstream of the 19-tube bundle, the pipeflow is dominated by the effects of multi-jets from individual tubes. The axial velocity profiles exhibit very smoothly varying velocity distributions in which the major portion of the center core of the pipeflow is quite slow in comparison with the fully developed distributions. The 19-tube bundle is quite effective in reducing transverse velocities and thus the dual eddy flow. Further downstream, the effect of the tube bundle diminishes but some of the upstream disturbance in the axial velocity distribution seems to persist. At 13D downstream of the tube bundle, the effect of pipe wall boundary layer has not yet completely propagated over the entire pipe cross section and thus the pipeflow is still in the process of evolving toward the fully developed distribution.

The performance of selected orifice flowmeters downstream of the 45° elbow and the two tube bundles were obtained using plate holders having both conventional pressure taps and scaled pressure taps. When the orifice meter is installed near the elbow the discharge coefficient is shifted negatively with respect to reference values. The negatively shifted values are similar to those for the 90° elbow and are larger than that for the tee-used-as-an-elbow or the double elbows-out-of-plane configuration. However, beyond the cross-over point, the discharge coefficients for the 45° elbow have the largest shifts reaching a maximum of +0.5% at the 53D location, while the shifts for both the 90° elbow and tee used as an elbow are less than 0.2%. For 45° elbow, an orifice meter of  $\beta=0.75$  requires more than 50 diameters of downstream distance before discharge coefficients attain values equal to those pertinent to fully developed pipeflow conditions.



The effectiveness of the 19- and 7-tube bundles was assessed for these installation positions. The orifice meter was located at a fixed position of 17.95D downstream from the elbow and the tube bundle was installed at various locations upstream of the meter. This arrangement is analogous to the sliding vane test condition tested in other laboratories. For 19 tube bundle, the meter performance for a  $\beta=0.4$  is within  $\pm 0.25\%$  of reference values for all the bundle locations tested and the performances for  $\beta=0.6$  and  $0.75$  are only acceptable ( $< \pm 0.25\%$ ) when the 19-tube bundle is located at a C/D within the range of 11~14 with the cross over point at about C/D=13. For 7 tube bundle, there is no cross-over point and all discharge coefficients are negatively shifted. The maximum negative value of the shift is about  $-2.2\%$  for  $\beta=0.75$  when the 7-tube bundle is installed at C/D=7.16. These data indicate that the 19-tube bundle conditioner is more effective than the 7-tube bundle in these conditions. This result is different from the result for the case of the tee-used-as-an-elbow where the 7-tube bundle seemed to produce better meter performance.

The 5 cm (2") scaled tap orifice plate holder is scaled to conventional 10cm (4") diameter meters. This arrangement is expected to set precedence for larger meter tests. The discharge coefficients for the scaled ports are smaller than those of the conventional ports for both  $\beta$  of 0.6 and 0.75 but are essentially the same for the  $\beta=0.4$  geometry.

By comparing the discharge coefficients from both the conventional and scaled port orifice meters it appears that the corrections for the pressure tap separations are not same for all flow conditions. That is, it appears that the pressure tap correction also is susceptible to installation effects.

The effects of pressure tap orientation on orifice meter performance has also been examined. Results show there are some differences for different tap locations, however these differences are smaller than the change due to the  $45^\circ$  elbow itself. The effect due to the tap location is of the order of 0.5% of the reference discharge coefficient, while the change in discharge coefficient due to the elbow is as much as 4%. These data also indicate that the pressure distributions conform to expected results, i.e., lower pressure at the lower axial velocity region downstream of the inside of the elbow turn; higher pressure at the higher axial velocity region at the outside of the turn, and a moderate pressure at the two symmetric locations.



However, the pressure difference (or the discharge coefficient) does not necessarily give the same result as that corresponding to the individual pressure distribution. Some of the uncertainty in these results could be due to the small uncertainty of the measurement system. For the tests involving tube bundles, the data seem to indicate that the effects of pressure tap orientation are primarily due to anomalies associated with the tube bundle construction details.

Turbine meter characteristics do not seem to be so radically affected by the pipeflows downstream from the 45° elbow and tube bundles as compared to the orifice meters tested. At the nearest installation position of 2.8D downstream of the 45° elbow, the meter factor shift is -0.45%. For further positions, this shift approaches and reaches zero for the position about 18D downstream. If one places a tolerance of  $\pm 0.25\%$  about the reference meter constant, the minimal pipe length required to ensure an acceptable meter performance for the turbine meter is about 7 pipe diameters.

These results indicate that, the turbine meter factor is within  $\pm 0.25\%$  of the reference value for all tube bundle installation positions tested. That is, this turbine meter is not affected by the pipeflows exiting from the combination of the 45° elbow and the 19- or 7-tube bundle.

## REFERENCES

- [1] Mattingly, G.E. and Yeh, T.T., Summary Report of NIST's Industry-Government Consortium Research Program on Flowmeter Installation Effects With Emphasis on the Research Period January-September 1991: The Reducer, NISTIR 4779, December 1991.
- [2] Mattingly, G.E. and Yeh, T.T., NIST's Industry-Government Consortium Research Program on Flowmeter Installation Effects: Report of Results for the Research Period Feb-Dec. 1990: Tee Used As An Elbow, NISTIR 4753, December 1990.
- [3] Mattingly, G.E. and Yeh, T.T., NIST's Industry-Government Consortium Research Program on Flowmeter Installation Effects: Report of Results for the Research Period May 1989 - Feb. 1990: Tube Bundle, NISTIR 4751, Nov. 1990.
- [4] Mattingly, G.E. and Yeh, T.T., NIST's Industry-Government Consortium Research Program on Flowmeter Installation Effects: Report of Results for the Research Period Nov. - May 1989, NISTIR 4310, April. 1990.
- [5] Mattingly, G.E. and Yeh, T.T., NIST's Industry-Government Consortium Research Program on Flowmeter Installation Effects: Report of Results for the Research Period Jan. - July 1988, NISTIR-89-4080, April 1989.
- [6] Mattingly, G.E. and Yeh, T.T., NIST's Industry-Government Consortium Research Program on Flowmeter Installation Effects: Report of Results for the Research Period July - December 1987. NISTIR-88-3898, May 1988.
- [7] ASME MFC-10M, Method for Establishing Installation Effects on Flowmeter, Amer. Soc. of Mech. Engr., Nov. 1988, New York, NY.
- [8] Yeh, T.T. and Mattingly, G.E., Secondary Flows in Pipes, (Submitted for publication in the ASME Journal of Fluid Engineering).
- [9] Mattingly, G.E. and Yeh, T.T., Robertson, B. and Kothari, K., NBS Research on In-Situ Flowmeter Installations, Procs. AGA Distribution and Transmission Confr. Las Vegas NV, May 1987.
- [10] Mattingly, G.E. and Yeh, T.T., Effects of Non-Ideal Pipeflows and Tube Bundles on Orifice and Turbine Meters, Flow Measurement and Instrumentation Journal, Special Issue on Flowmeter Installation Effects, Butterworth Publ., Guildford, U.K., Feb. 1991, pp. 1-19.
- [11] Orifice Metering of Natural Gas and other Related Hydrocarbon Fluids, Part 2, Specification and Installation Requirements, AGA Report No.3, API 14.3, GPA 8185-90, 3rd Ed., February 1991.
- [12] Bogue, D.C. and Metzner, A.B., Velocity Profiles in Turbulent Pipe Flow, I&EC Fundamentals Vol. 2, No. 2, May 1963, pp 143-9.

- [13] Laufer, J., The Structure of Turbulence in Fully Developed Pipe Flow, NBS Rept. 1974, Sept. 1952.
- [14] Orifice Metering of Natural Gas and other Related Hydrocarbon Fluids, ANSI/API 2530, AGA Report No.3, 2nd Ed., American Gas Association, Arlington, VA, May 1985.
- [15] Orifice Metering of Natural Gas and other Related Hydrocarbon Fluids, Part 1, General Equations and Uncertainty Guidelines, AGA Report No.3, API 14.3, GPA 8185-90, 3rd Ed., October 1990.
- [16] Morrow, T.B. and Park, J.T., Orifice Meter Installation Effects: Sliding Vane Test with a 17 D Meter Tube and a 19 Tube Bundle Straightening Vane Downstream of a 45° Elbow Technical Memorandum MRF-UE-10, GRI, July 1992
- [17] Measurement of Fluid Flow by Means of Orifice Plates, Nozzles, and Venturi Tubes Inserted in Circular Cross-section Conduits Running Full, ISO 5167 - 1980 (E), International Organization for Standardization, Geneva, 1980.
- [18] Fluid Meters- Their Theory and Applications 6th ed, ASME, New York, 1971, ed. by Bean, H.S., Chapter I-5.
- [19] Davis, R.W. and Mattingly, G.E., Numerical Modeling of Turbulent Flow Through Thin Orifice Plates, NBS Special Publication 484, Proceedings of the Symposium on Flow in Open Channels and Closed Conduits held at NBS, Gaithersburg, MD, Feb. 23-25, 1977.
- [20] Morrison, G.L., 3-D Laser Anemometer Study of Compressible Flow Through Orifice Plates Gas Research Institute Annual Report Number GRI-90/0036, December 1990.



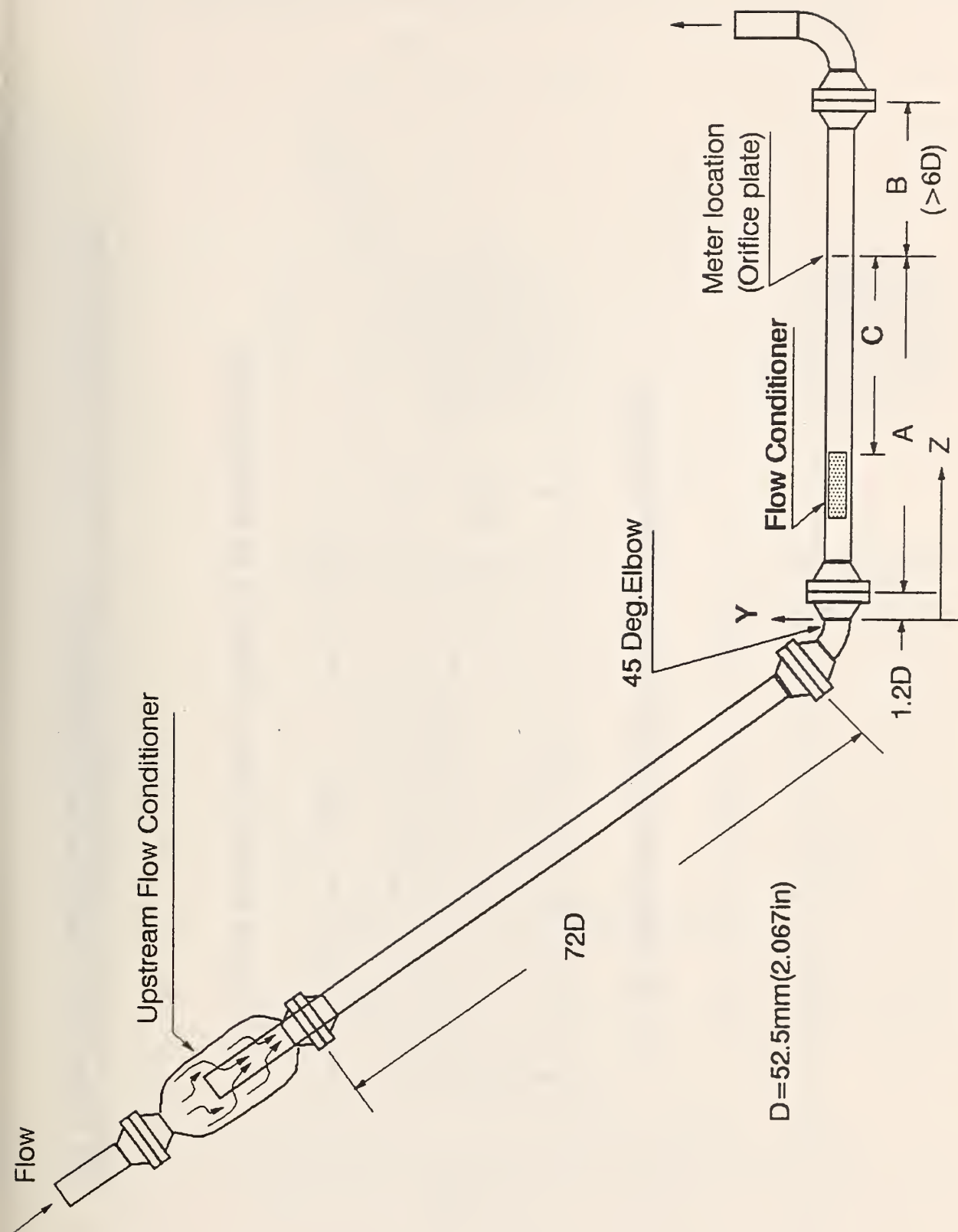
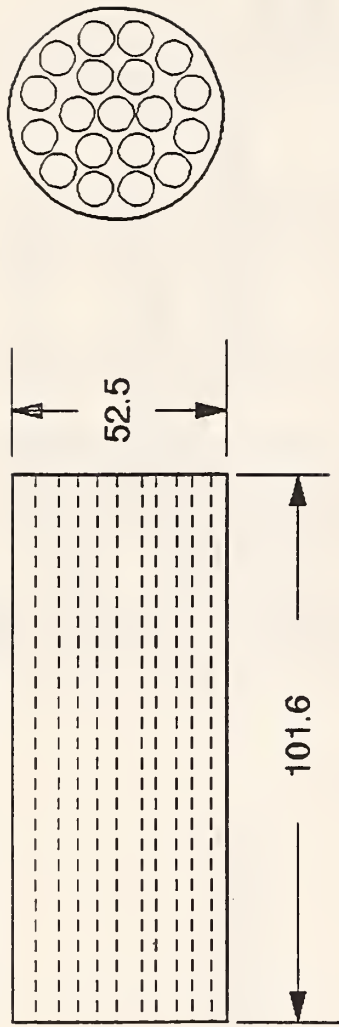
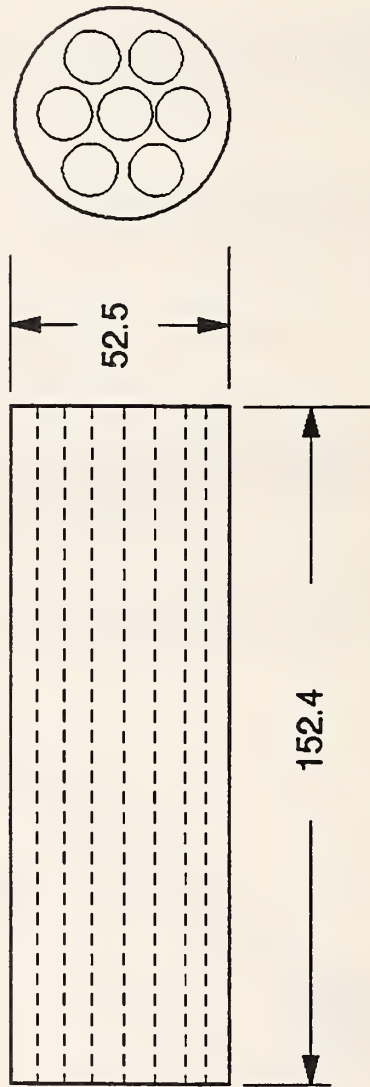


**Figure 1** Sketch of the 45° Elbow Piping Arrangement and Coordinate System.

Dimensions are in millimeters



(a) 19-Tube Bundle (Tubes: 9.5 ID; 0.4 wall thickness)



(b) 7-Tube Bundle (Tubes: 13.39 ID; 1.26 wall thickness)

Figure 2 Sketches of Tube Bundles: (a) 19 Tube, Concentric Arrangement and (b) 7 Tube Unit. Dimensions are in millimeters.

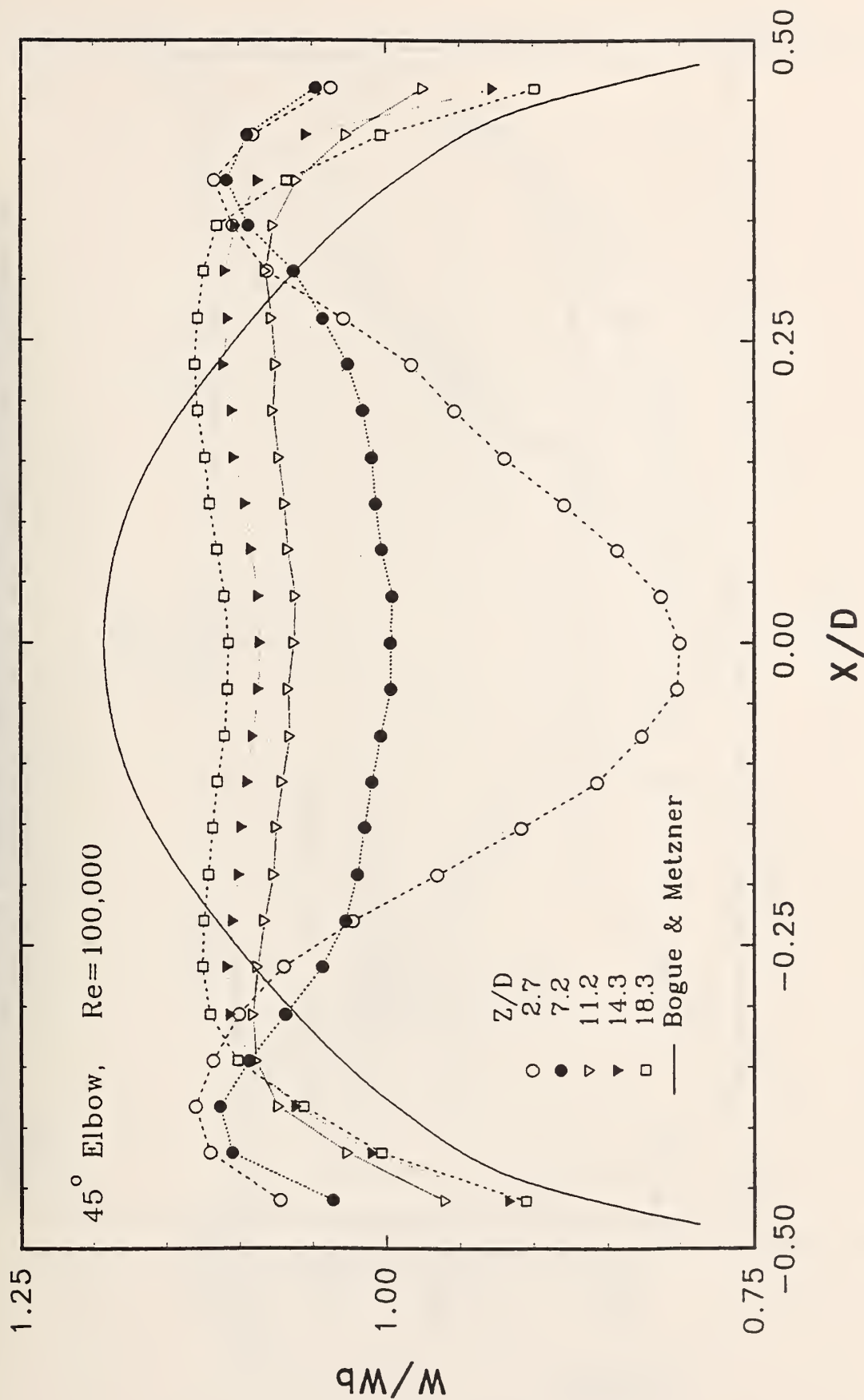


Figure 3 Axial Velocity Profile Results vs. Horizontal Radial Position at Different Downstream Locations from the 45° Elbow for  $Re = 100,000$ . The solid line shows the ideal profile of Bogue & Metzner.



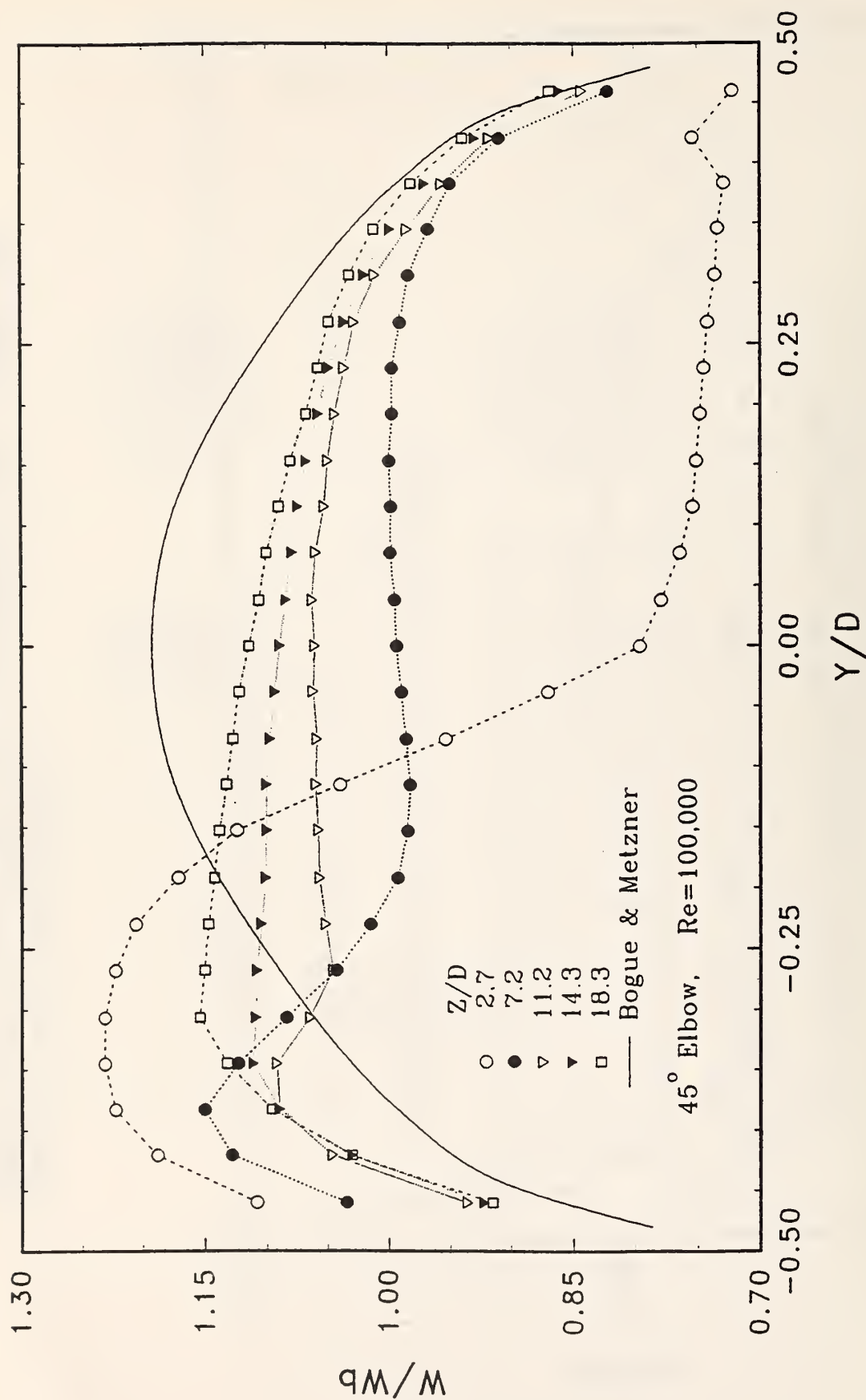
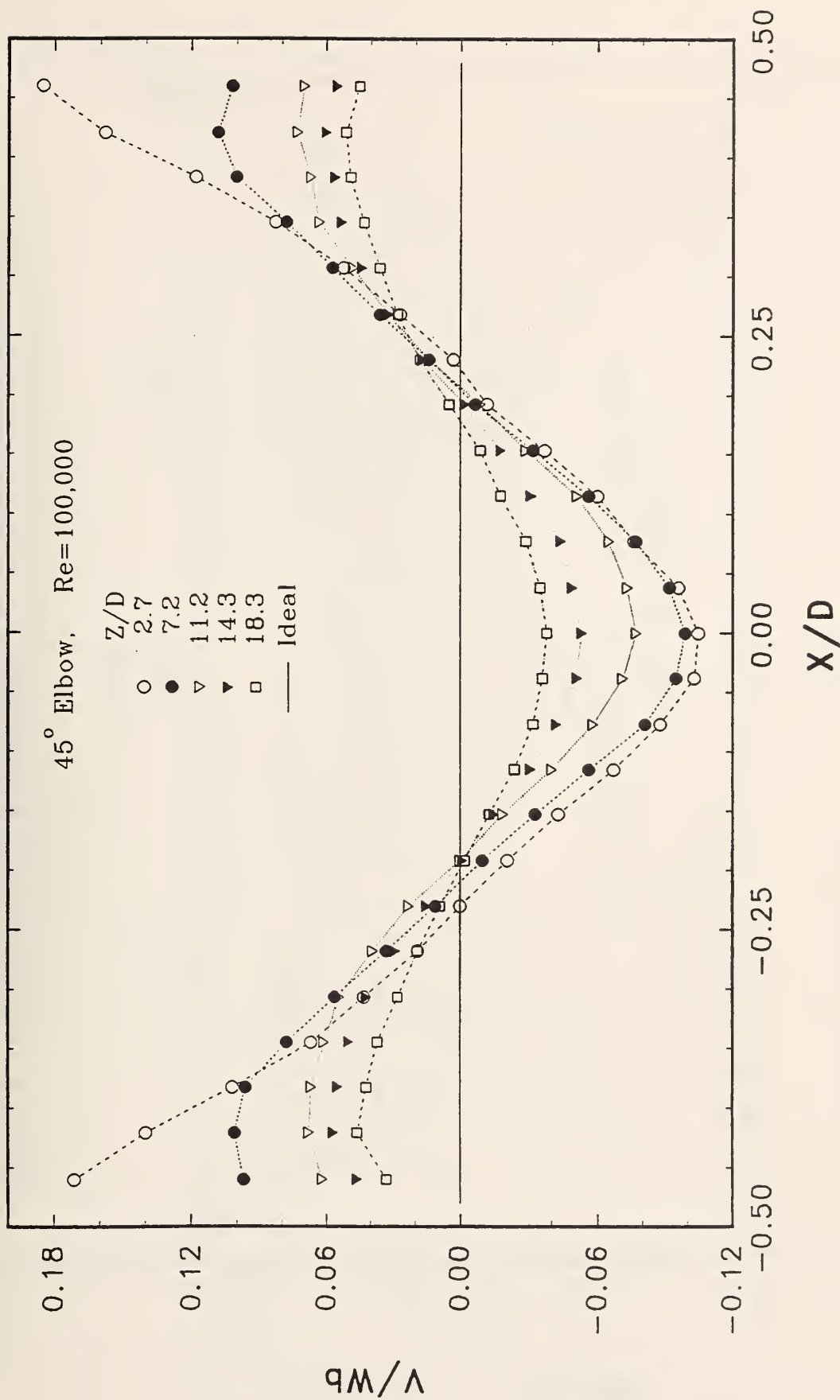
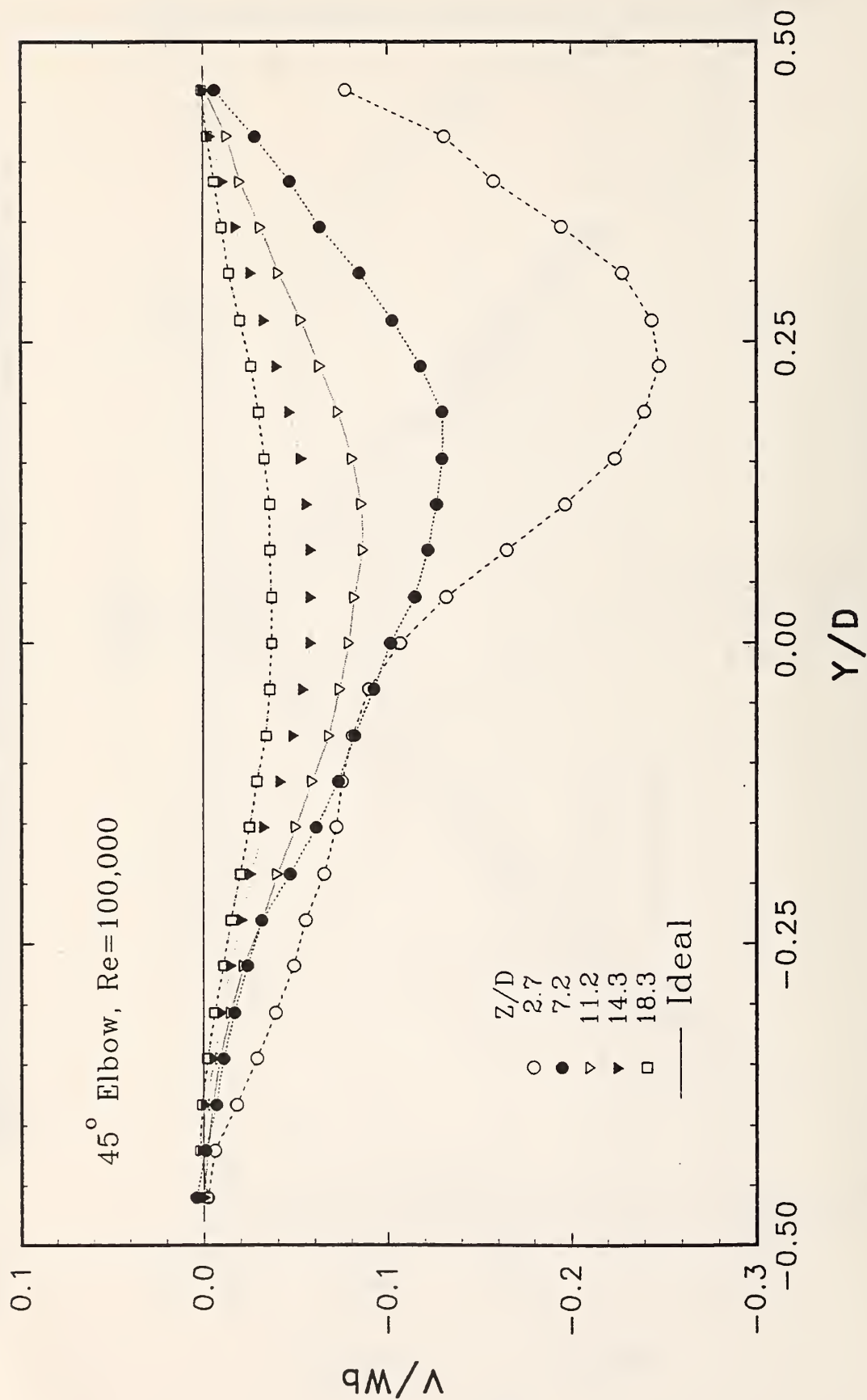


Figure 4 Axial Velocity Profile Results vs. Vertical Radial Position at Different Downstream Locations from the  $45^\circ$  Elbow for  $Re = 100,000$ . The solid line shows the ideal profile of Bogue & Metzner.



**Figure 5** Vertical Velocity Profile Results vs. Horizontal Radial Position at Different Downstream Locations from the 45° Elbow for  $Re = 100,000$ .



**Figure 6** Vertical Velocity Profile Results vs. Vertical Radial Position at Different Downstream Locations from the  $45^\circ$  Elbow for  $Re = 100,000$ .



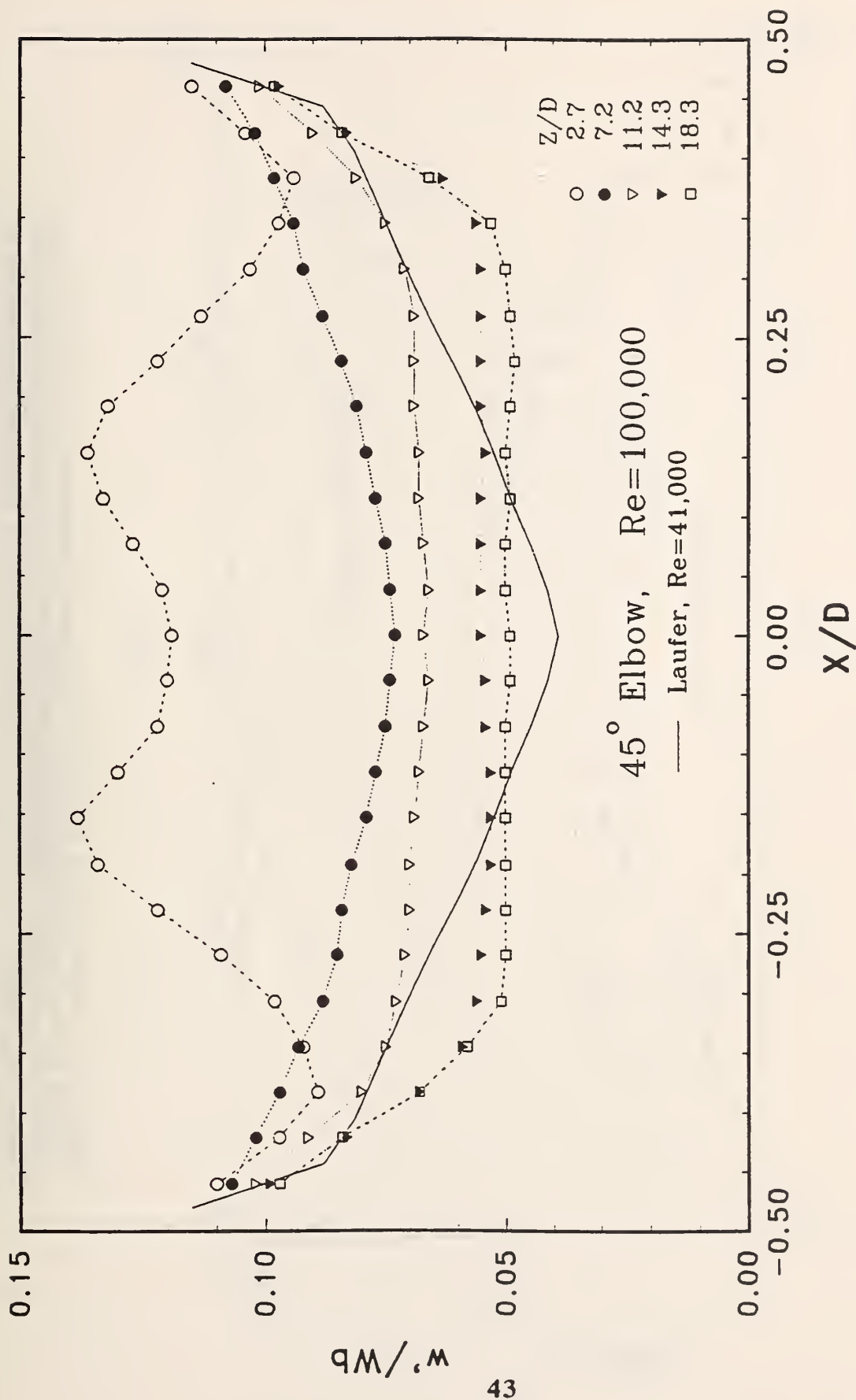


**Figure 7** Profiles of the R.M.S. of the Axial Component of the Turbulent Velocity vs. Horizontal Radial Position at Different Downstream Locations from the 45° Elbow for  $Re = 100,000$ . The solid line shows the profile measured by Laufer, for  $Re=41,000$ .

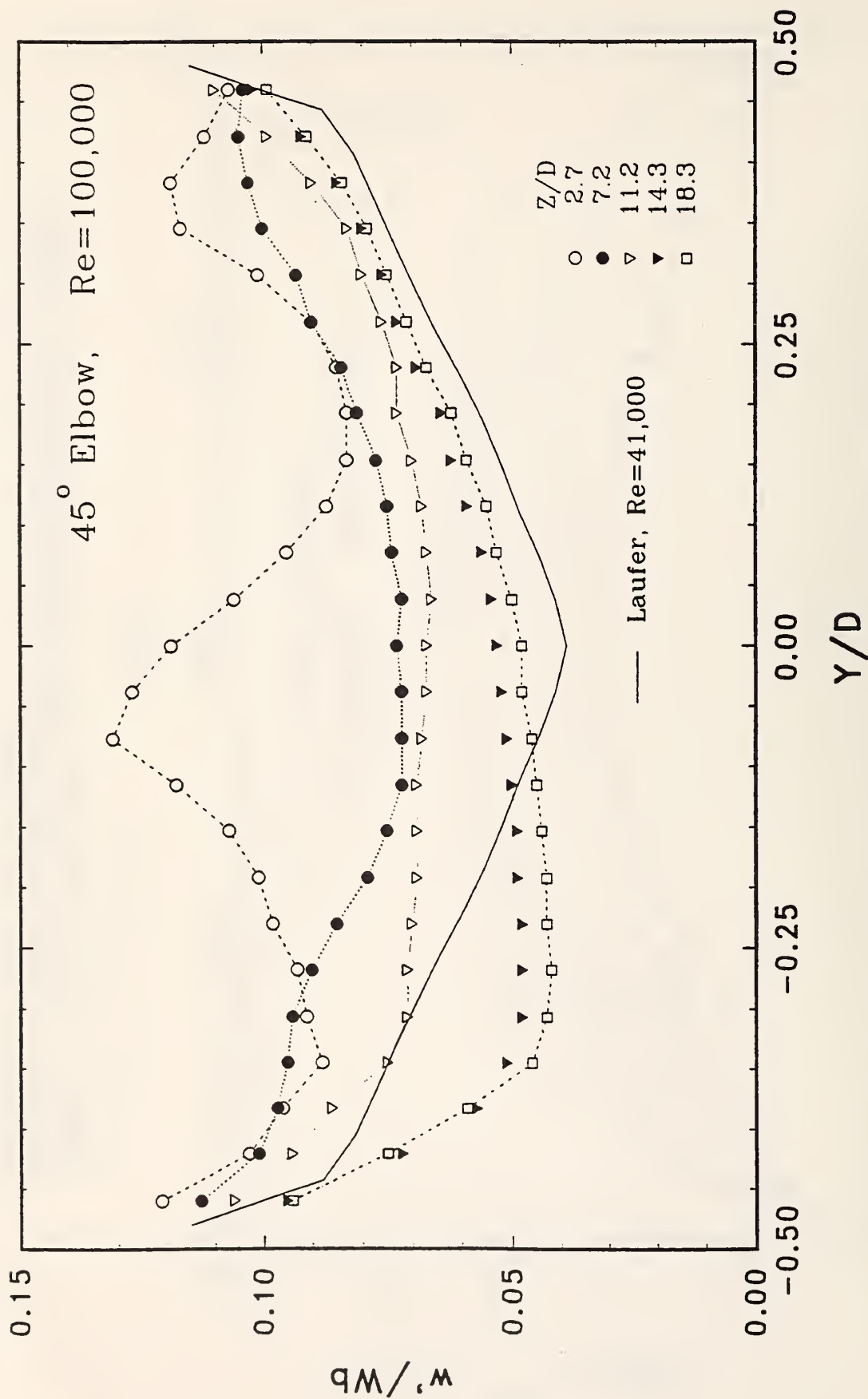


**Figure 8** Profiles of the R.M.S. of the Axial Component of the Turbulent Velocity vs. Vertical Radial Position at Different Downstream Locations from the  $45^\circ$  Elbow for  $Re = 100,000$ . The solid line shows the profile measured by Laufer,  $Re=41,000$ .

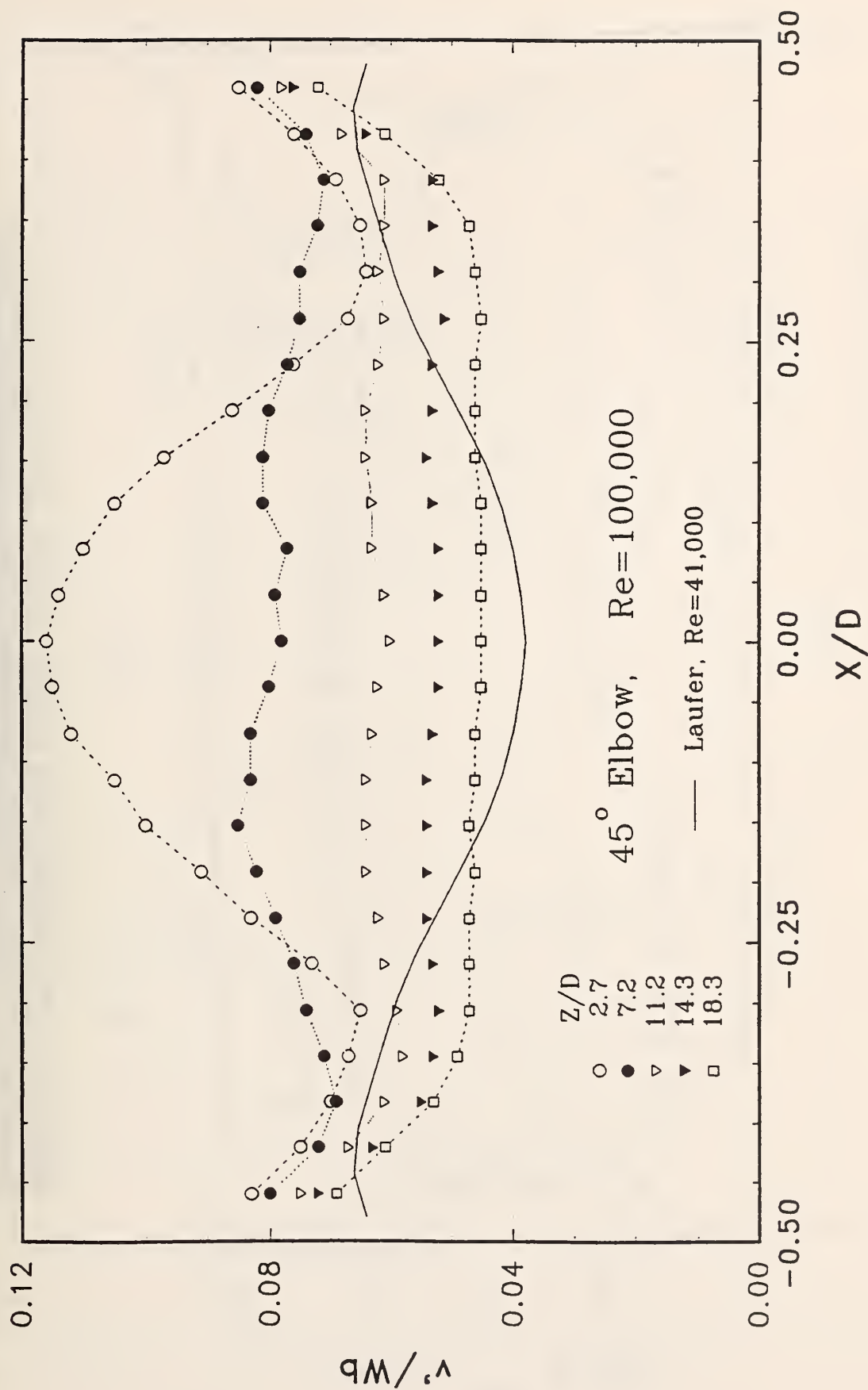
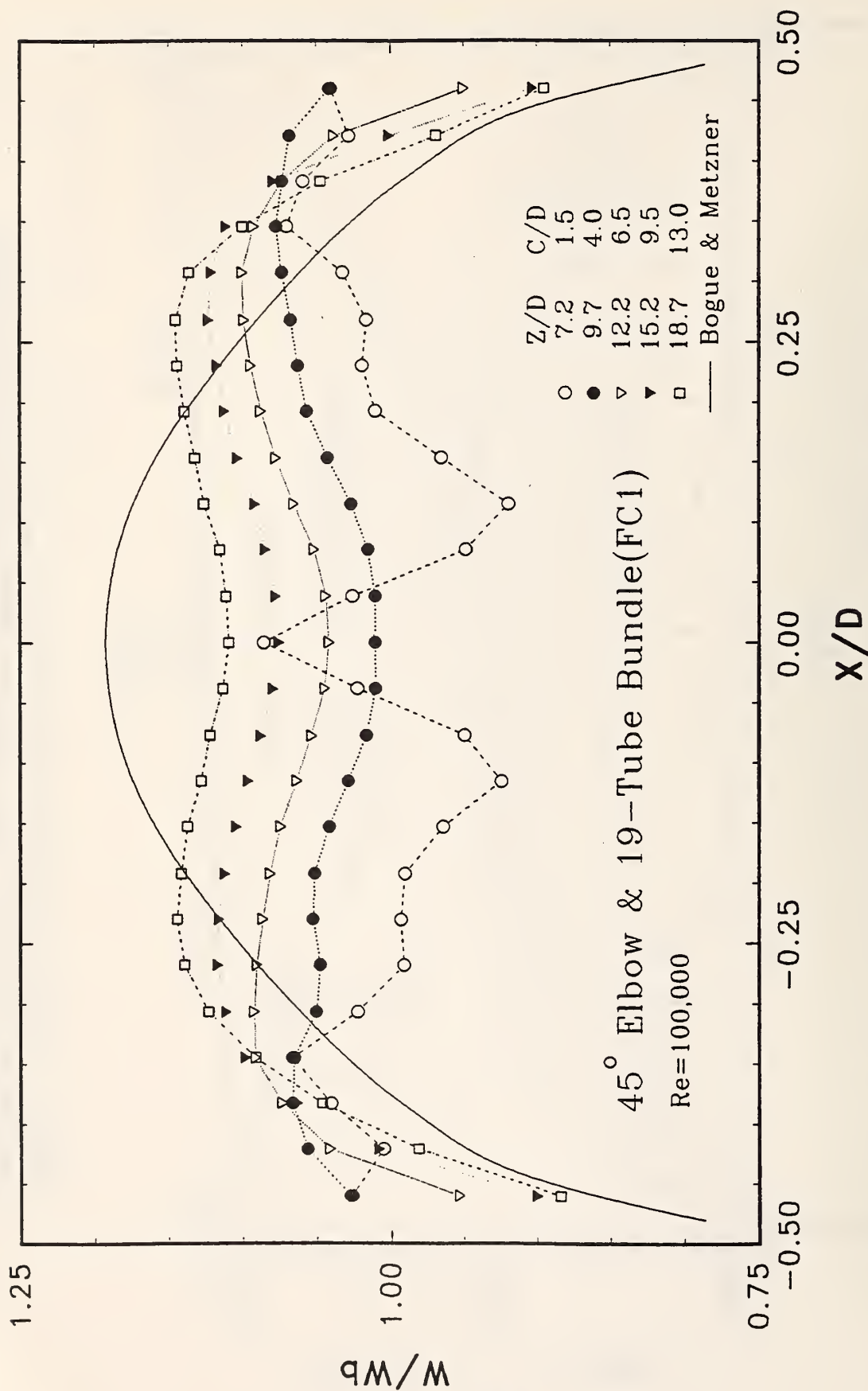
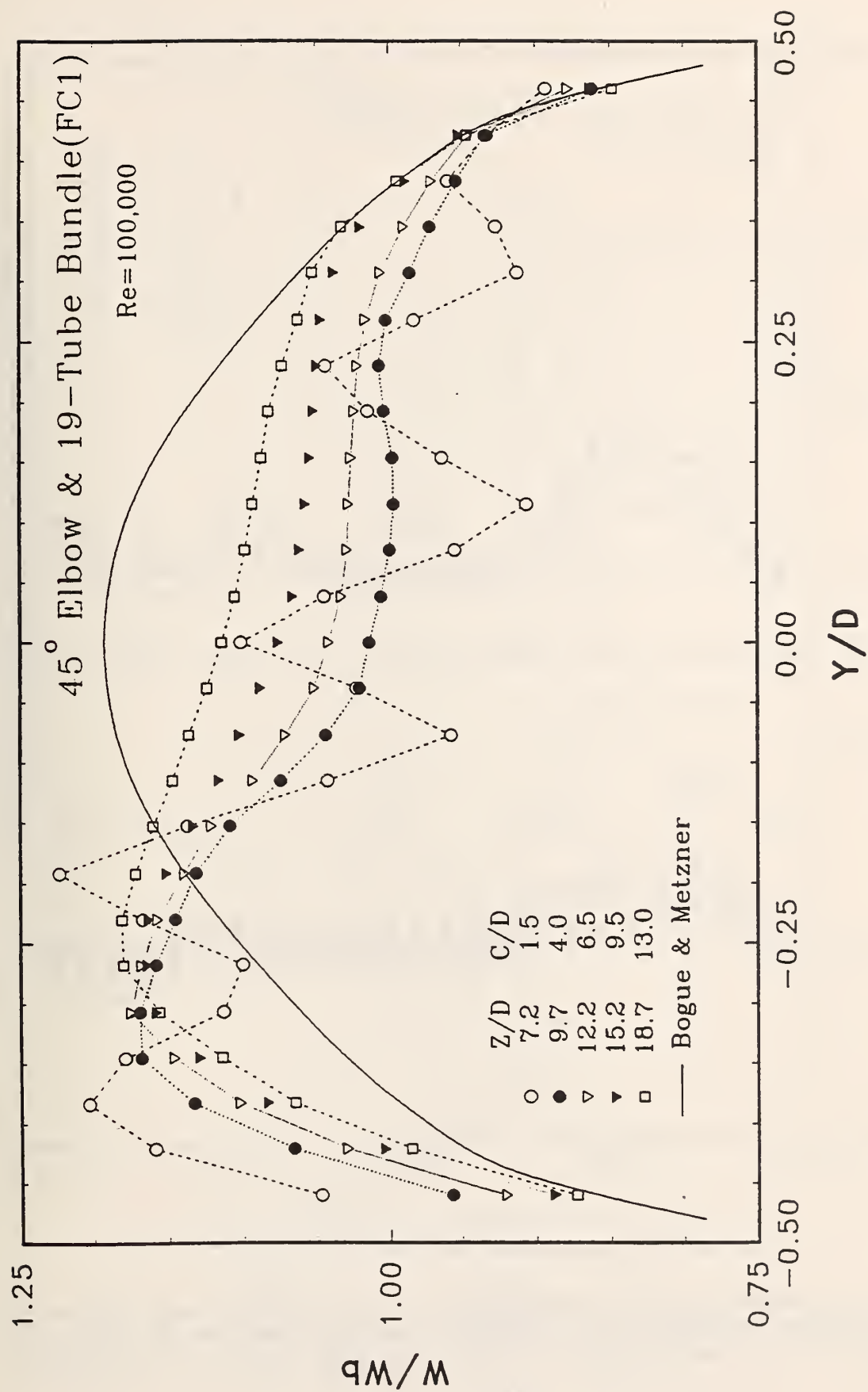


Figure 9 Profiles of the R.M.S. of the Vertical Component of the Turbulent Velocity vs. Horizontal Radial Position at Different Downstream Locations from the  $45^\circ$  Elbow for  $Re = 100,000$ . The solid line shows the profile measured by Laufer,  $Re=41,000$ .





**Figure 10** Axial Velocity Profile Results vs. Horizontal Radial Position at Different Downstream Locations from the  $45^\circ$  Elbow and the 19-Tube Tube Bundle for  $Re = 100000$ . The solid line shows the profile measured by Bogue & Metzner.



**Figure 11** Axial Velocity Profile Results vs. Vertical Radial Position at Different Downstream Locations from the 45° Elbow and the 19-Tube Tube Bundle for  $Re = 100000$ . The solid line shows the ideal profile of Bogue & Metzner.

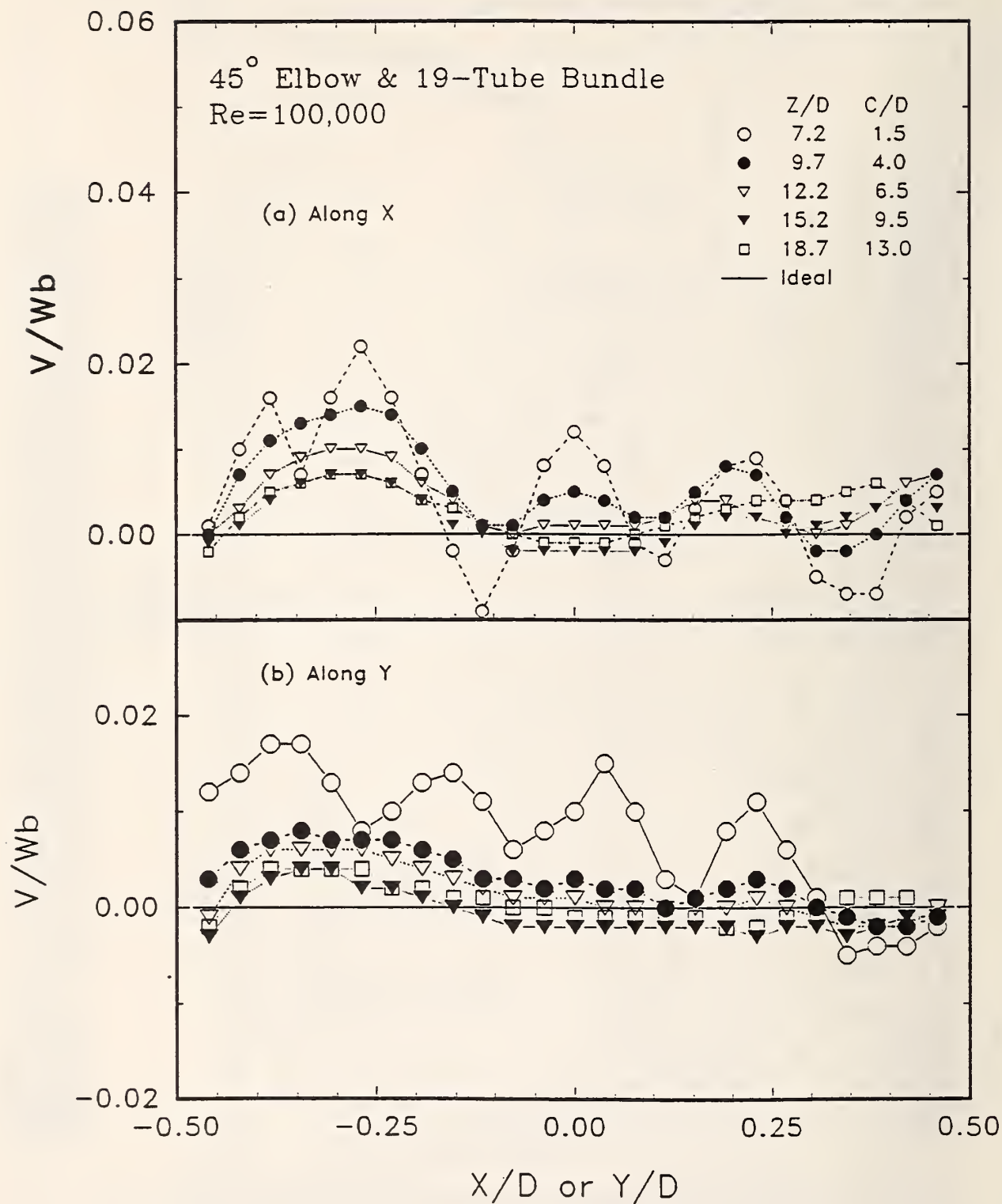


**Figure 12** Vertical Velocity Profile Results vs. Horizontal (a) and Vertical (b) Radial Positions at Different Downstream Locations from the 45° Elbow and the 19-Tube Tube Bundle for Re = 100000. The solid lines show the profile of ideal flow.



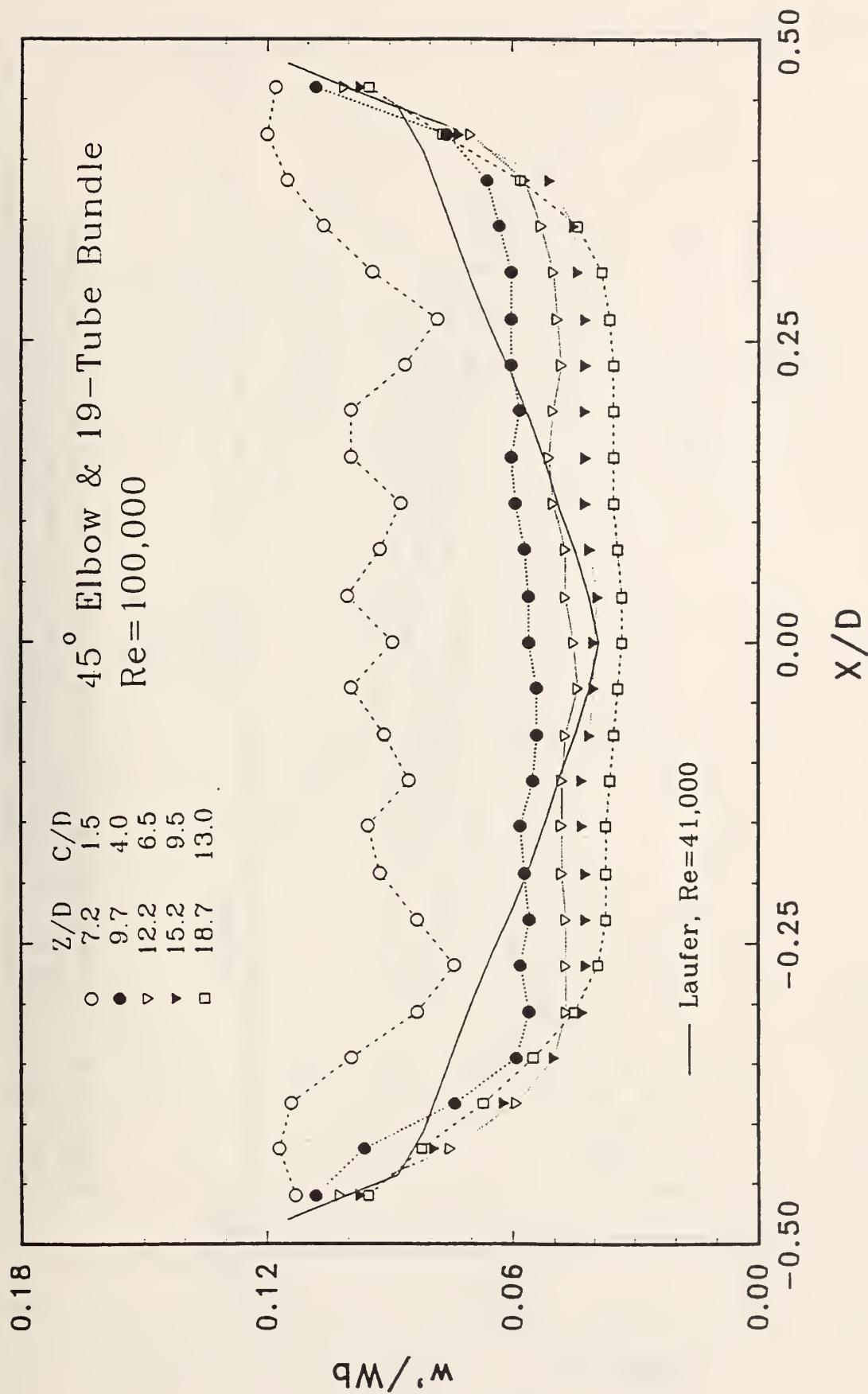
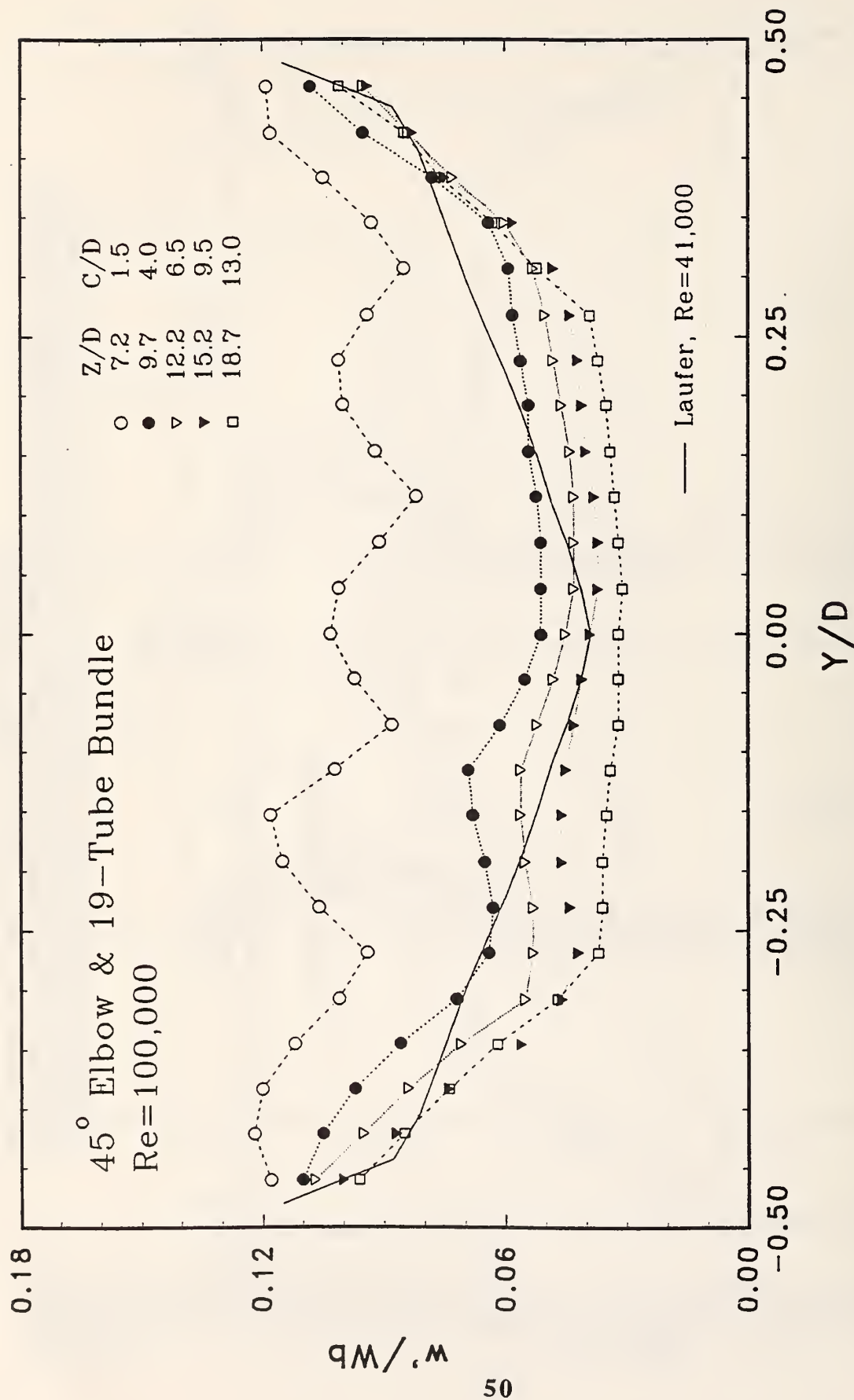
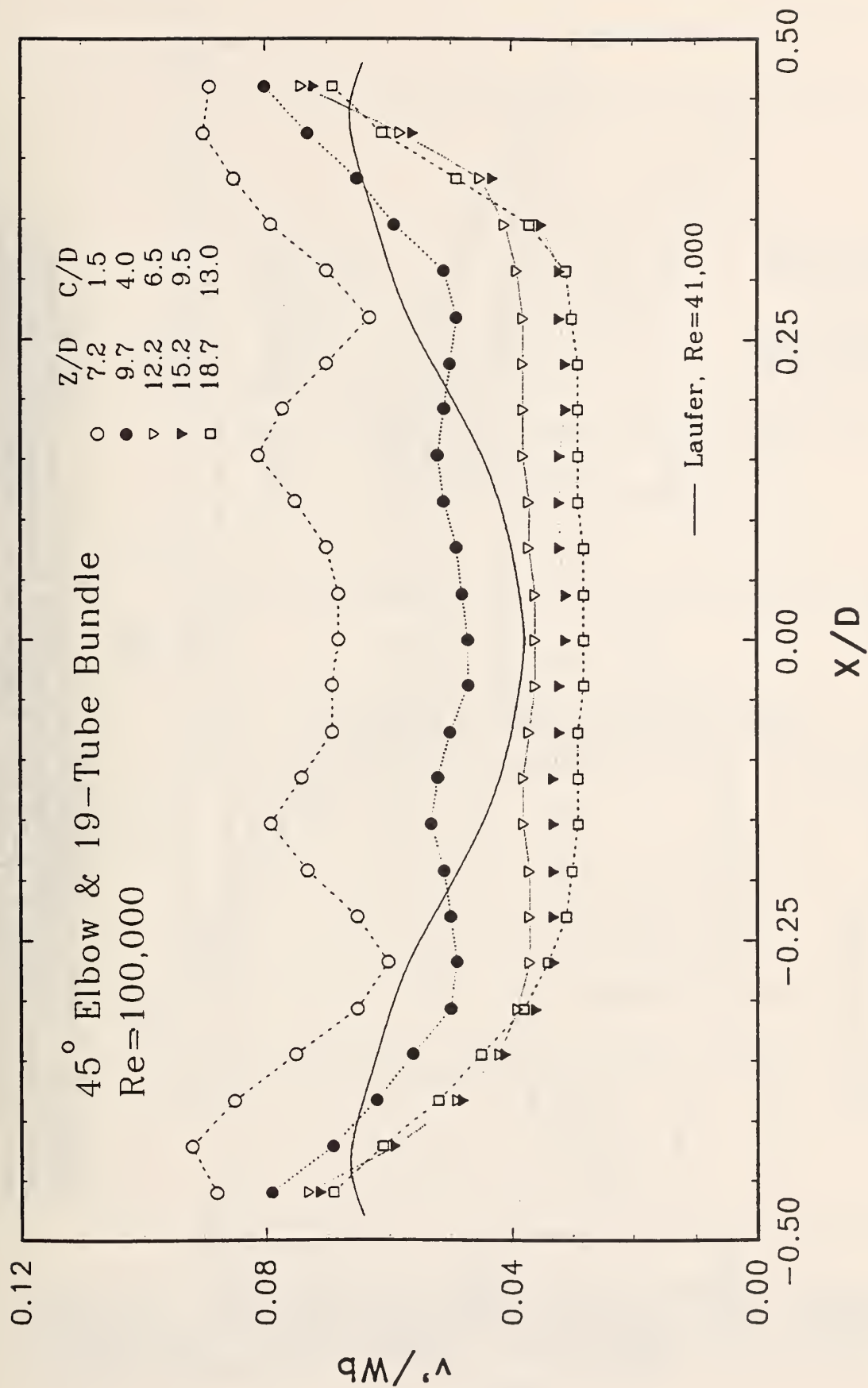


Figure 13 Profiles of the R.M.S. of the Axial Component of the Turbulent Velocity vs. Horizontal Radial Position at Different Downstream Locations from the 45° Elbow and the 19-Tube Bundle for  $Re = 100,000$ . The solid line shows the ideal profile of Laufer,  $Re=41,000$ .



**Figure 14** Profiles of the R.M.S. of the Axial Component of the Turbulent Velocity vs. Vertical Radial Position at Different Downstream Locations from the  $45^\circ$  Elbow and the 19-Tube Tube Bundle for  $Re = 100,000$ . The solid line shows the ideal profile of Laufer,  $Re=41,000$ .



**Figure 15** Profiles of the R.M.S. of the Vertical Component of the Turbulent Velocity vs. Horizontal Radial Position at Different Downstream Locations from the 45° Elbow and the 19-Tube Bundle for Re = 100000. The solid line shows the ideal profile of Laufer, Re=41000.



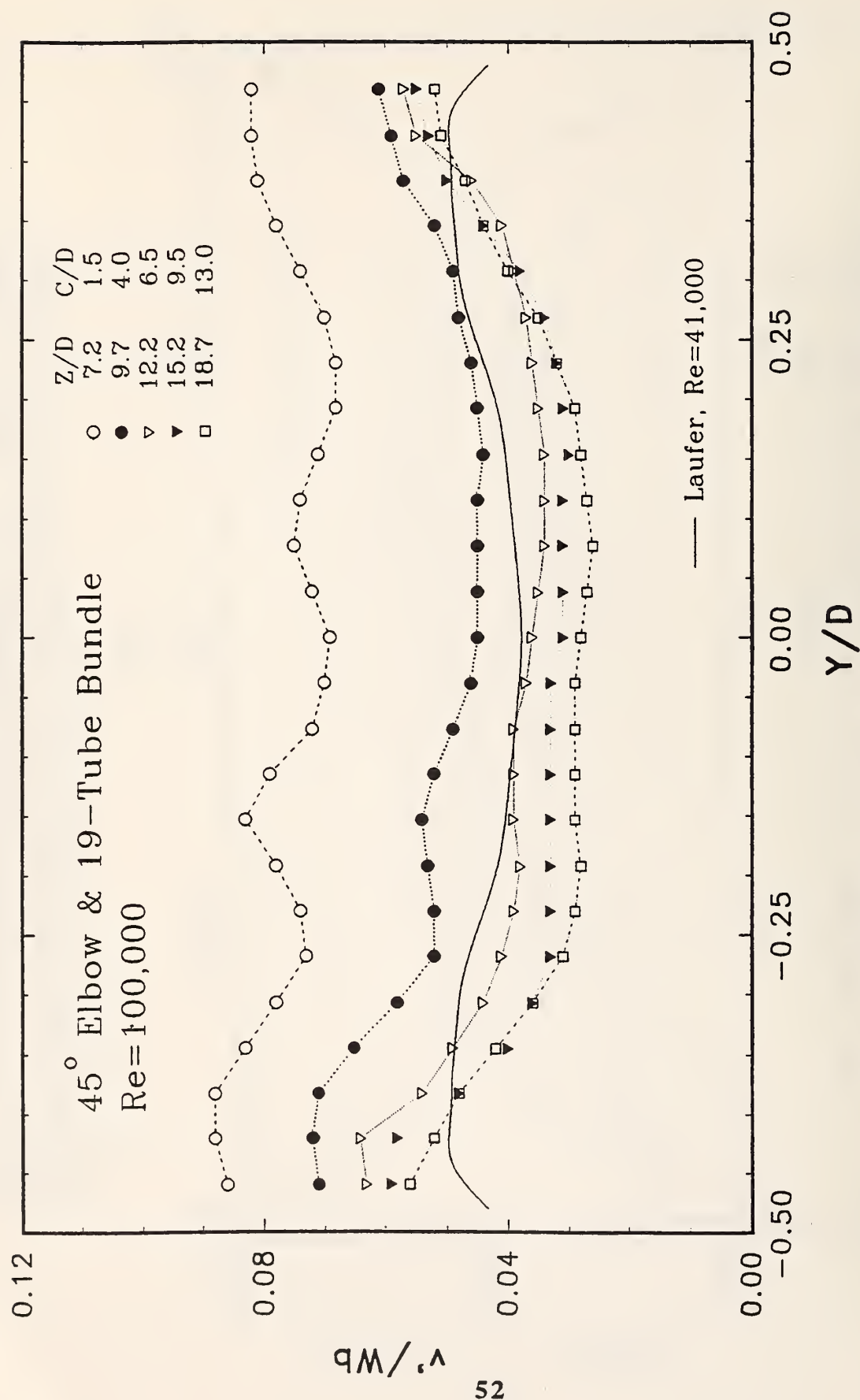
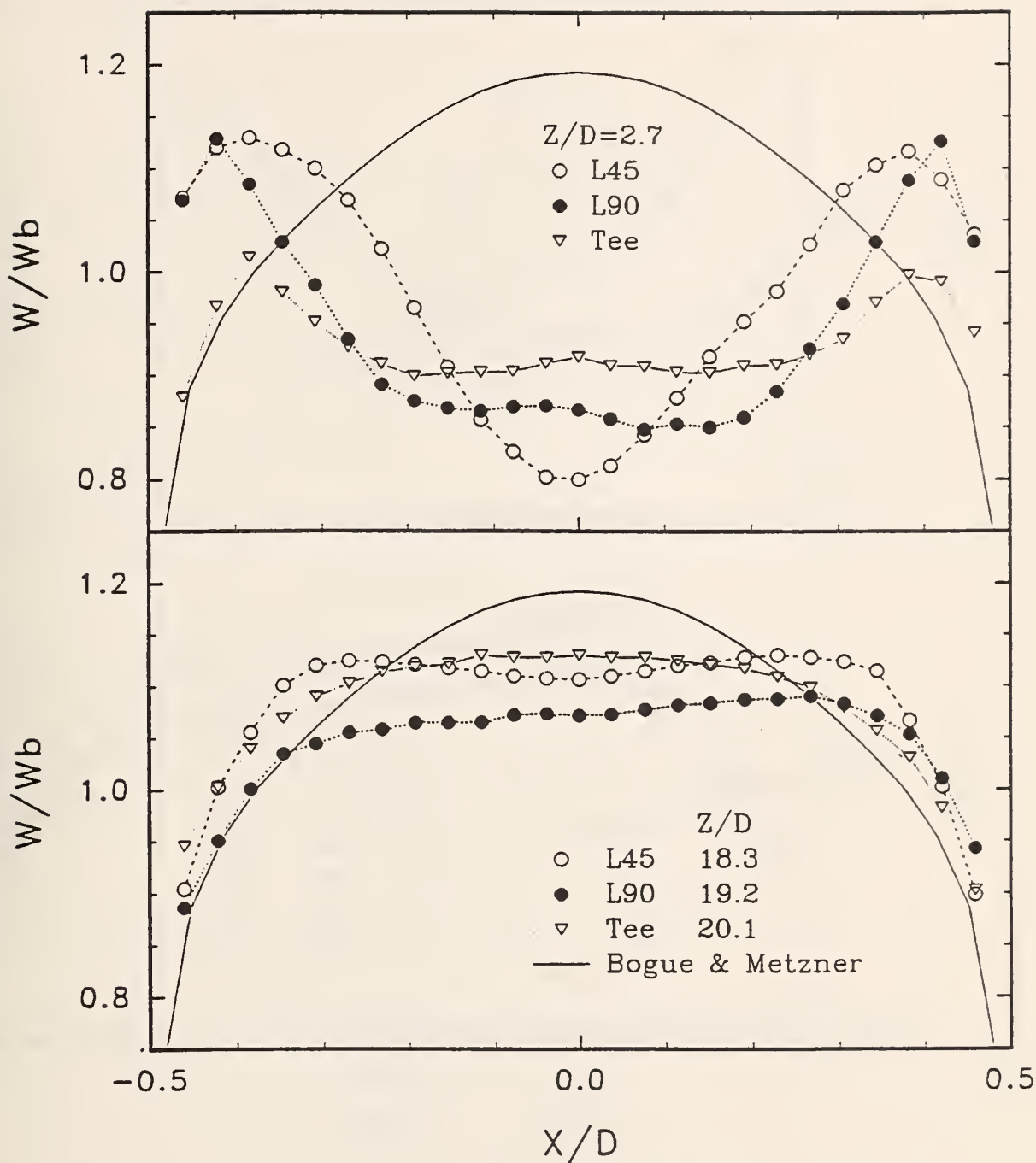
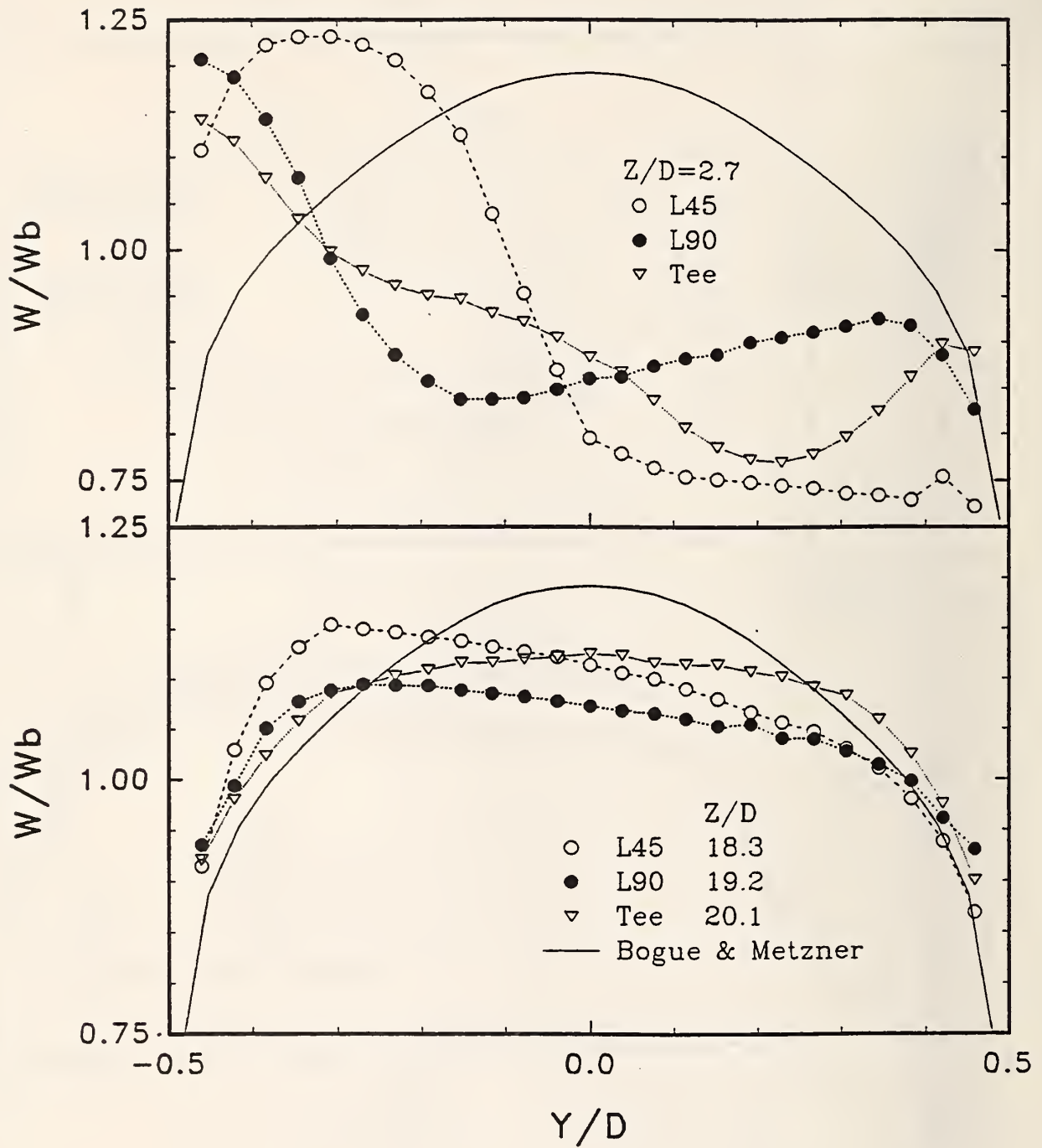


Figure 16 Profiles of the R.M.S. of the Vertical Component of the Turbulent Velocity vs. Vertical Radial Position at Different Downstream Locations from the  $45^\circ$  Elbow and the 19-Tube Bundle for  $Re = 100000$ . The solid line shows the ideal profile of Laufer,  $Re=41000$ .



**Figure 17** Comparison of the Axial Velocity Profile vs. Horizontal Radial Position at Two Axial Locations Downstream from Different Piping Configurations for  $Re = 100000$ . The solid lines show the ideal profile of Bogue & Metzner.



**Figure 18** Comparison of the Axial Velocity Profile vs. Vertical Radial Position at Two Axial Locations Downstream from Different Piping Configurations for  $Re = 100000$ . The solid lines show the ideal profile of Bogue & Metzner.



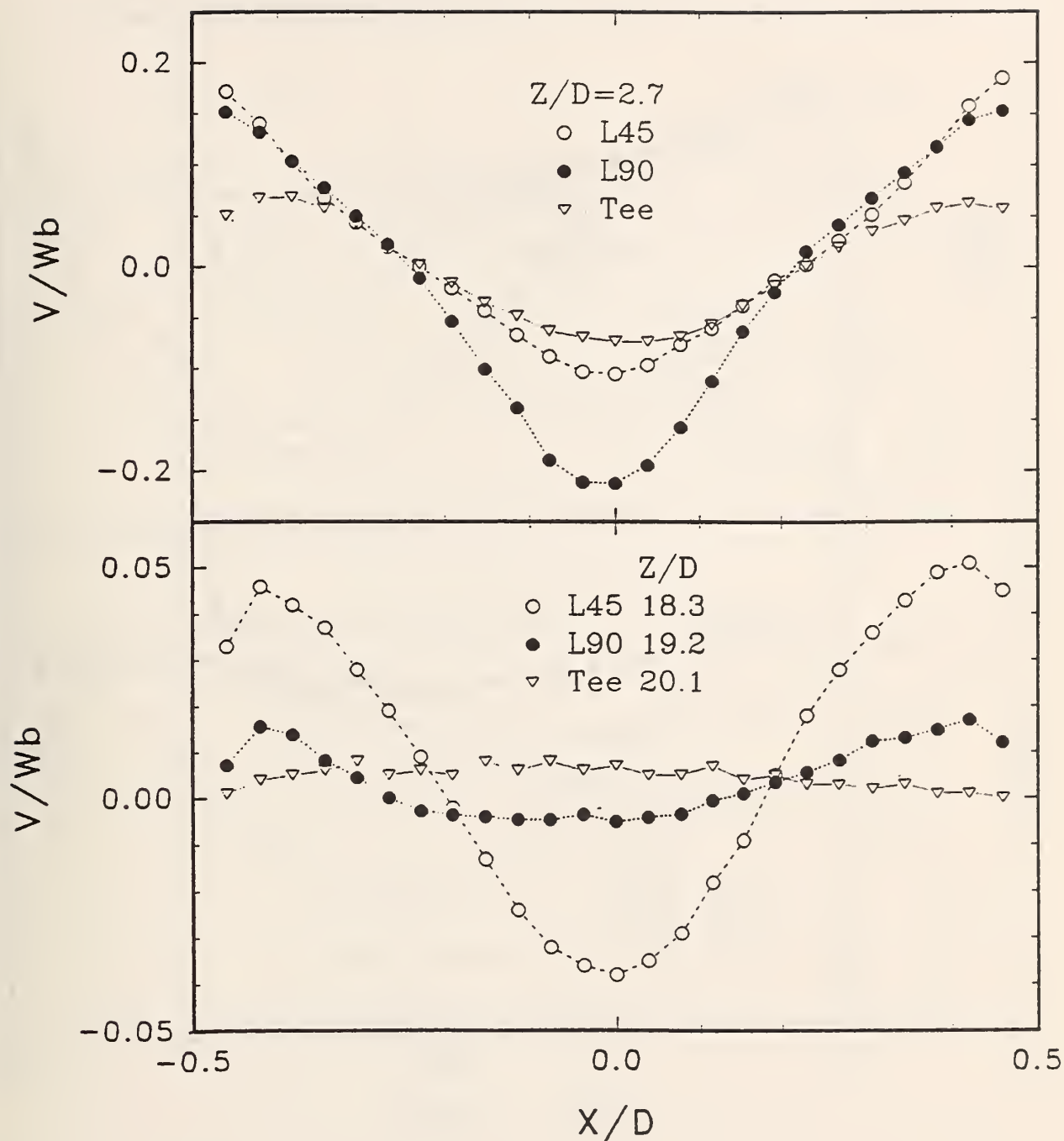


**Figure 19** Comparison of the Vertical Velocity Profile vs. Horizontal Radial Position at Two Axial Locations Downstream from Different Piping Configurations for  $Re = 100000$ .

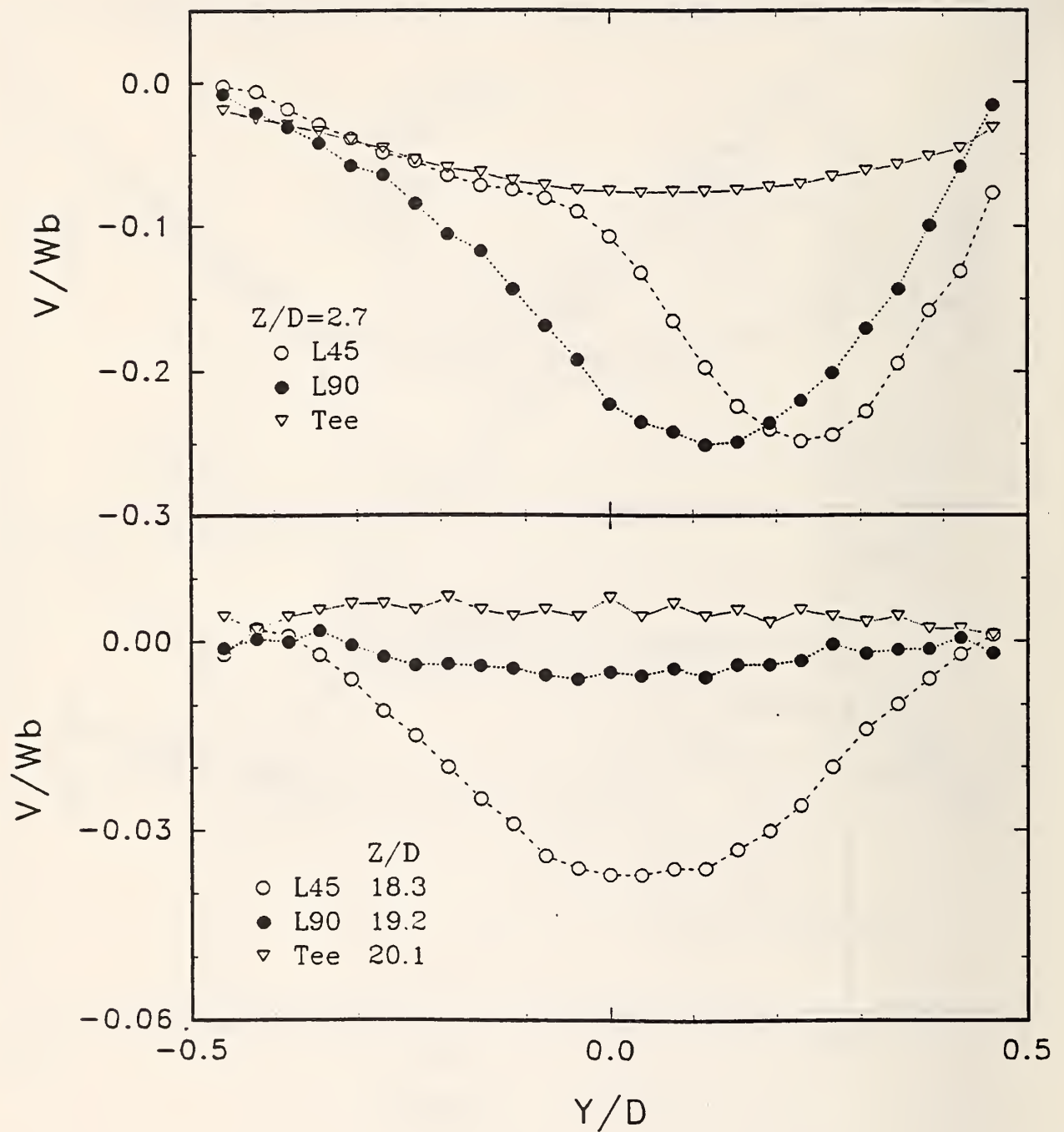


**Figure 20** Comparison of the Vertical Velocity Profile vs. Vertical Radial Position at Two Axial Locations Downstream from Different Piping Configurations for  $Re = 100000$ .

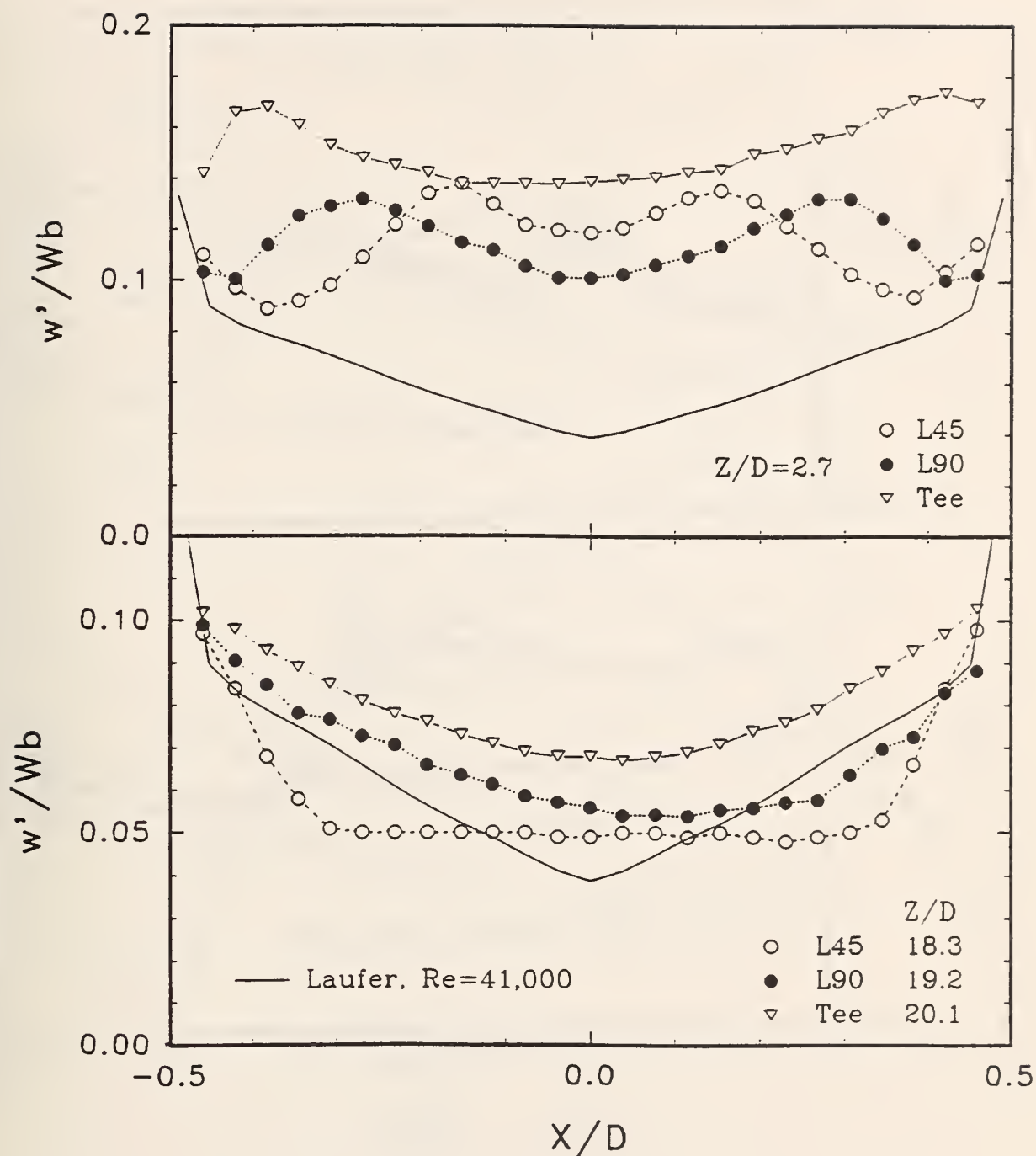


**Figure 21** Comparison of the Profiles of the R.M.S. of the Axial Component of the Turbulent Velocity vs. Horizontal Radial Position at Two Axial Locations Downstream from Different Piping Configurations for  $Re = 100000$ . The solid lines show the ideal profile of Laufer,  $Re = 41000$ .



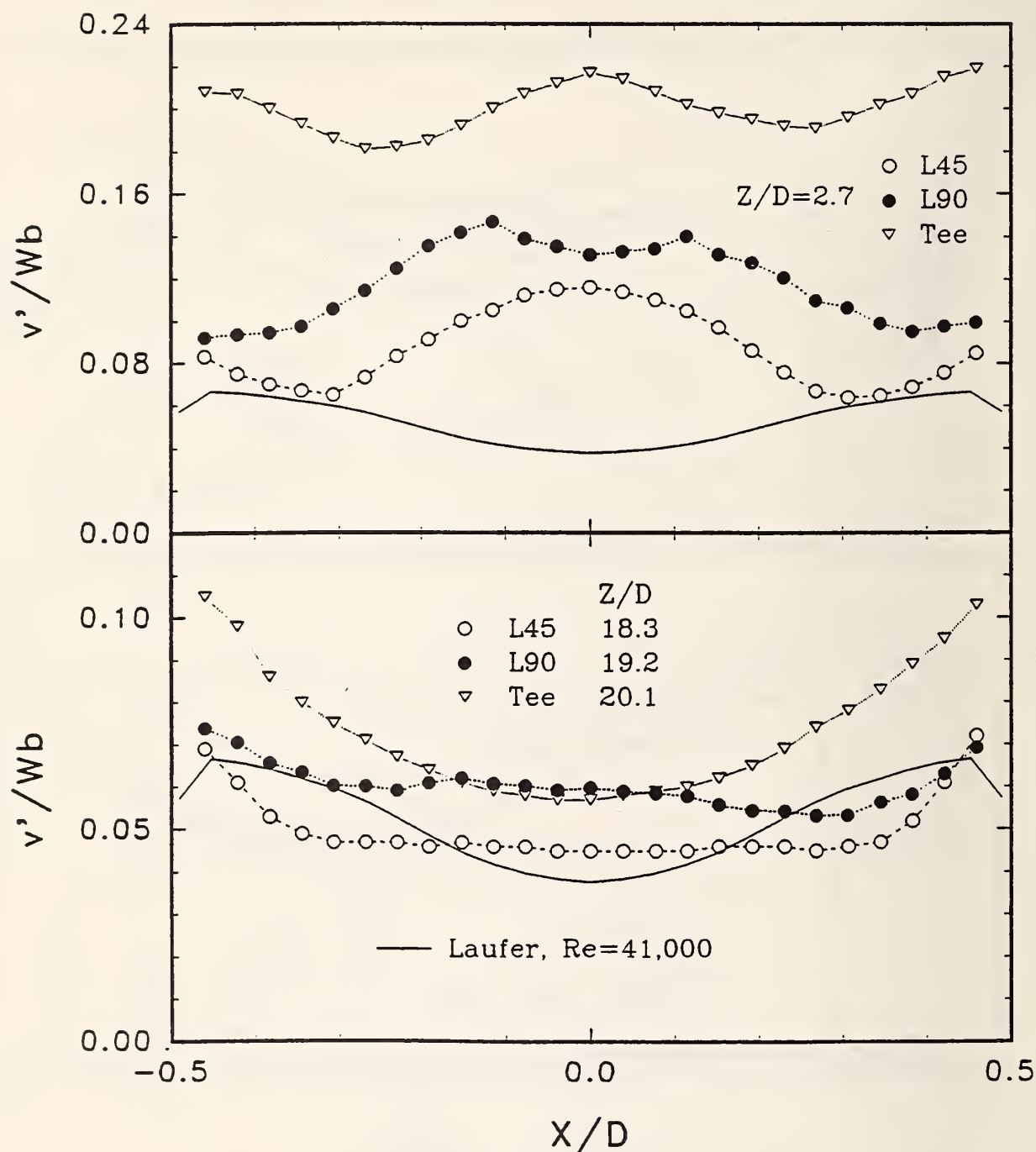


**Figure 22** Comparison of the Profiles of the R.M.S. of the Vertical Component of the Turbulent Velocity vs. Horizontal Radial Position at Two Axial Locations Downstream from Different Piping Configurations for  $Re = 100,000$ . The solid lines show the ideal profile of Laufer,  $Re = 41,000$ .

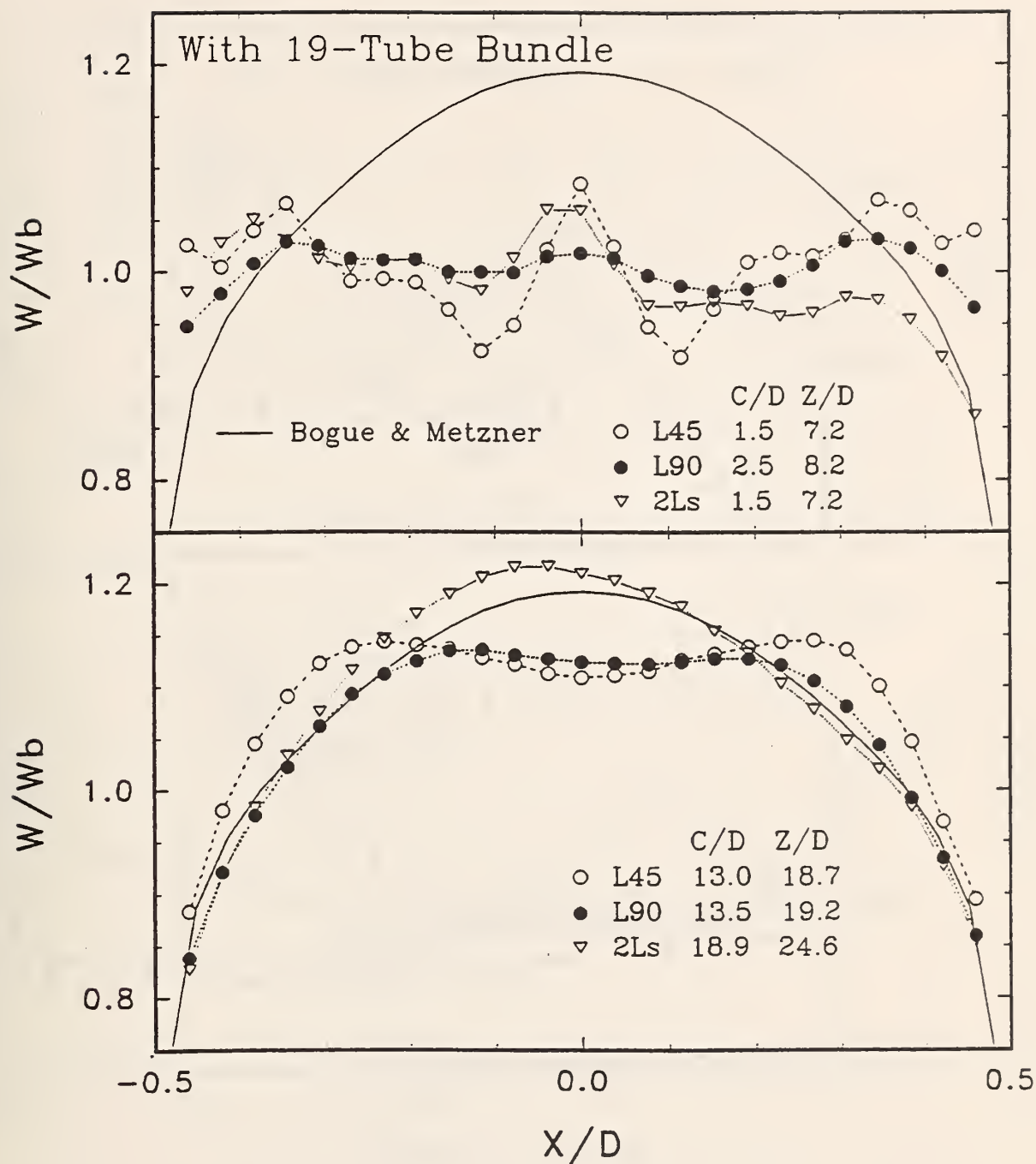


**Figure 23** Comparison of the Axial Velocity Profile vs. Horizontal Radial Position at Two Axial Locations Downstream of the 19-Tube Tube Bundles in Different Piping Configurations for  $Re = 100000$ . The solid lines show the ideal profile of Bogue & Metzner.

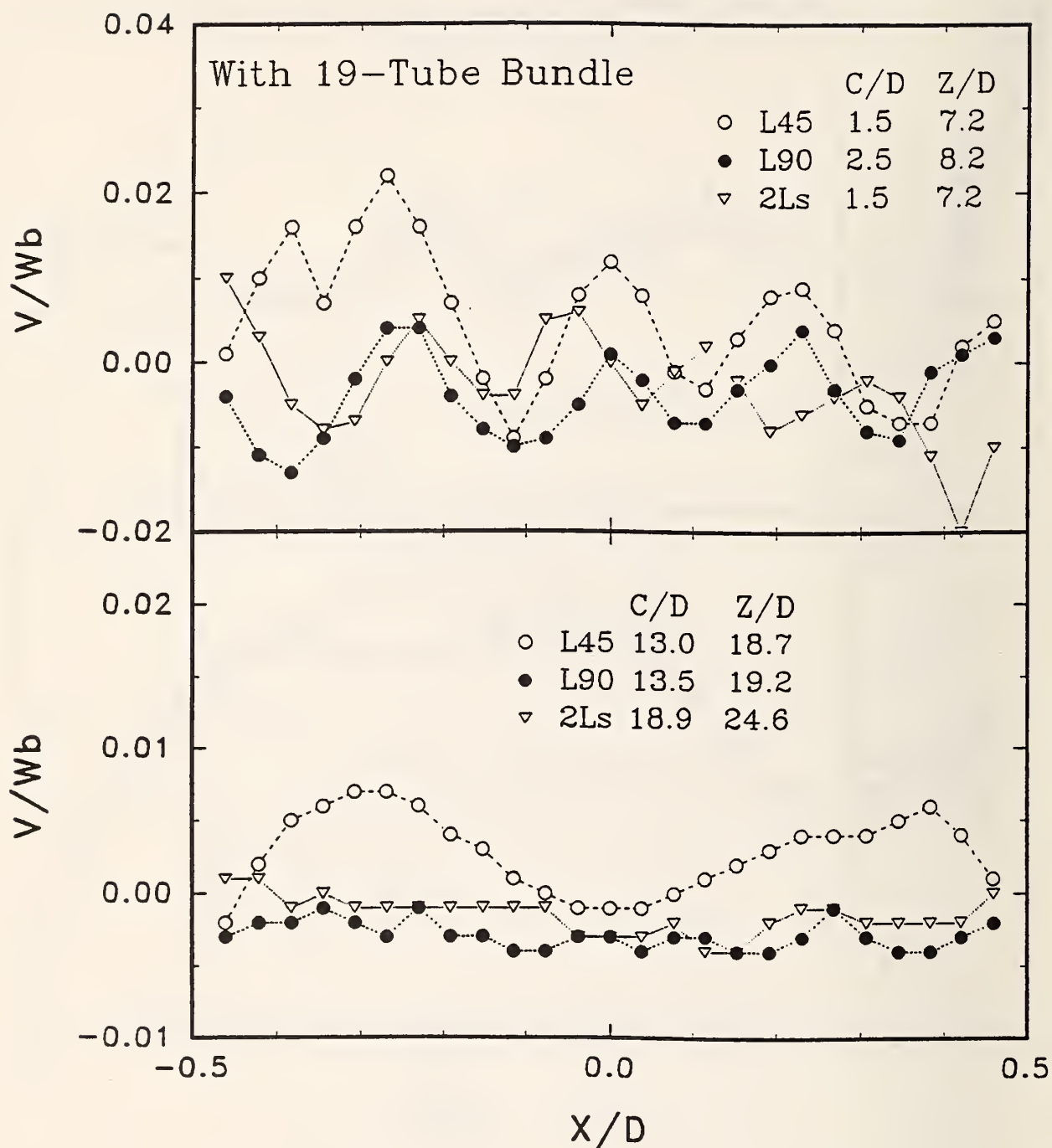


**Figure 24** Comparison of the Vertical Velocity Profile vs. Horizontal Radial Position at Two Axial Locations Downstream of the 19-Tube Tube Bundle in Different Piping Configurations for  $Re = 100000$ .



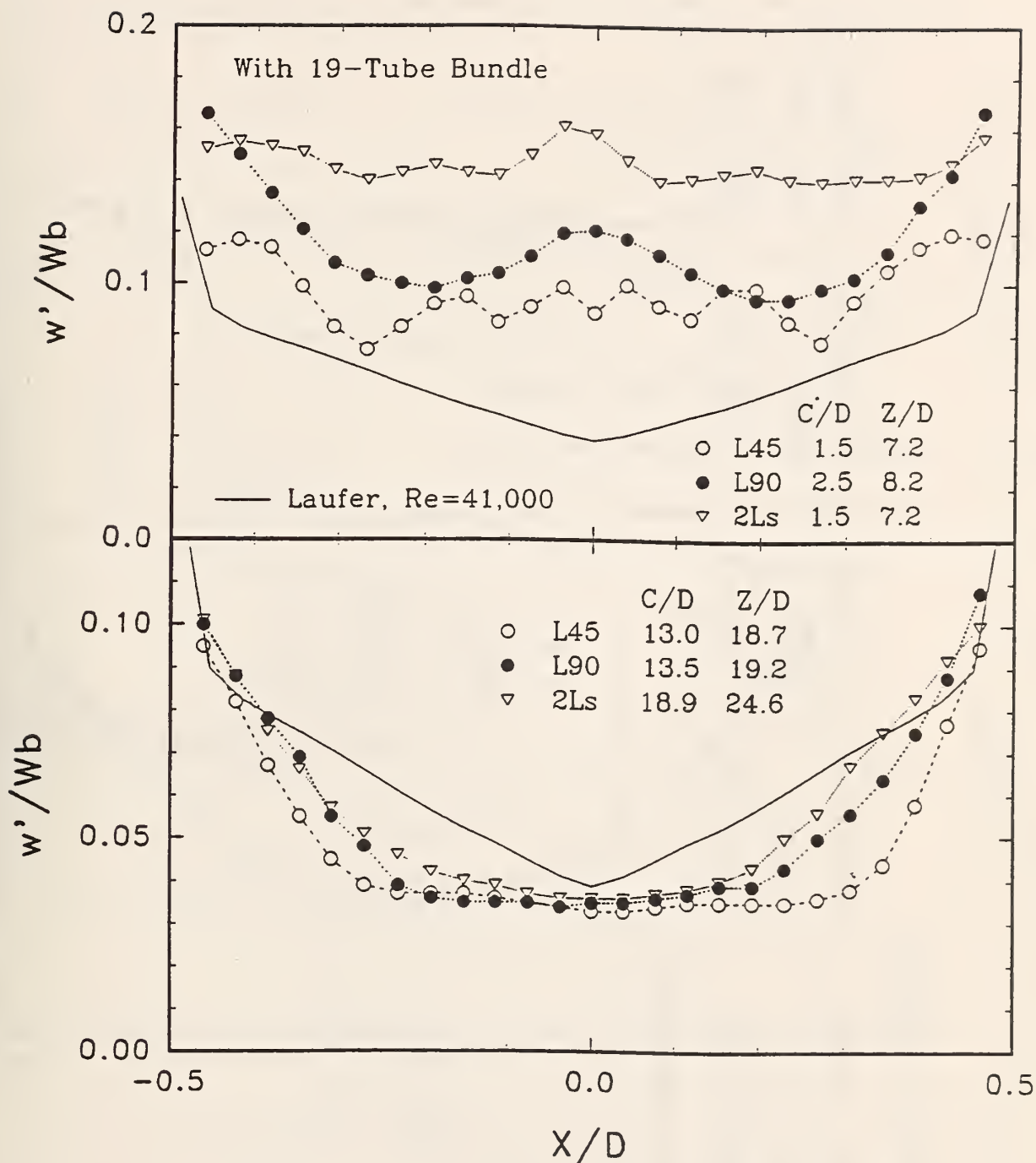


**Figure 25** Comparison of the Profiles of the R.M.S. of the Axial Component of the Turbulent Velocity vs. Horizontal Radial Position at Two Axial Locations Downstream of the 19-Tube Tube Bundle in Different Piping Configurations for  $Re = 100000$ . The solid lines show the ideal profile of Laufer,  $Re=41000$ .

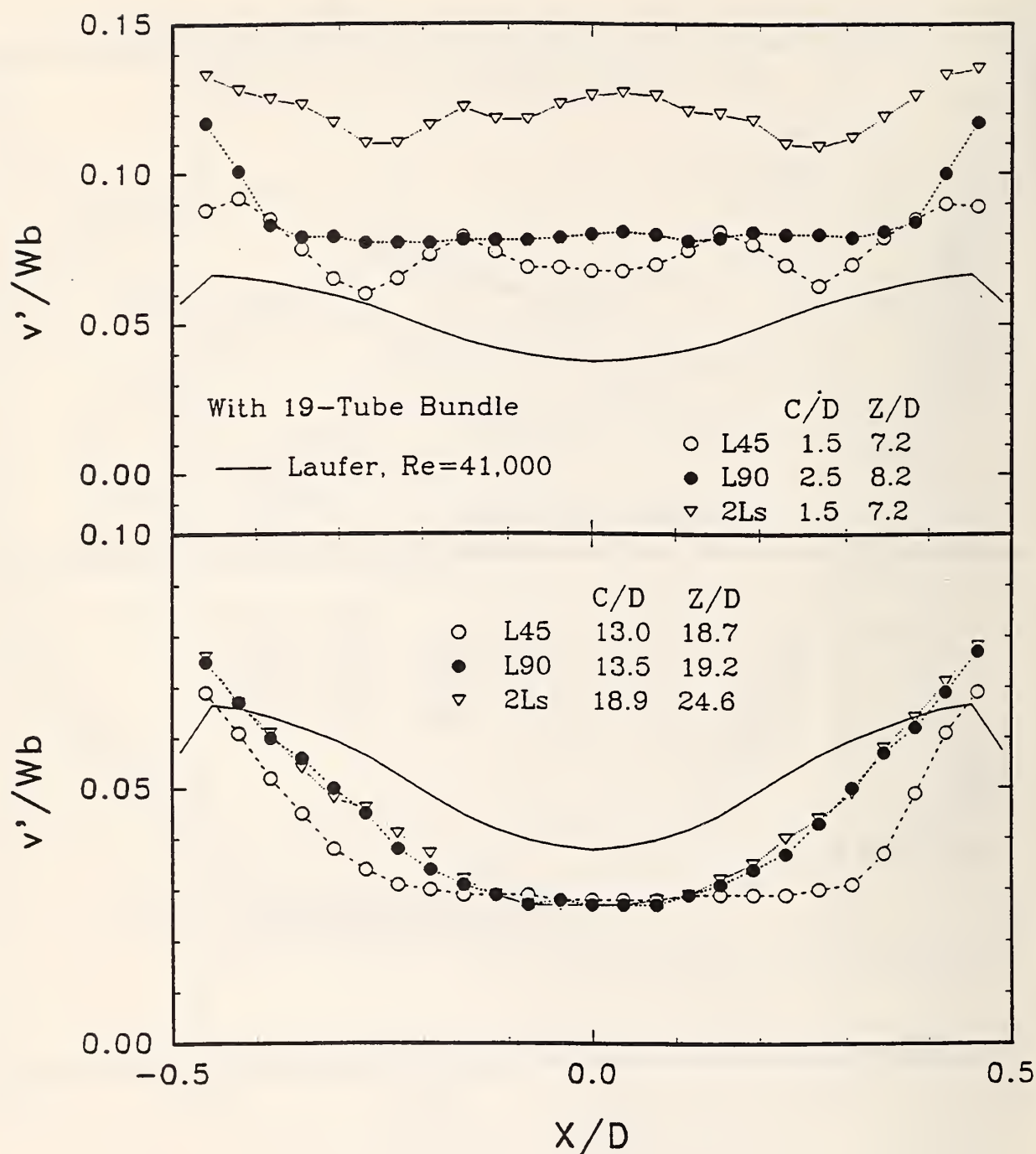
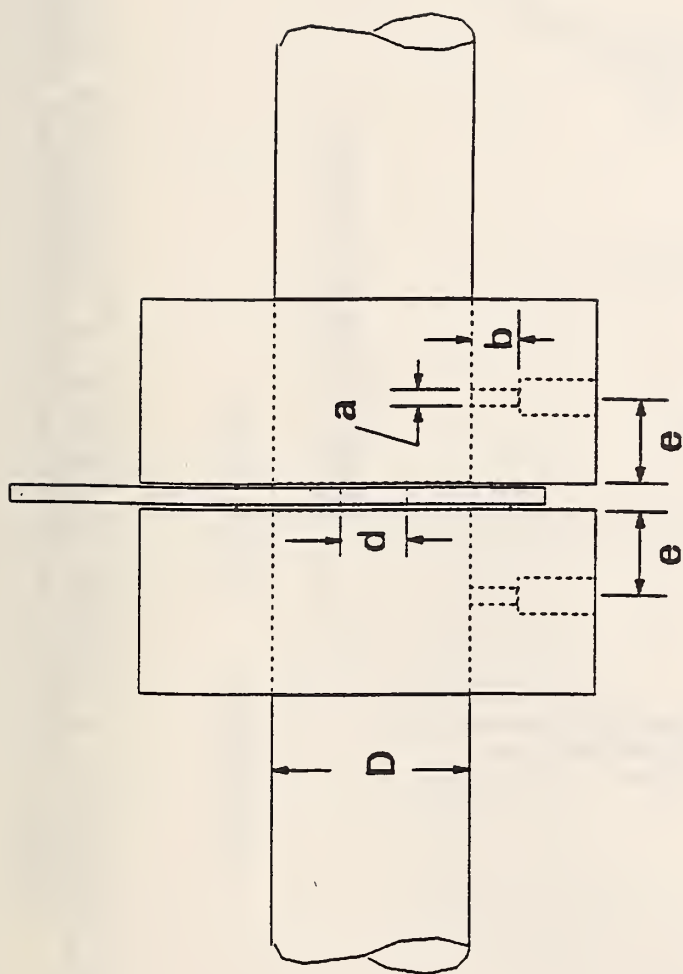


**Figure 26** Comparison of the Profiles of the R.M.S. of the Vertical Component of the Turbulent Velocity vs. Horizontal Radial Position at Two Axial Locations Downstream of the 19-Tube Tube Bundle in Different Piping Configurations for Re = 100000. The solid lines show the ideal profile of Laufer, Re=41000.



Orifice Plate Holder	D	e	a	b
4" Meter, Conv.	10.23(4.025)	2.54(1.0)	1.26(0.495)	4.76(1.875)
2" Meter, Conv.	5.26(2.07)	2.54(1.0)	0.95(0.375)	2.86(1.125)
2" Meter, Scaled	5.26(2.07)	1.27(0.5)	0.64(0.25)	2.38(0.9375)
Dimension in cm(inch)				

**Figure 27** Sketch of Pressure Ports and the Orifice Plate Holder



# Two Port Orifice Plate Holder

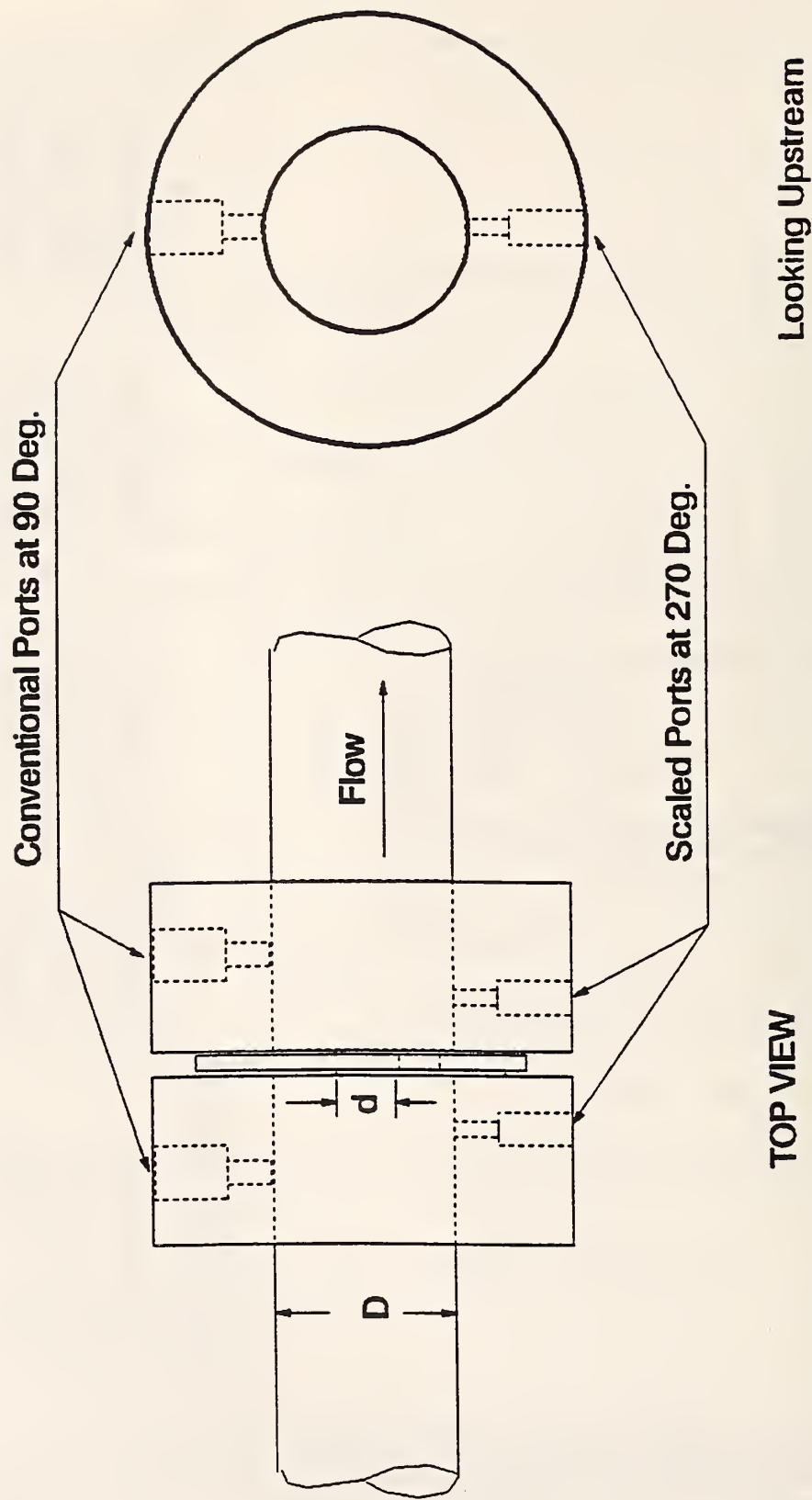
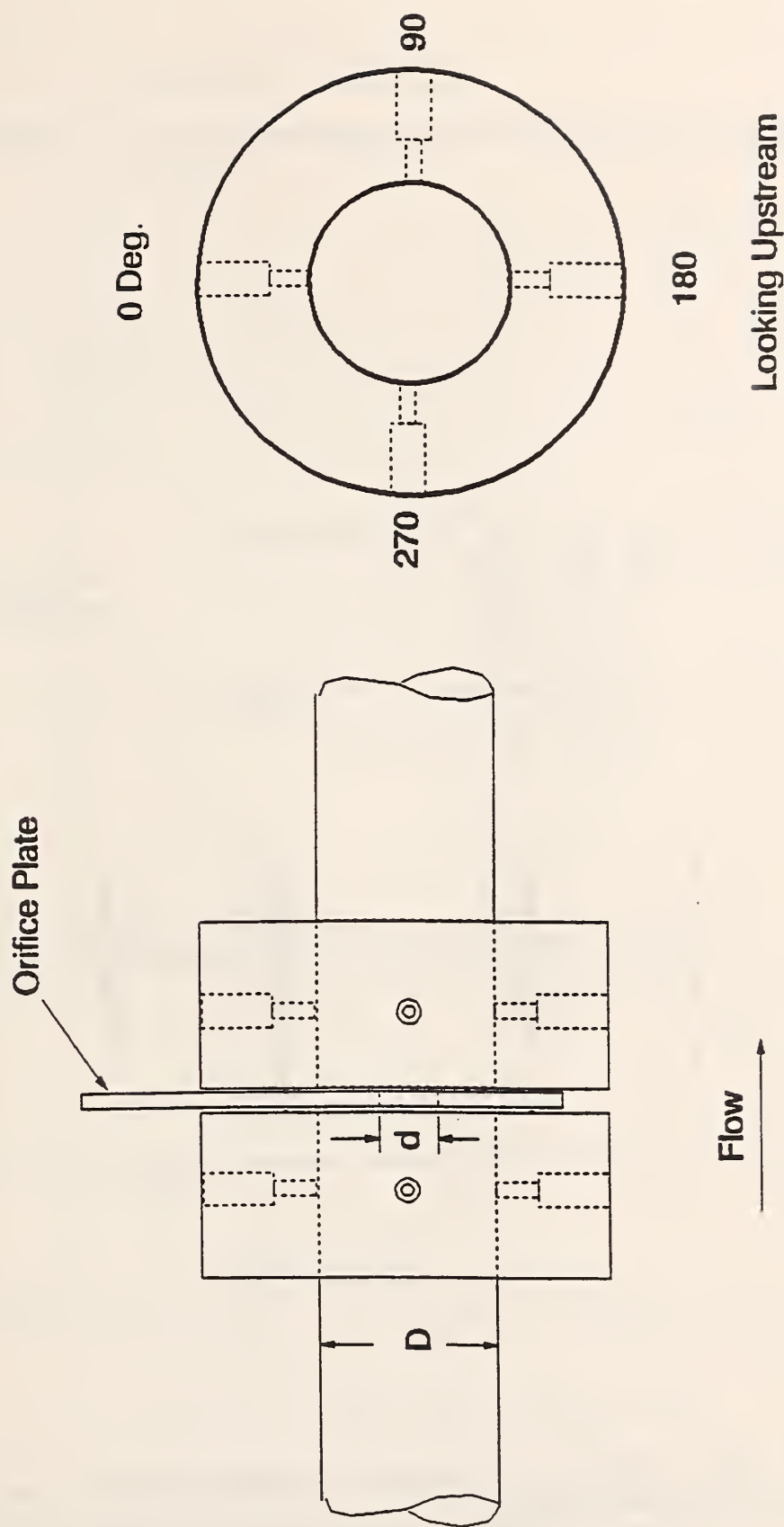
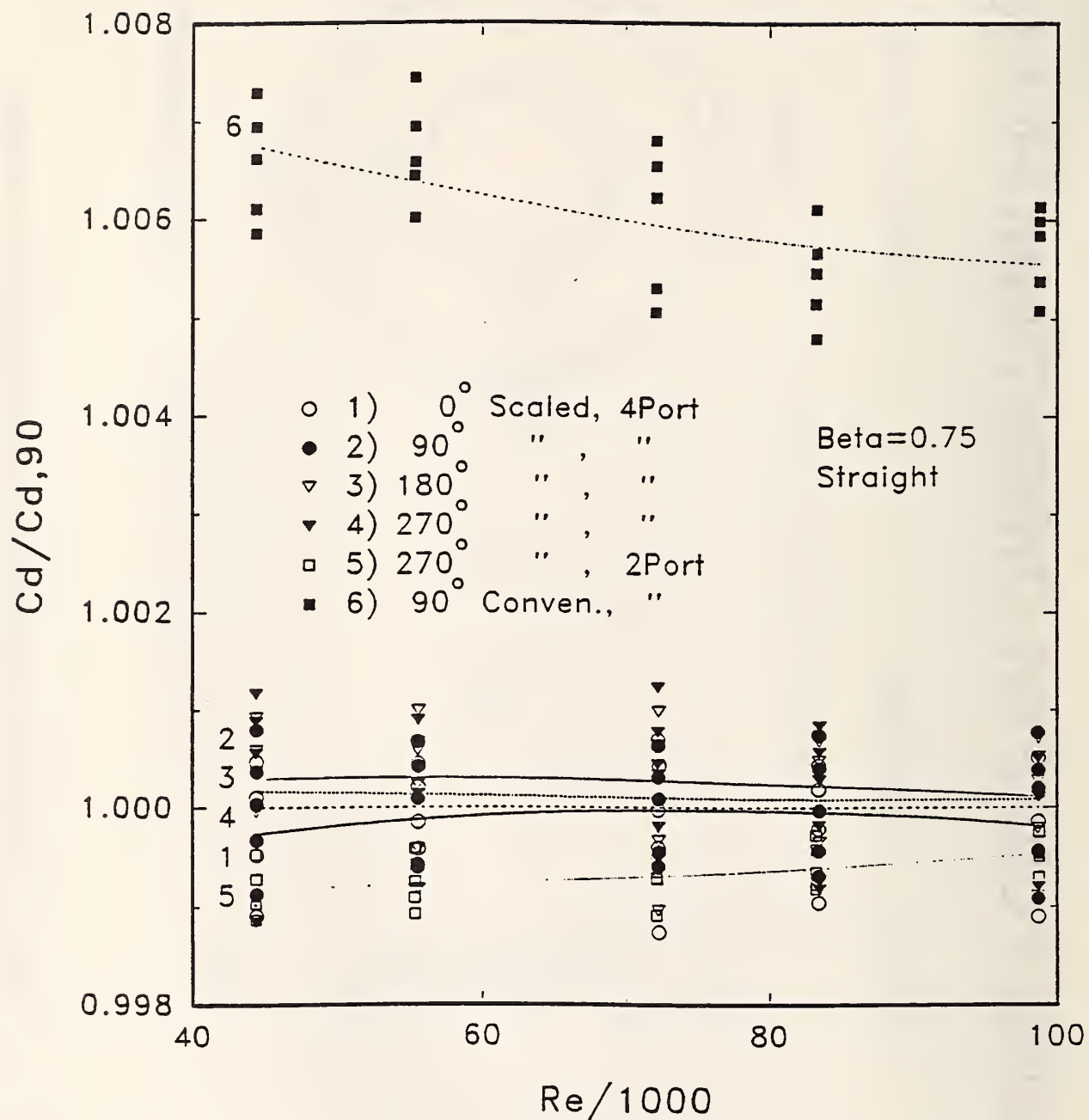


Figure 28 Sketch of the Two-Ports Orifice Plate Holder

# Scaled Four Port Orifice Plate Holder



**Figure 29** Sketch of the Scaled Four Port Orifice Plate Holder



**Figure 30** The Reference Discharge Coefficients for the Scaled and Conventional Ports for Beta=0.75



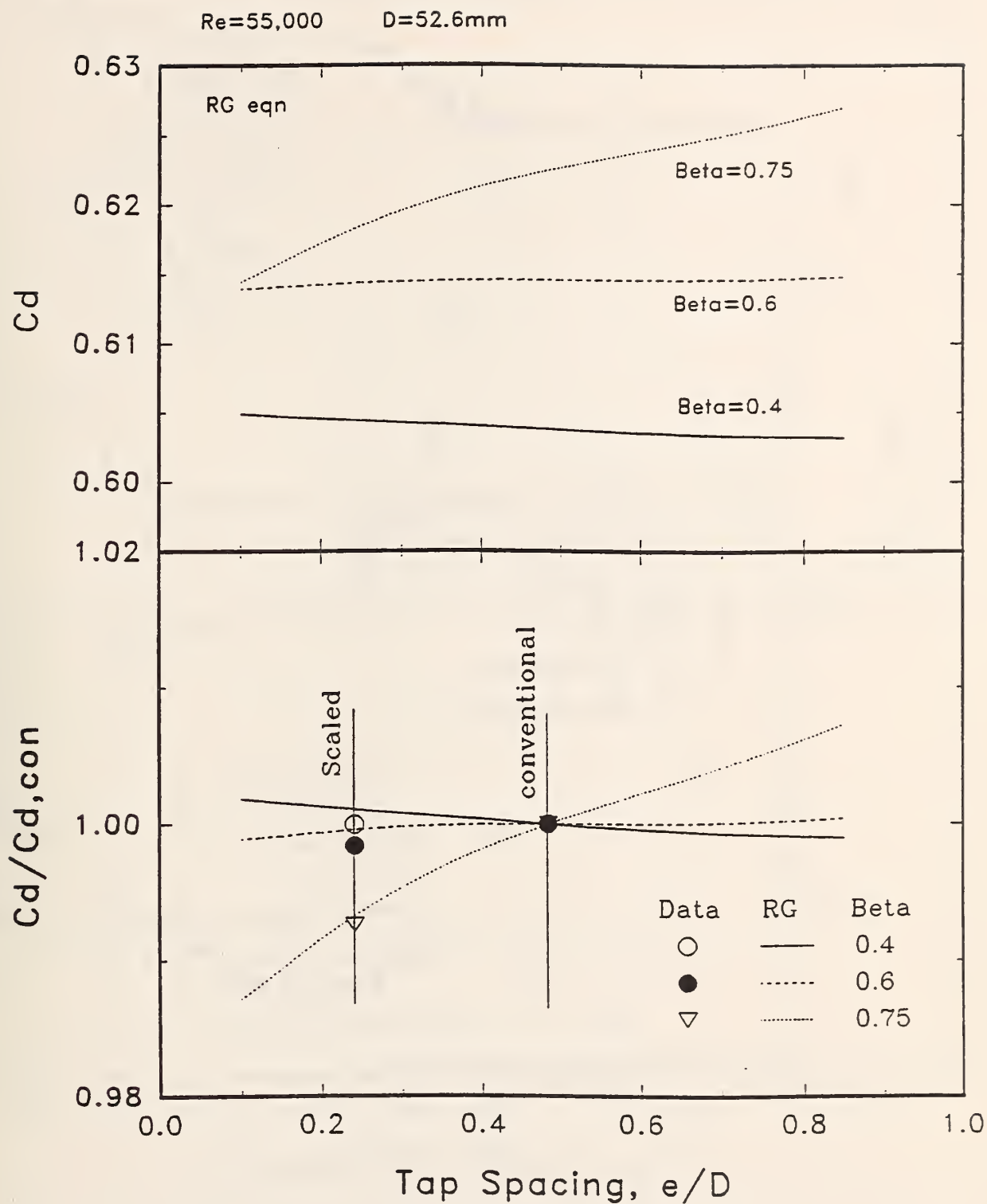


**Figure 31** Variation of the Reference Discharge Coefficients as Functions of the Tap Separation for  $Re=55000$

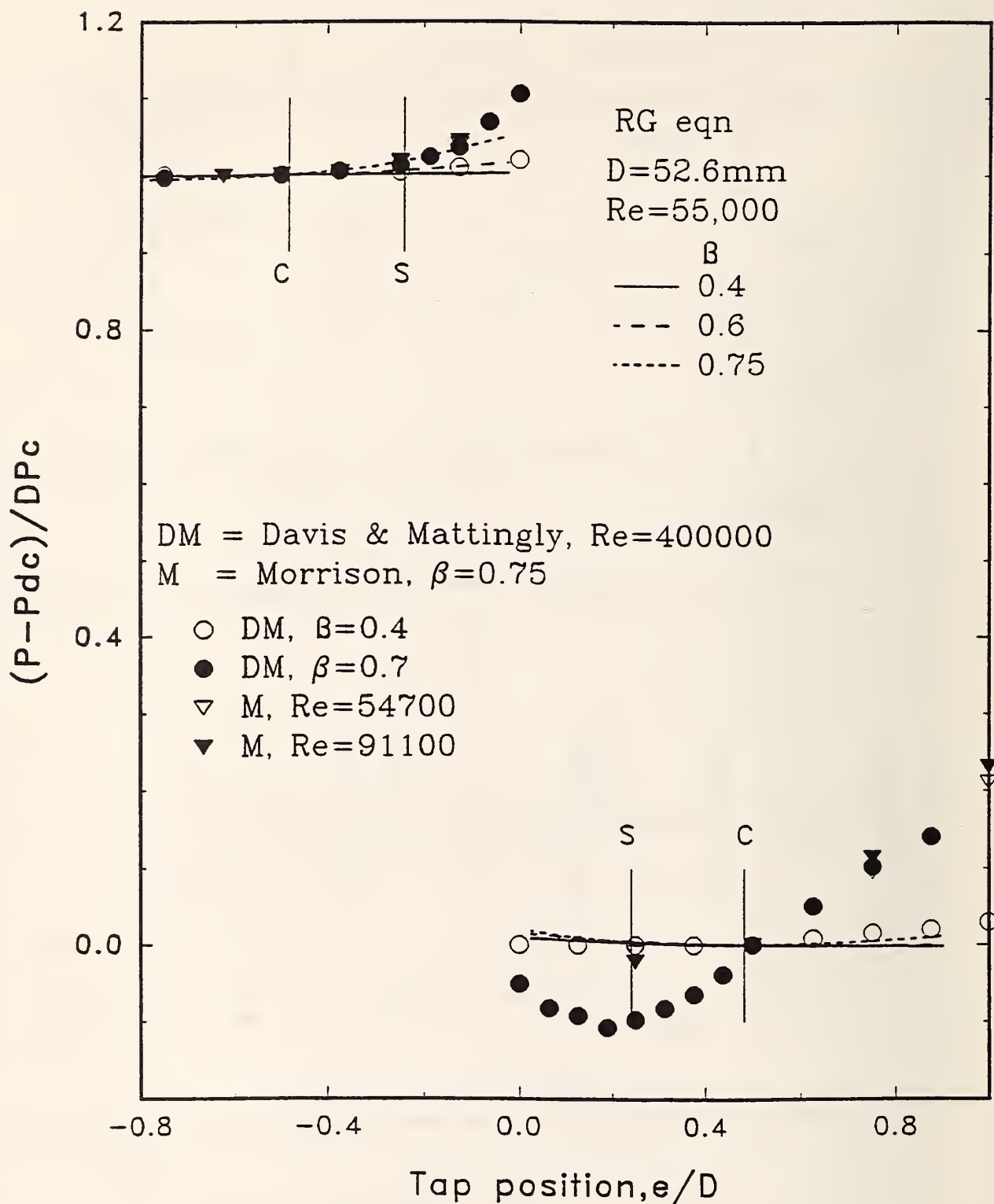


**Figure 32(a)** Wall Pressure Distributions near an Orifice Plate for Beta=0.4, 0.6, and 0.75

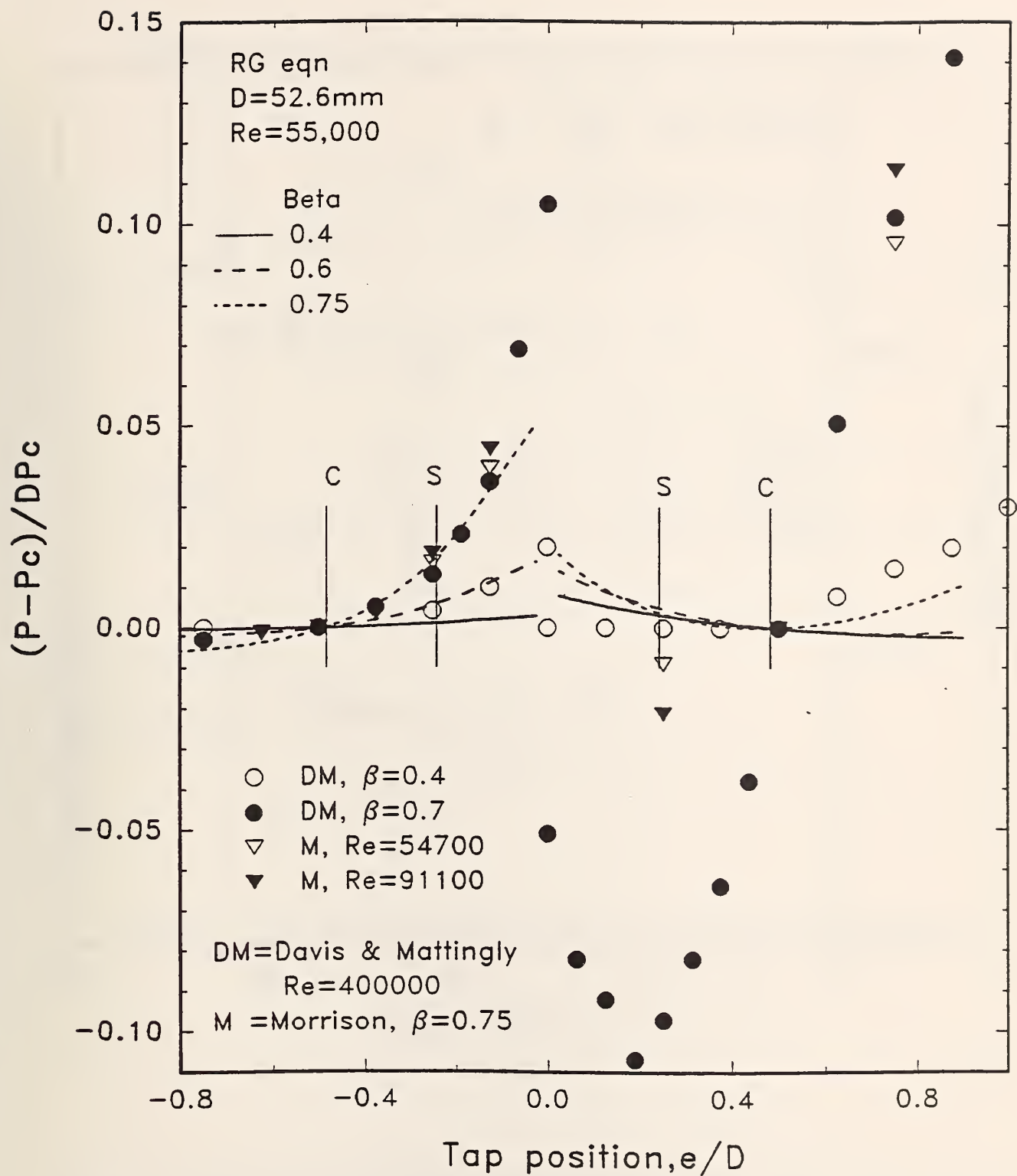


**Figure 32(b)** Wall Pressure Distributions near an Orifice Plate for Beta=0.4, 0.6, and 0.75

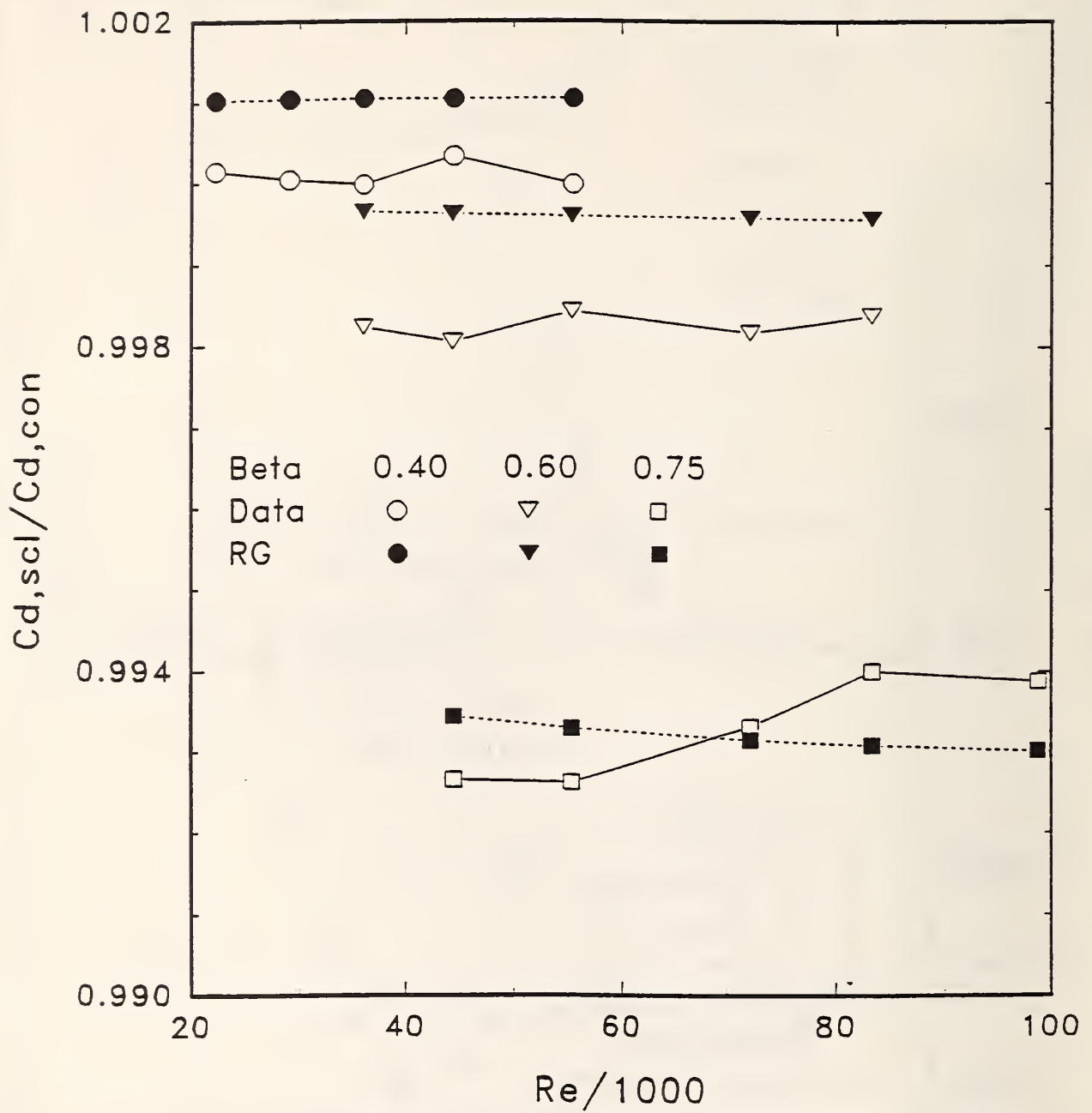


**Figure 33** Ratio of the Reference Discharge Coefficients between the Scaled Ports and the Conventional Ports as Functions of Reynolds Number.



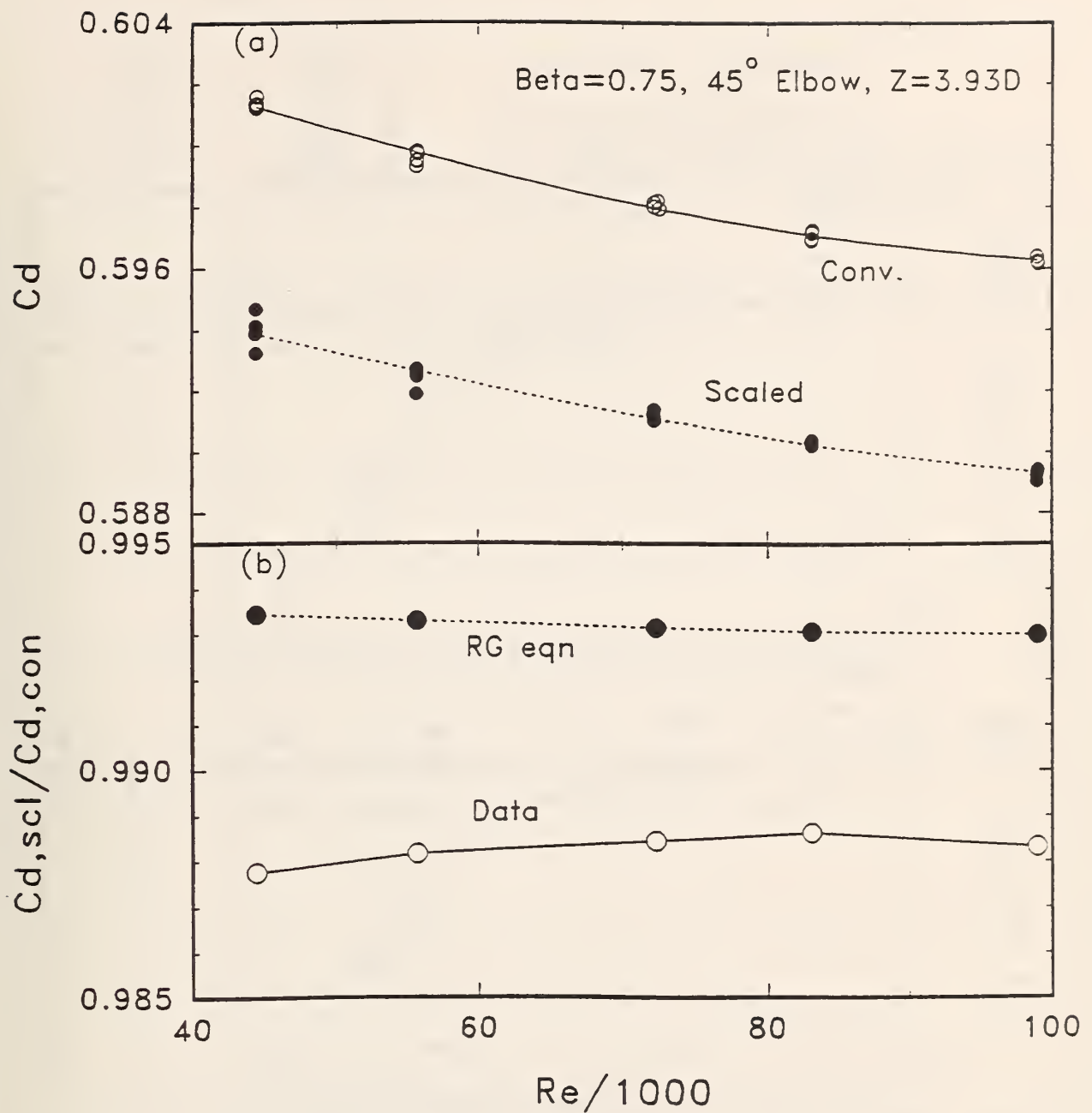


**Figure 34** Discharge Coefficients Obtained from the scaled and conventional ports as functions of Reynolds Number for a  $\beta=0.75$  Orifice Meter at a location of  $Z=3.93D$  Downstream of a  $45^\circ$  Elbow. (a) Discharge Coefficients, (b) Ratio of the Discharge Coefficients.

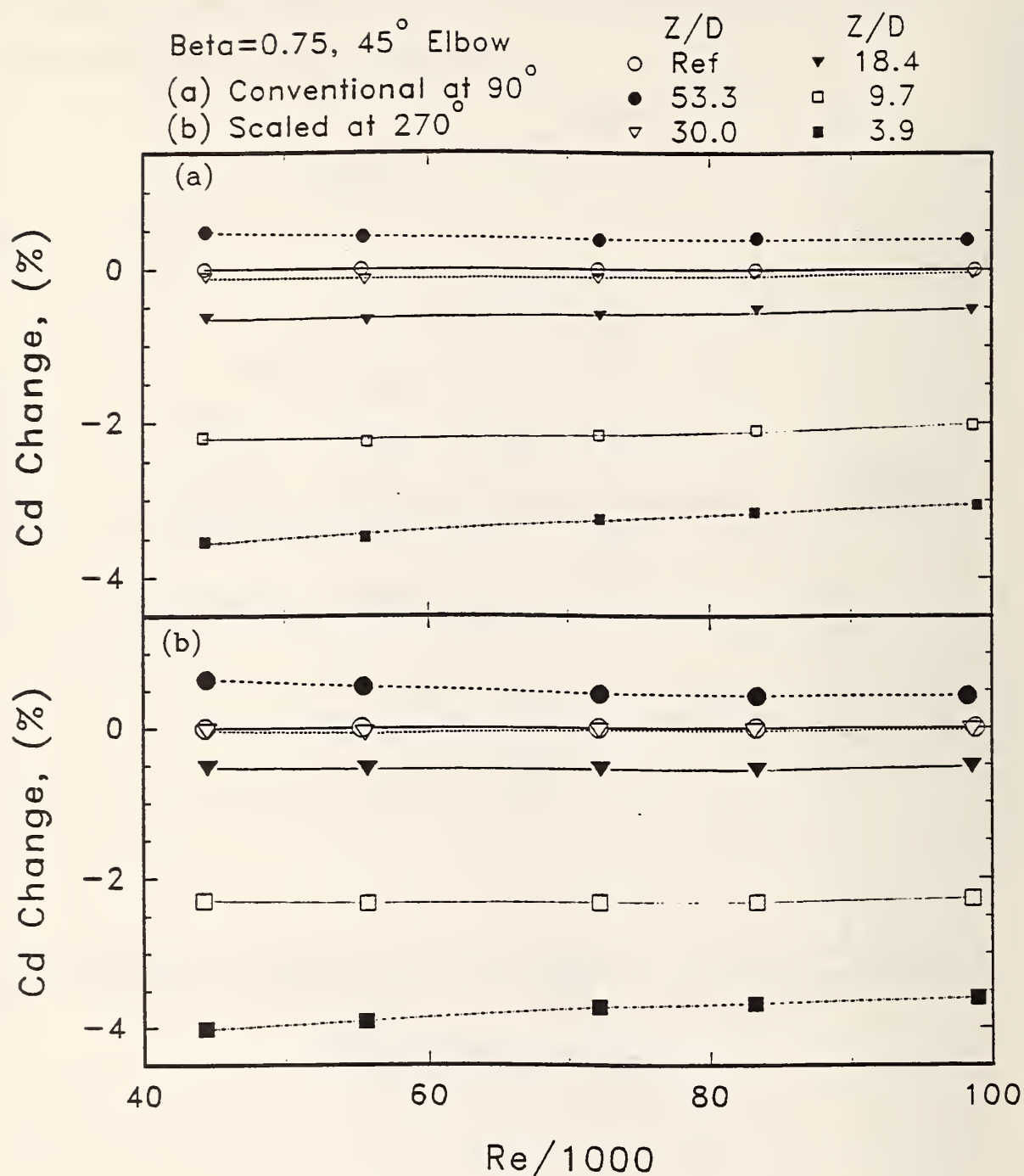


**Figure 35** Percentage Change in Discharge Coefficient for a Beta = 0.75 Orifice Meter Installed at Different Downstream Positions from a 45° Elbow. (a) Conventional Ports at 90° Position, (b) Scaled Ports at 270° Position.

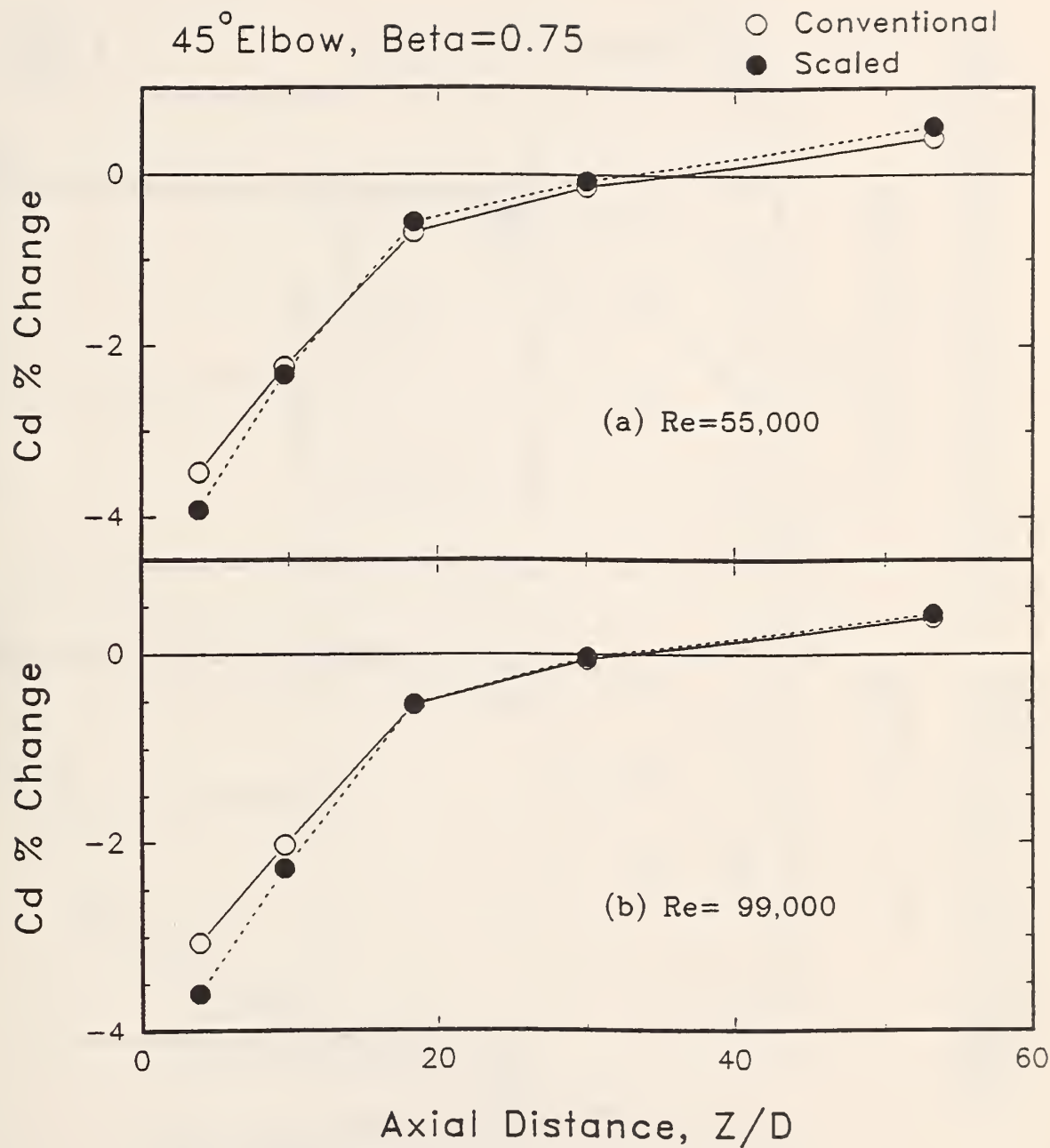


**Figure 36** Percentage Change in Discharge Coefficient for a Beta=0.75 Orifice Meter versus Location Downstream from a 45° Elbow for Re=55000 and 100000.

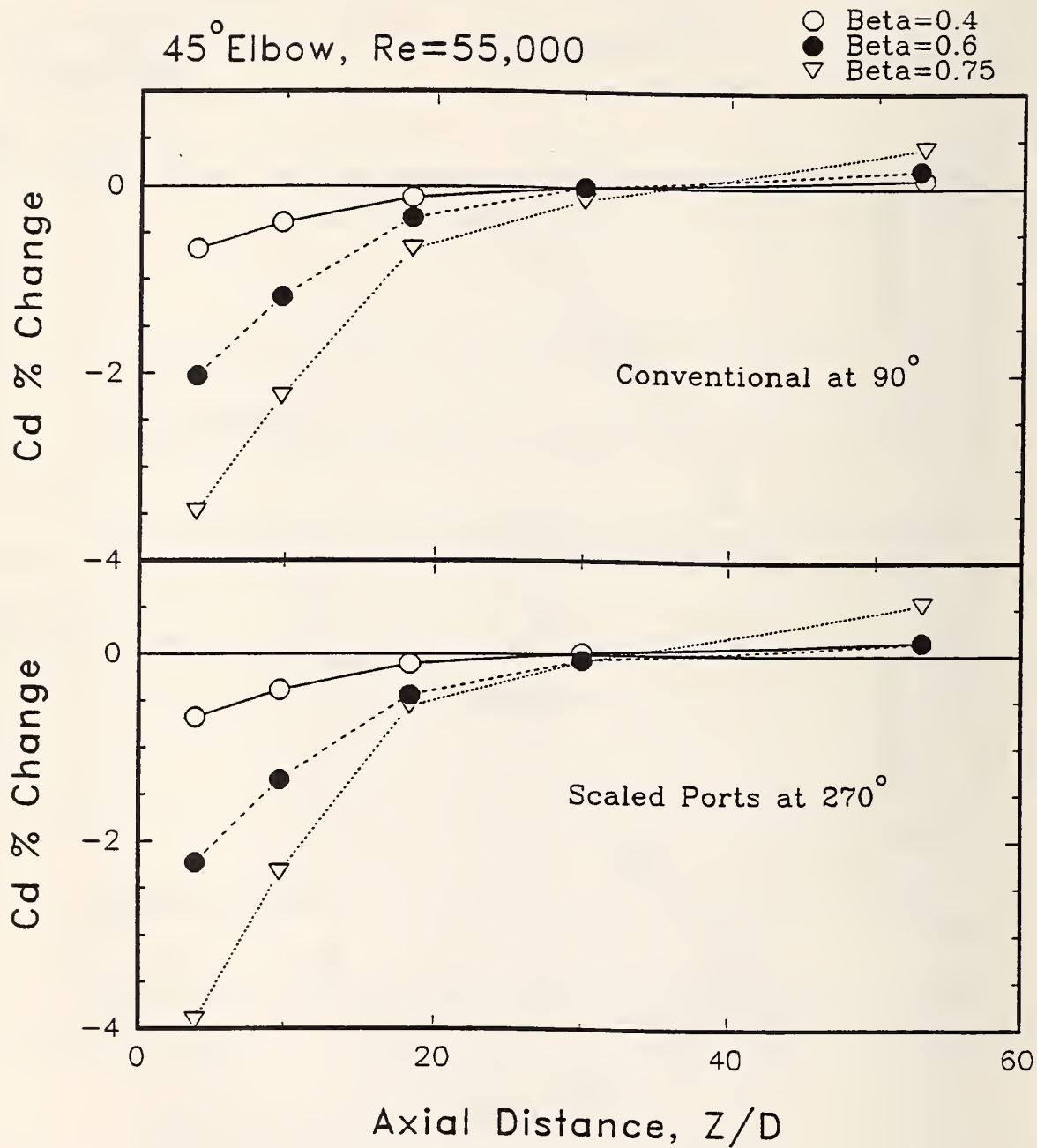


**Figure 37** Percentage Change in Discharge Coefficient for a Range of Orifice Meters at Different Downstream Installation Positions from a  $45^\circ$  Elbow for  $Re = 55000$ .



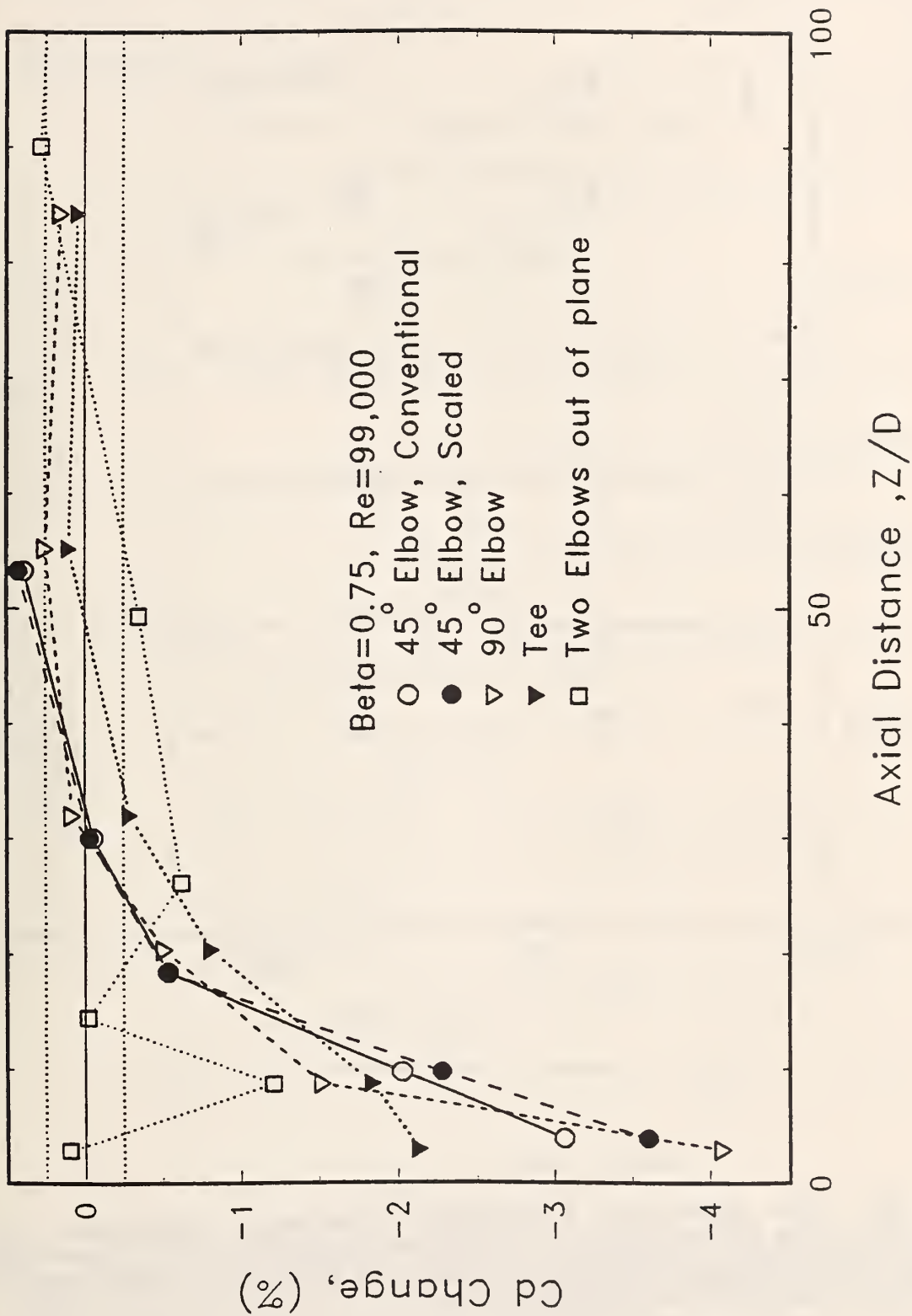


**Figure 38** Comparison of the Percentage Change in Discharge Coefficient for a Beta = 0.75 Orifice Meter Installed Downstream of Different Elbow Configurations for Re=100000.

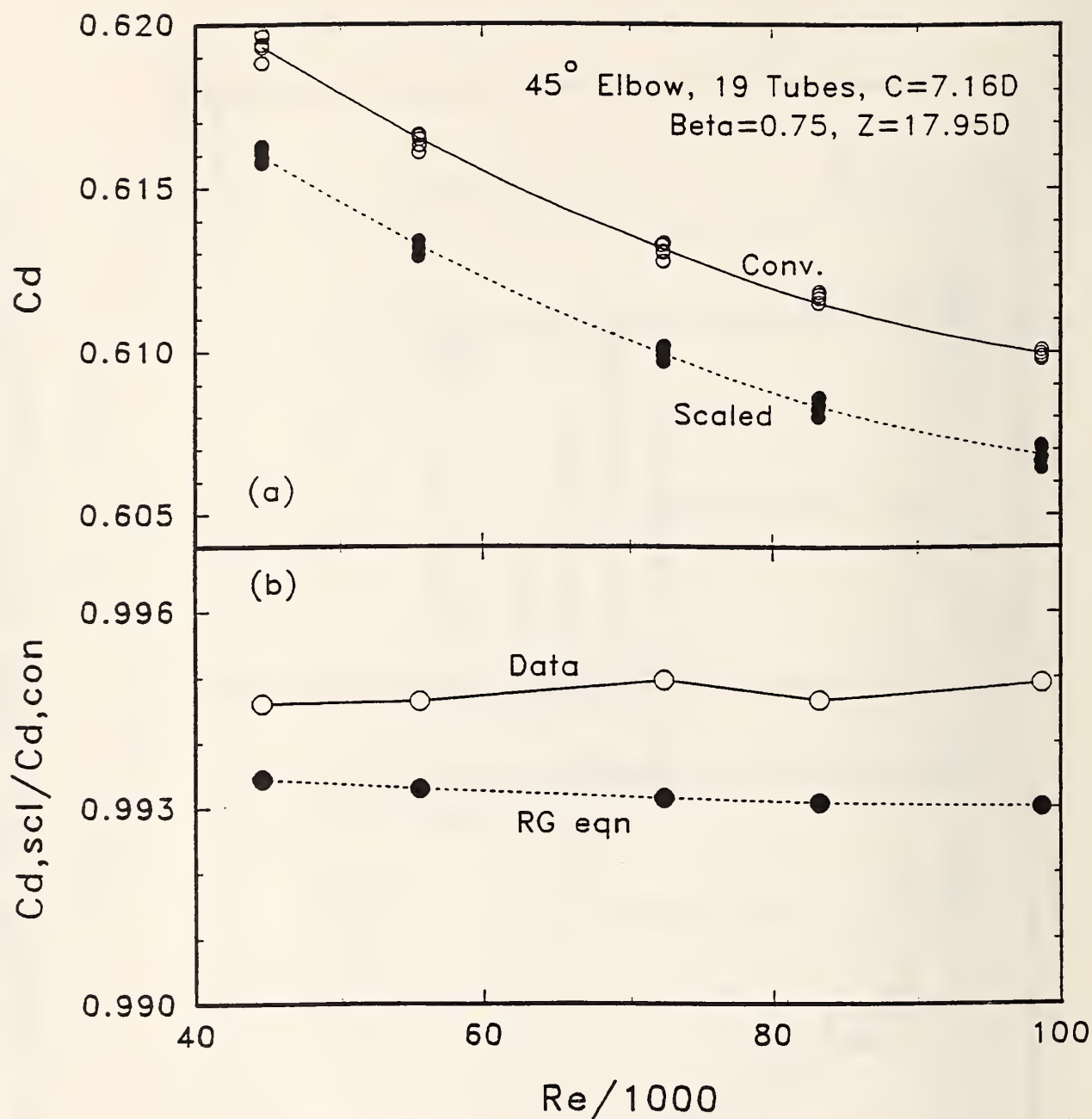


**Figure 39** The Scaled and Conventional Discharge Coefficients for a Beta=0.75 Orifice Meter Located 17.95D Downstream of a 45° Elbow with a 19-Tube Tube Bundle Located at  $C=7.16D$ . (a) Discharge Coefficients, (b) Ratio of the Discharge Coefficients.

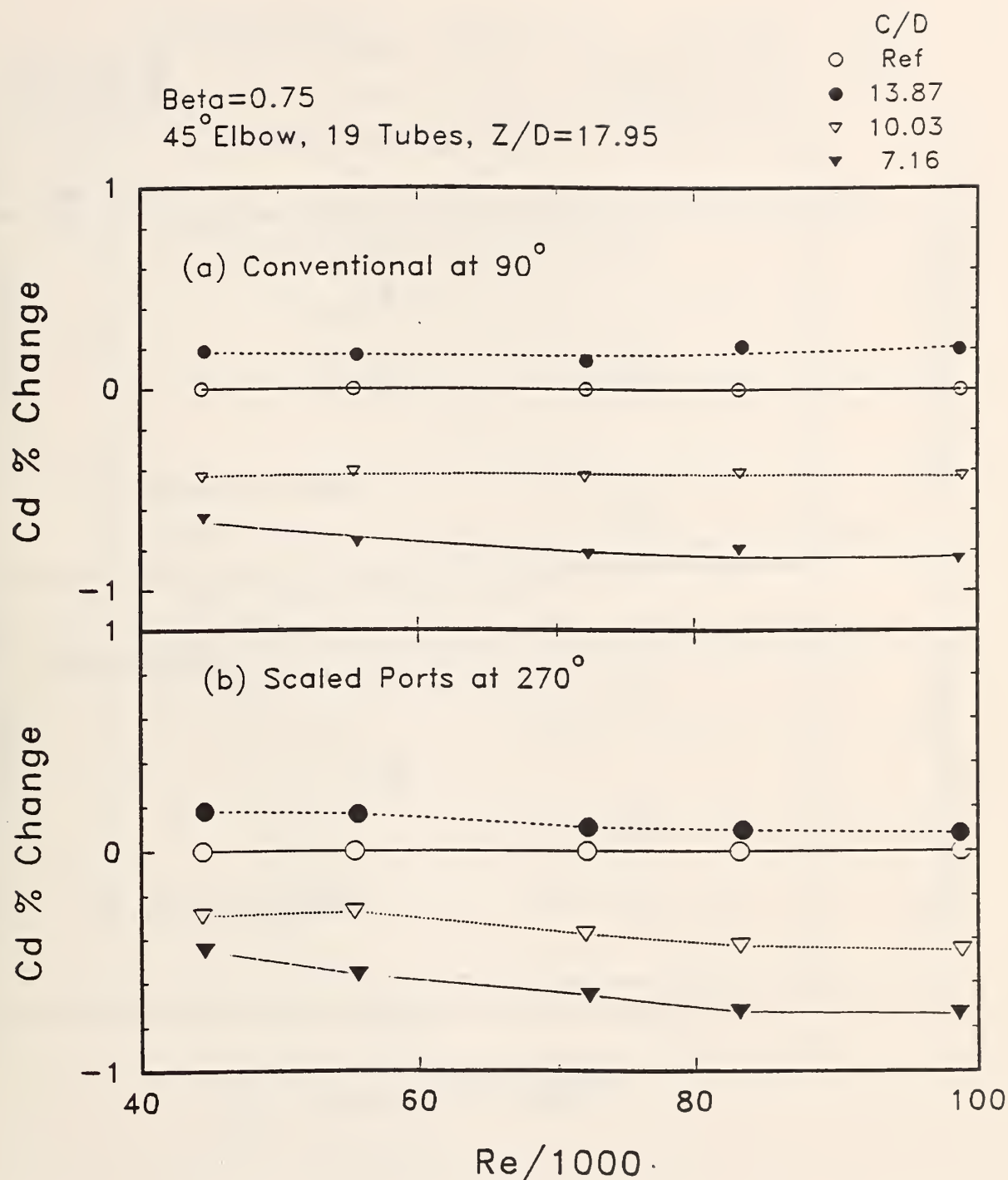


**Figure 40** Percentage Change in Discharge Coefficient for a Beta = 0.75 Orifice Meter Located 17.95D Downstream of a 45° Elbow with a 19-Tube Tube Bundle Located at Three Different Positions. (a) Conventional Ports at the 90° Position, (b) Scaled Ports at the 270° Position.

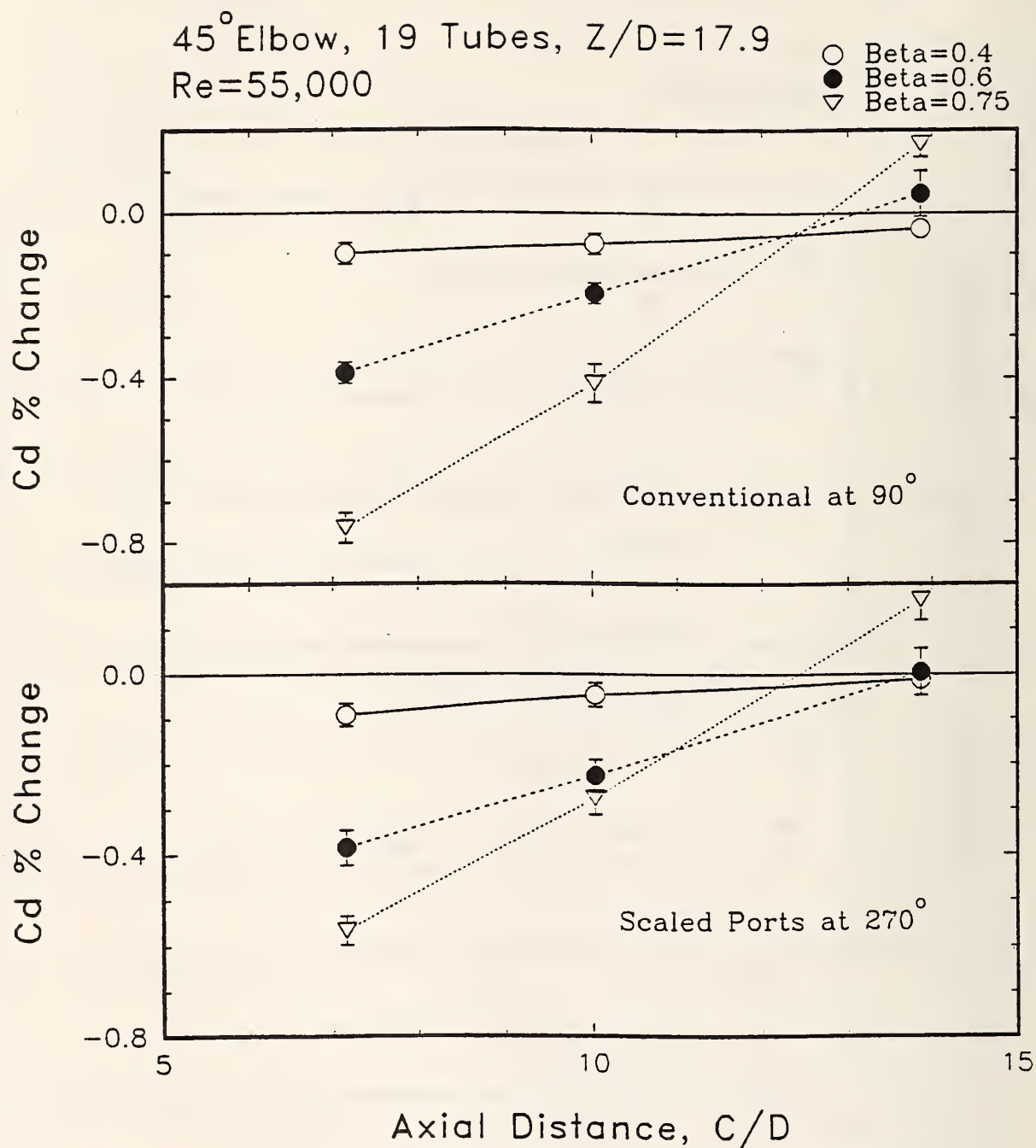


**Figure 41** Percentage Change in Discharge Coefficient for a Range of Orifice Meters Located 17.95D Downstream of a 45° Elbow with a 19-Tube Tube Bundles Located at Different Positions for  $Re = 55,000$ . (a) Conventional Ports at the 90° Position, (b) Scaled Ports at the 270° Position.



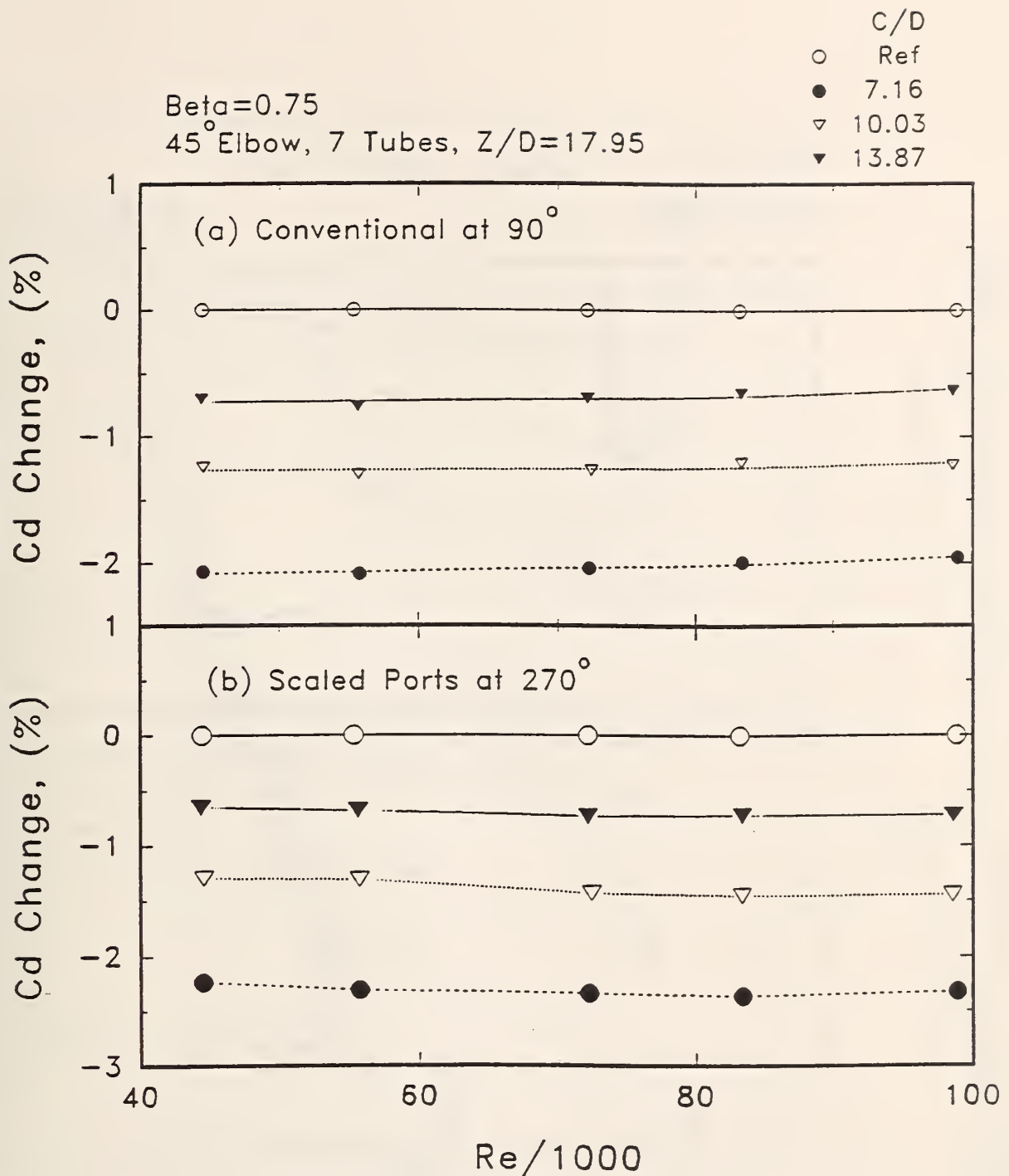


**Figure 42** Percentage Change in Discharge Coefficient for a Beta = 0.75 Orifice Meter Located 17.95D Downstream of a 45° Elbow with a 7-Tube Tube Bundle Located at Three Different C Positions. (a) Conventional Ports at the 90° Position, (b) Scaled Ports at the 270° Position.

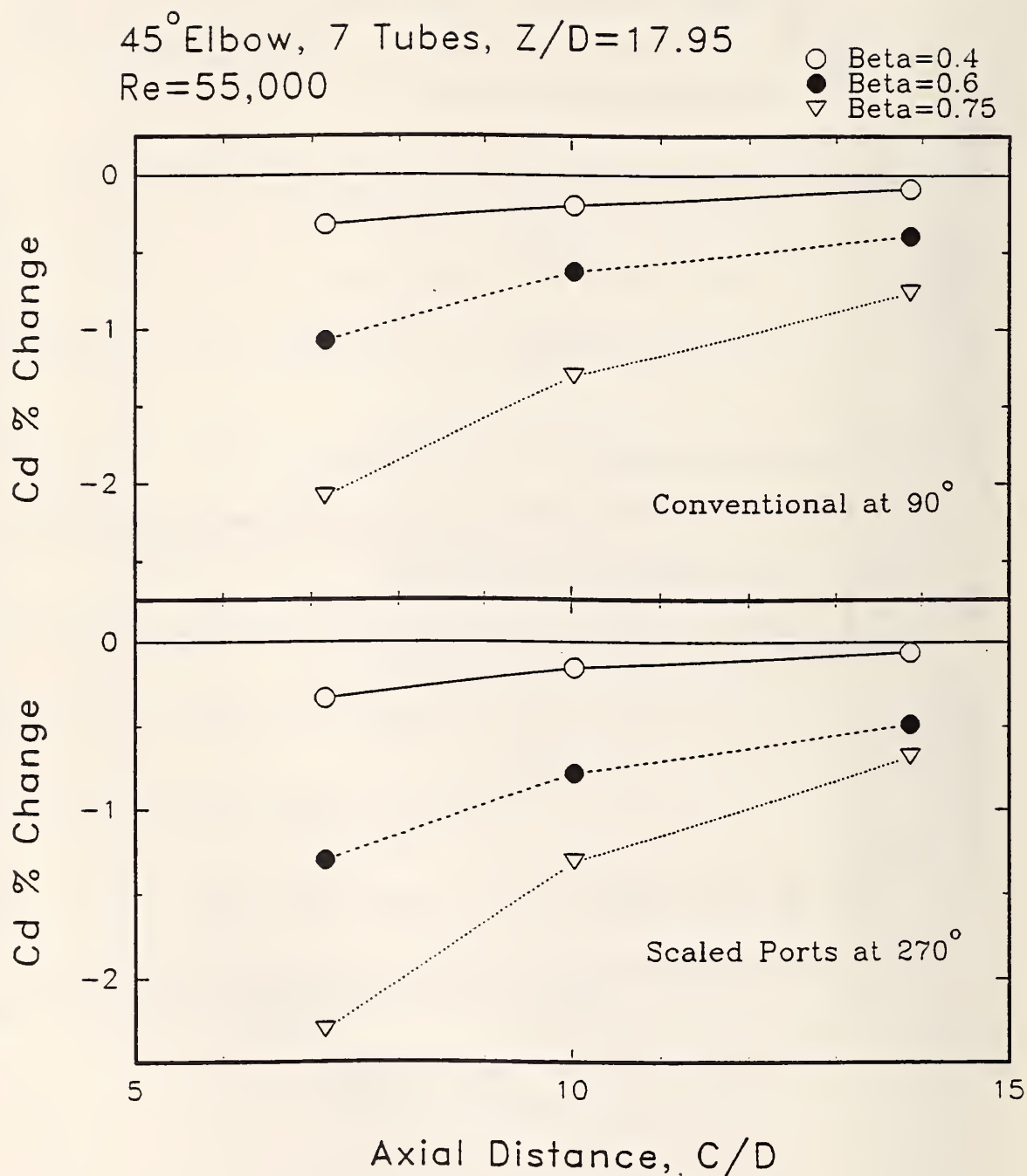


**Figure 43** Percentage Change in Discharge Coefficient for a Range of Orifice Meters Located 17.95D Downstream of a 45° Elbow with a 7-Tube Tube Bundle Located at Different C Positions for  $Re = 55000$ . (a) Conventional Ports at the 90° Position, (b) Scaled Ports at the 270° Position.

Beta=0.75, Re=99,000, Z/D=18

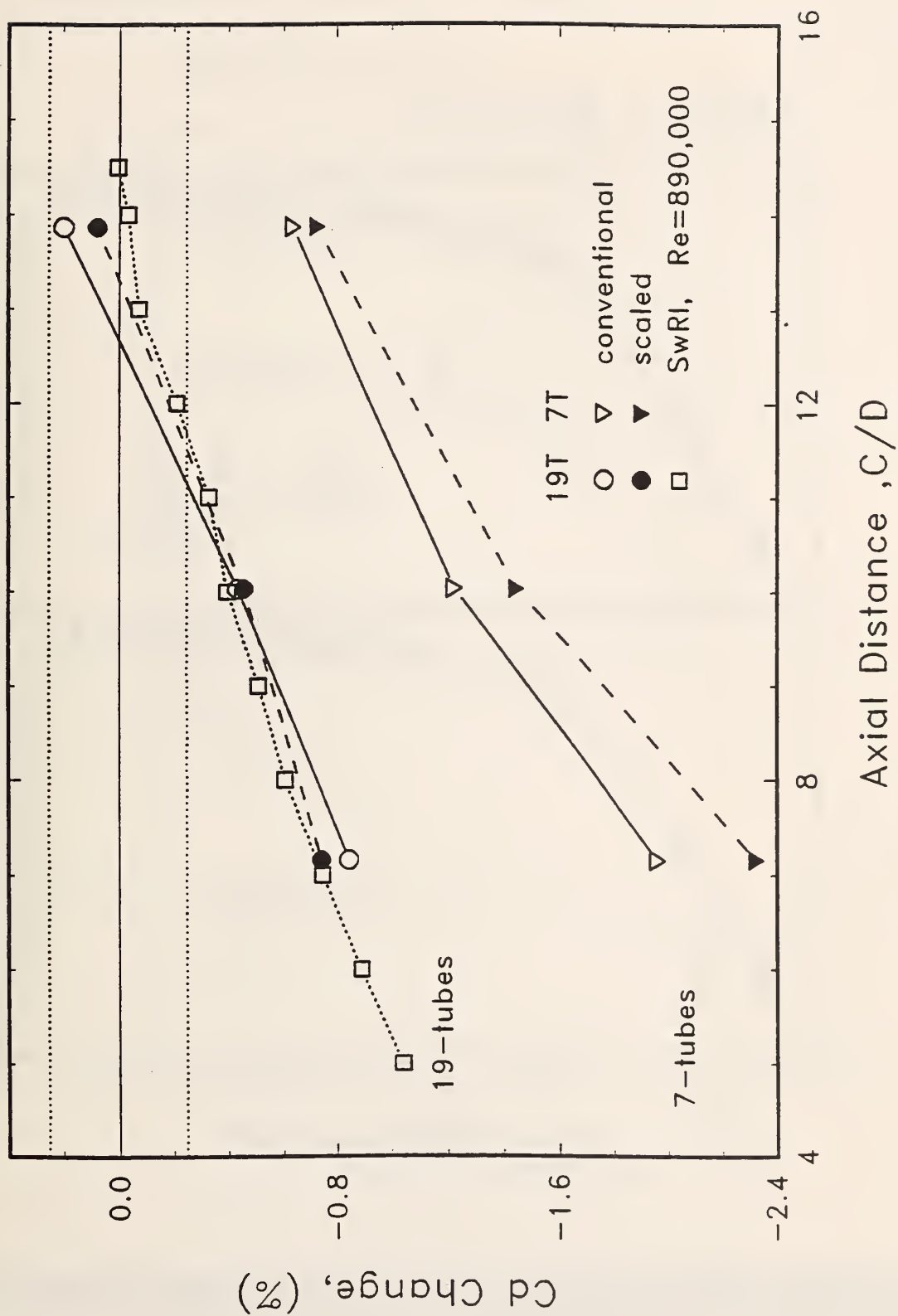
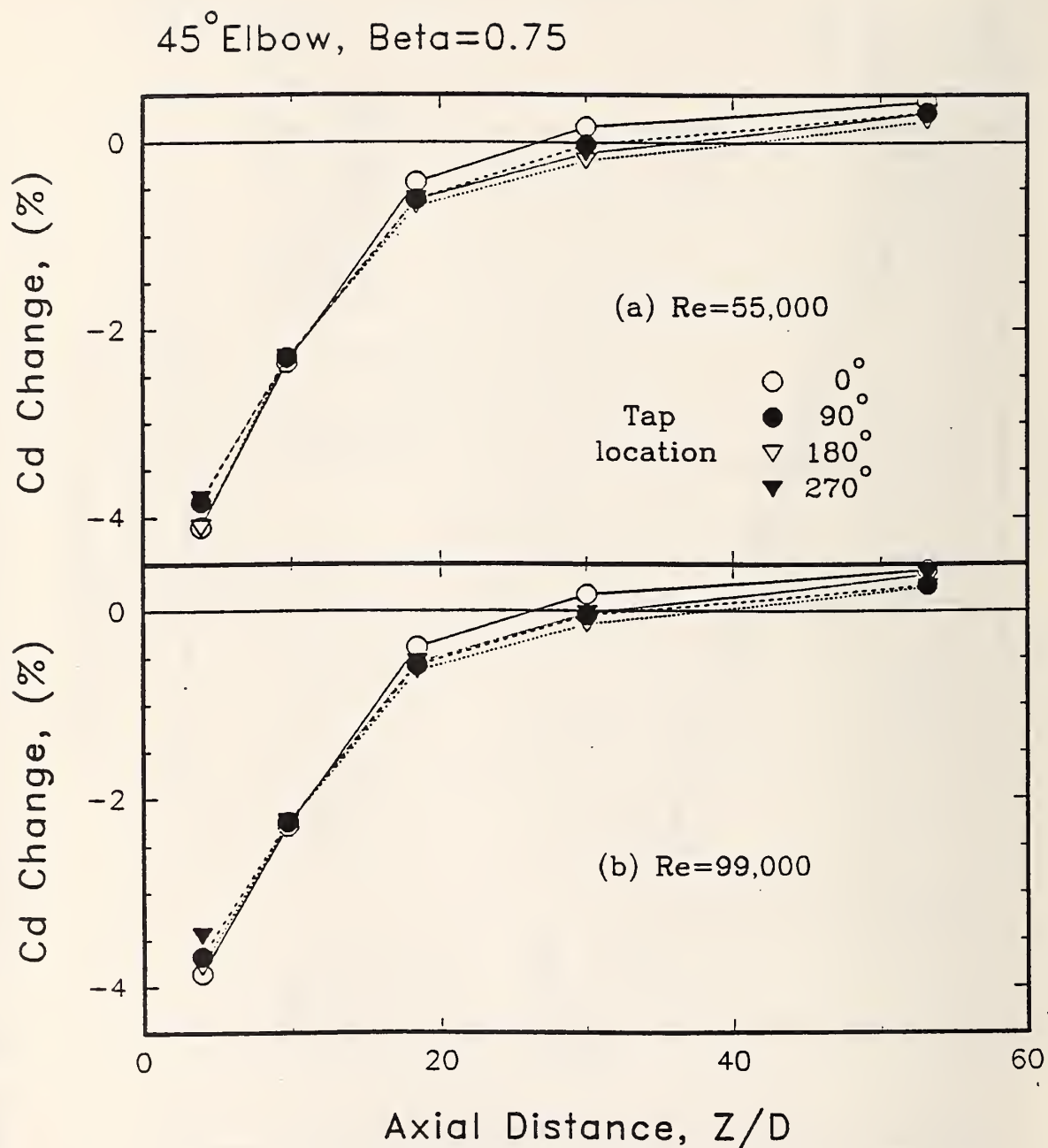
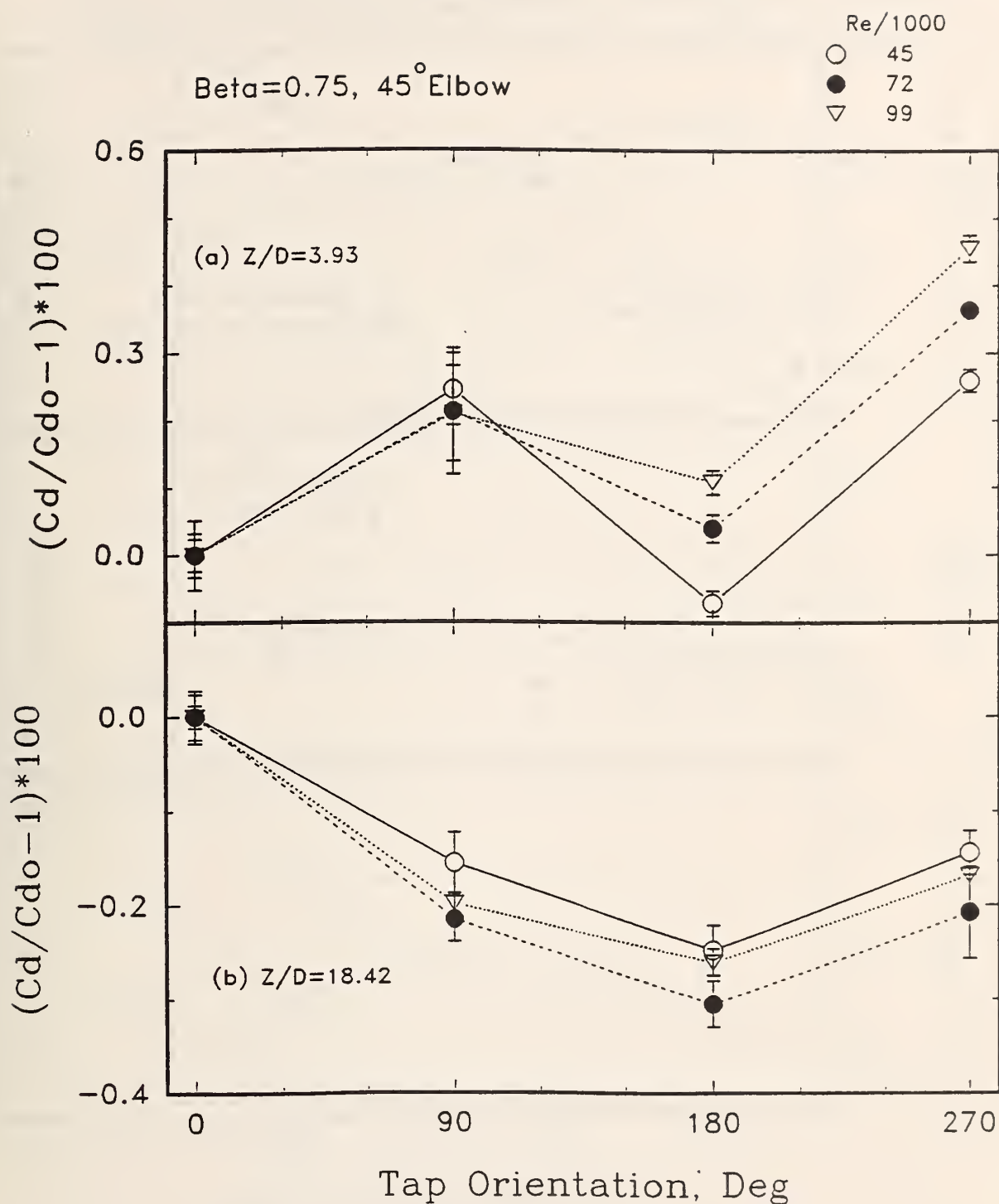


Figure 44 Comparison on the Change in Discharge Coefficients for a Beta = 0.75 Orifice Meter Downstream of a 45° Elbow and Two Tube Bundle Conditioners.



**Figure 45** The Change in Discharge Coefficient for a  $\text{Beta}=0.75$  Orifice Meter versus Location Downstream from a  $45^\circ$  Elbow for Four Pressure Tap Locations and  $\text{Re} = 55000$  and  $99000$ .





**Figure 46** Pressure Tap Orientation Effects on the Discharge Coefficient for a Beta=0.75 Orifice Meter Located at Two Different Downstream Positions from a 45° Elbow for Three Reynolds Numbers.

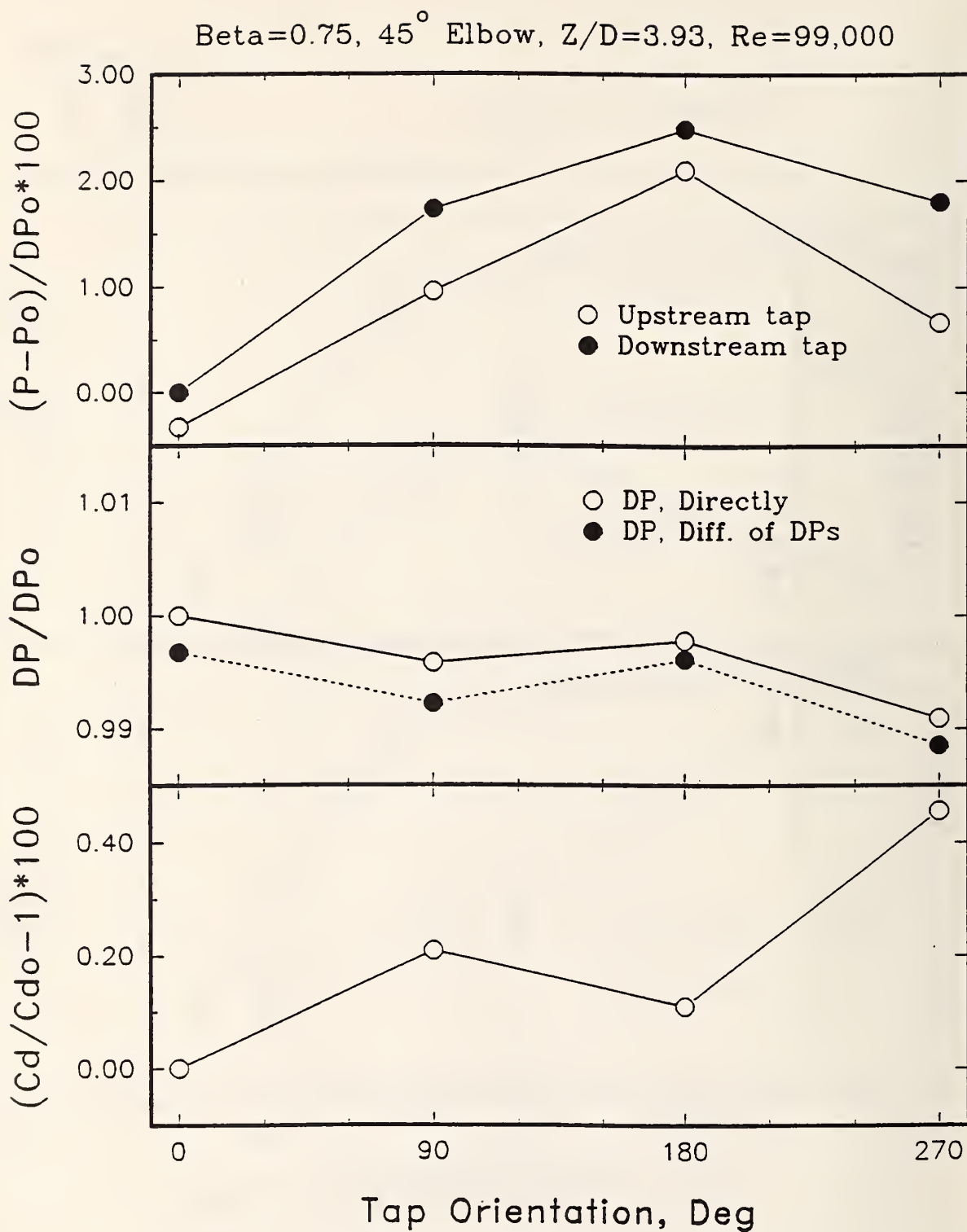


**Figure 47** Angular Distribution of the Wall Pressure, the Differential Pressure and the Discharge Coefficient for a Beta=0.75 Orifice Meter Located at 3.93D Downstream from a 45° Elbow for Re=99000.

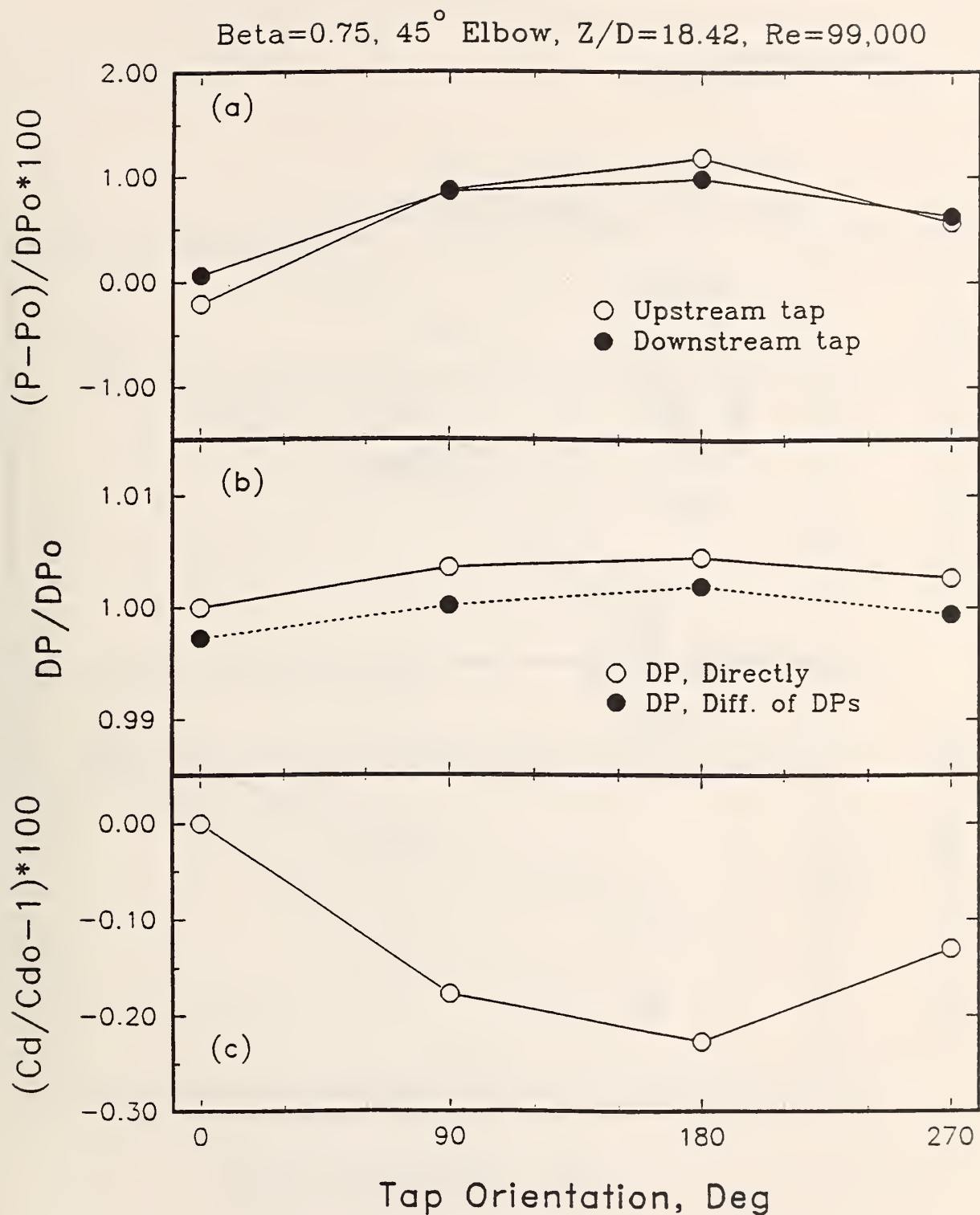


**Figure 48** Angular Distribution of the Wall Pressure, the Differential Pressure and the Discharge Coefficient for a Beta=0.75 Orifice Meter Located 18.42D Downstream from a 45° Elbow for Re=99000.

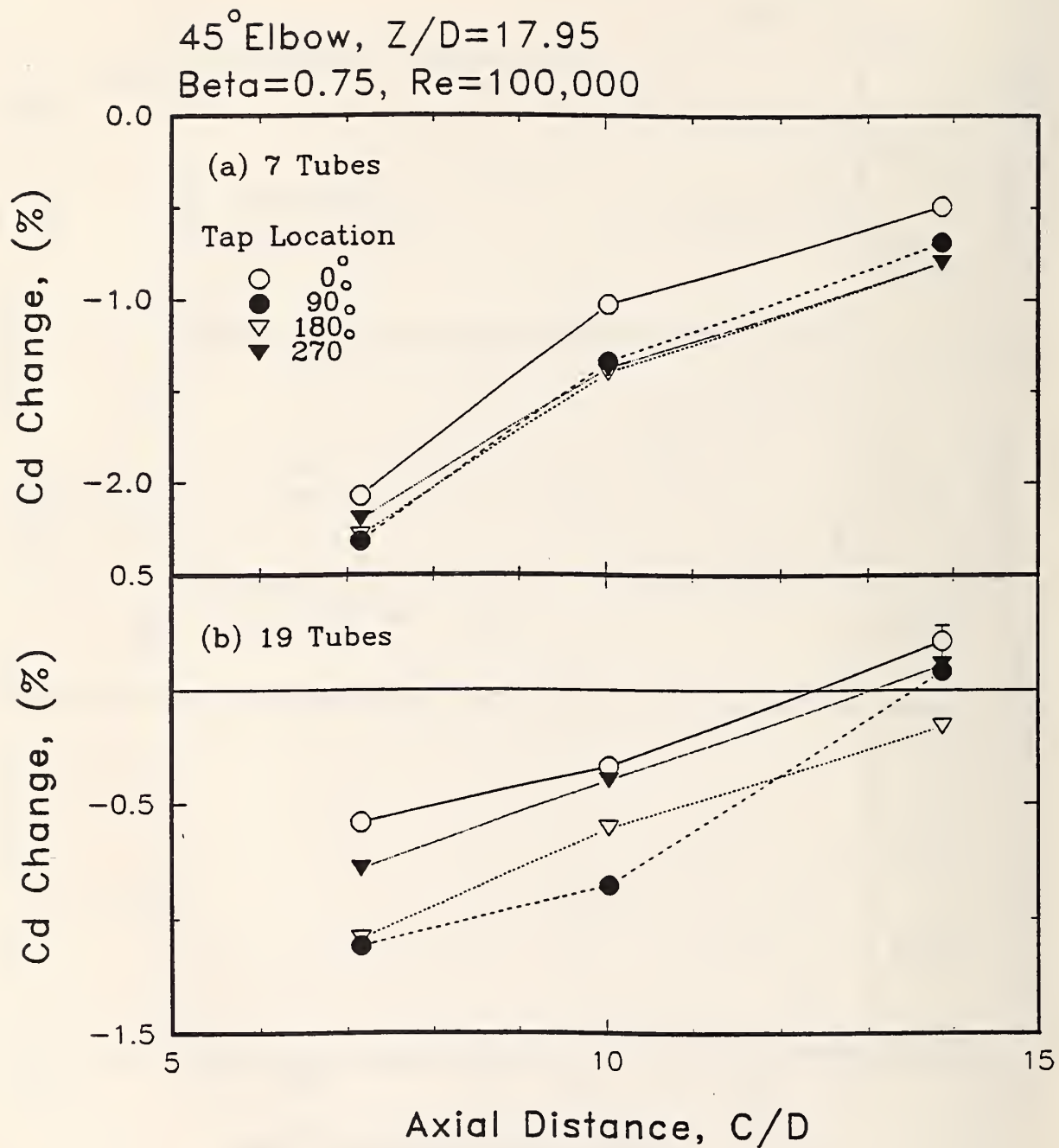


**Figure 49 The Change in Discharge Coefficient vs. Tube Bundle Positions for a  $\text{Beta}=0.75$  Orifice Meter Located  $17.95D$  Downstream from a  $45^\circ$  Elbow for Four Pressure Tap Locations and  $\text{Re} = 99000$ . (a) 7-Tube Tube Bundle, (b) 19-Tube Tube Bundle.**



45° Elbow, 19 Tubes, Z/D=17.95, C/D=10.03

Beta=0.75, Re=99,000

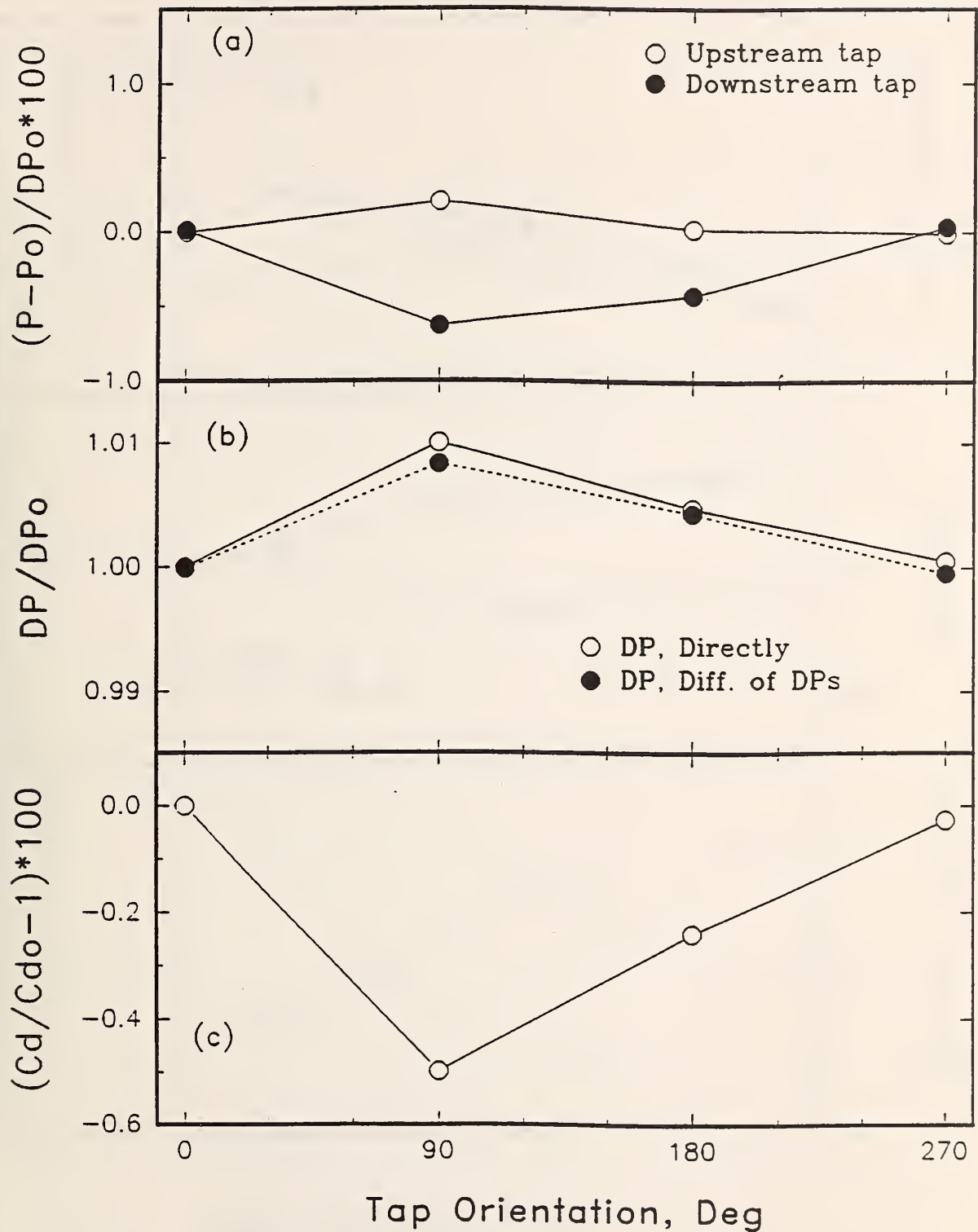


**Figure 50** Angular Distribution of the Wall Pressure, the Differential Pressure and the Discharge Coefficient for a Beta=0.75 Orifice Meter Located 17.95D Downstream from a 45° Elbow with a 19-Tube Tube Bundle Located at C=10.03D for Re=99000.

45° Elbow, 19 Tubes(180° Rotation), Z/D=17.95  
Beta=0.75, Re=99,000, C/D=10.03

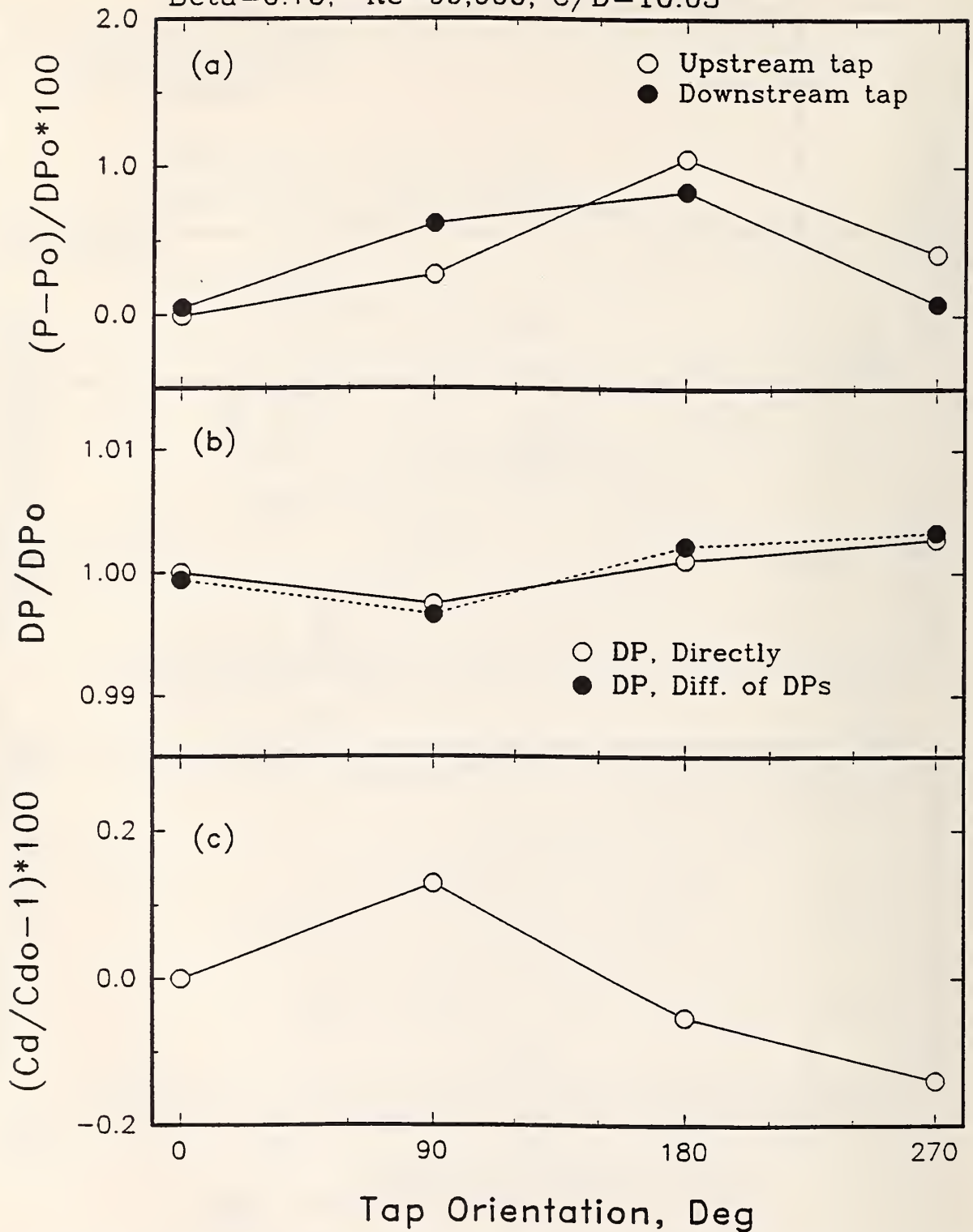


**Figure 51** Angular Distribution of the Wall Pressure, the Differential Pressure and the Discharge Coefficient for a Beta=0.75 Orifice Meter Located 17.95D Downstream from a 45° Elbow with a 19-Tube Tube Bundle Located at C=10.03D for Re=99000. The Bundle was rotated 180°.

45° Elbow, 7 Tubes, Z/D=17.95, C/D=10.03

Beta=0.75, Re=99,000

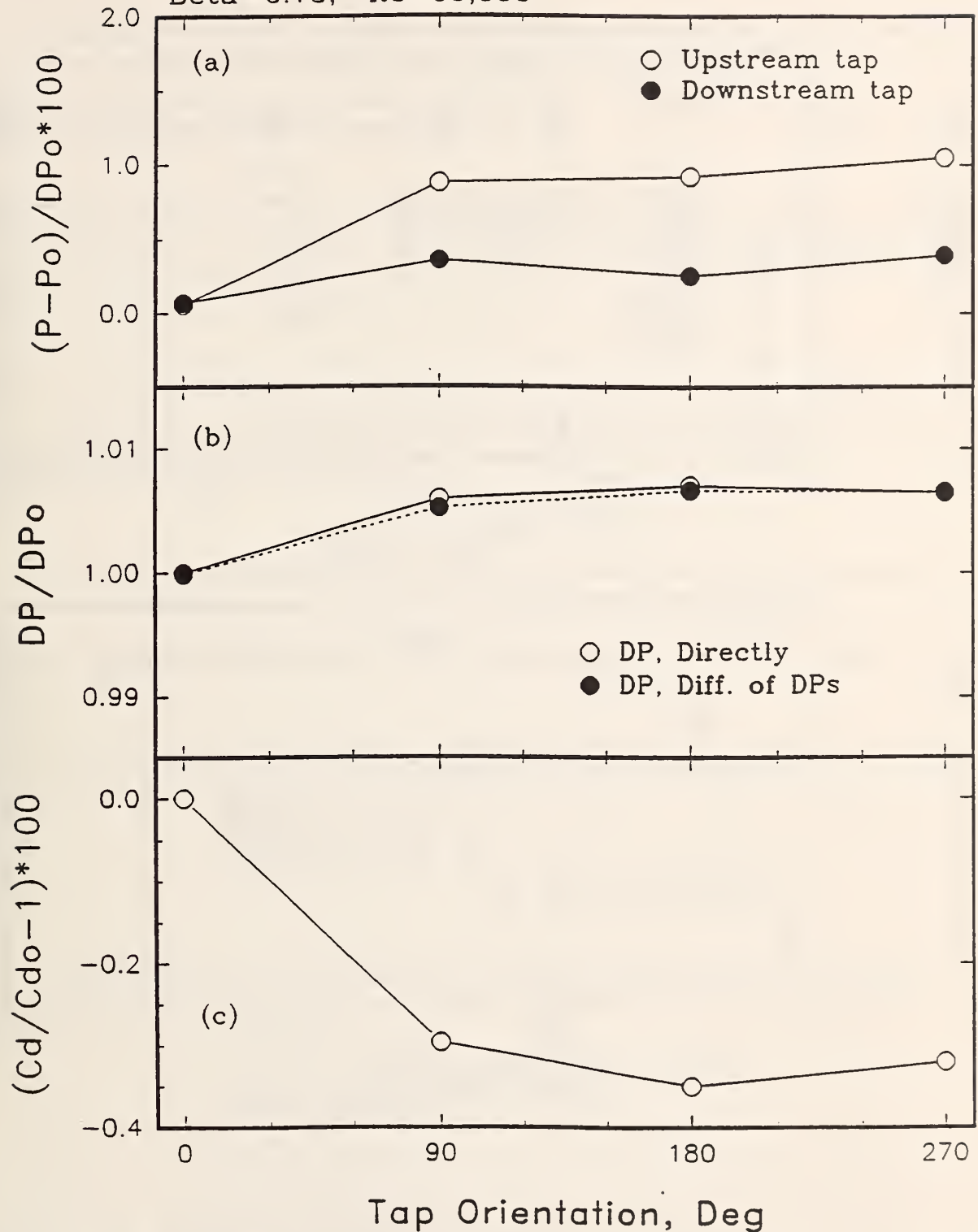


**Figure 52** Angular Distribution of the Wall Pressure, the Differential Pressure and the Discharge Coefficient for a Beta=0.75 Orifice Meter Located 17.95D Downstream from a 45° Elbow with a 7-Tube Tube Bundle Located at C=10.03D for Re=99000.

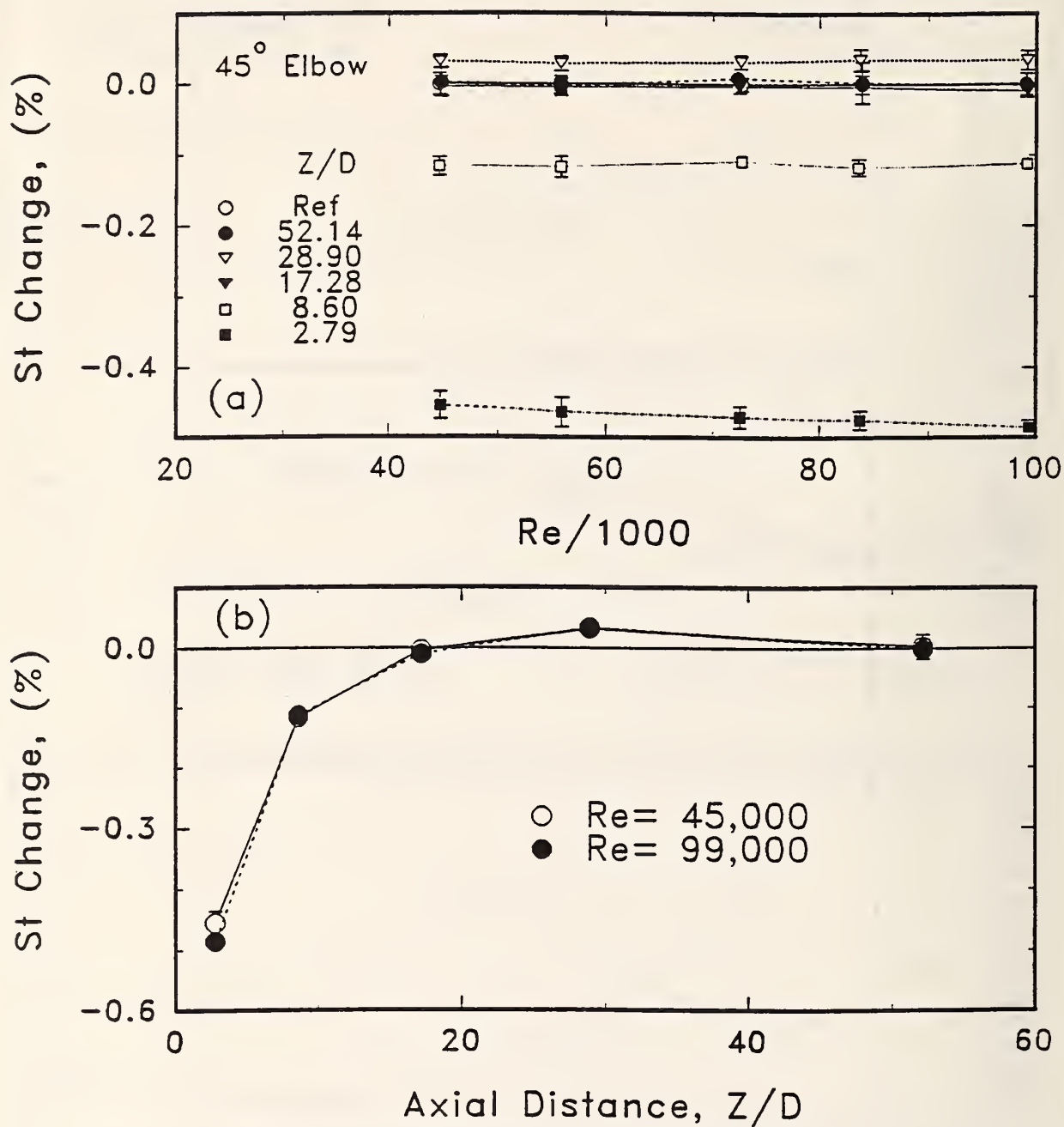


**Figure 53** Percentage Change in Strouhal Number for a Turbine Meter at Different Downstream Installation Positions from a 45° Elbow.



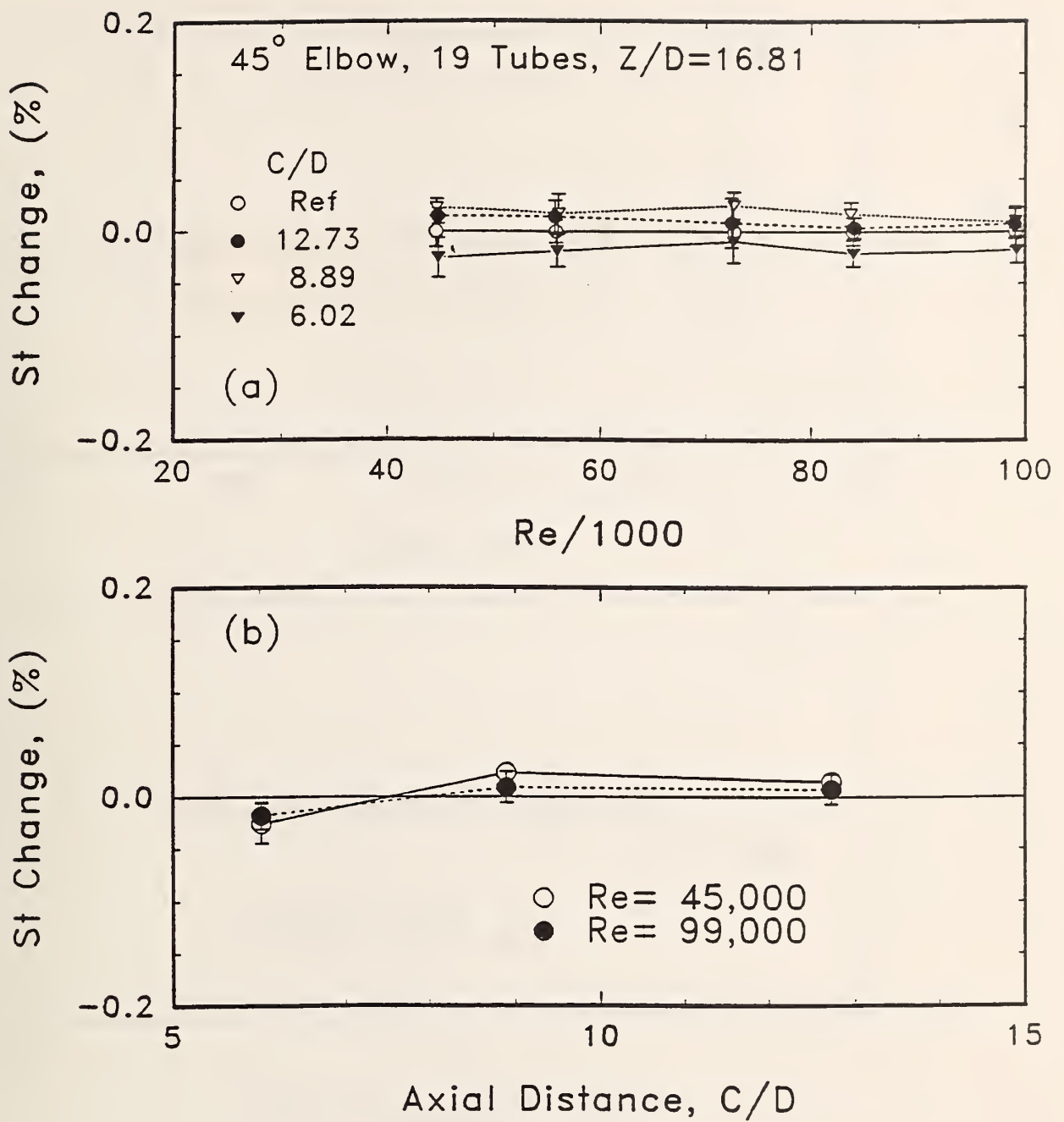


**Figure 54** Percentage Change in Strouhal Number for a Turbine Meter Located 16.81D Downstream of a 45° Elbow with a 19-Tube Tube Bundle Located at Different C Positions.

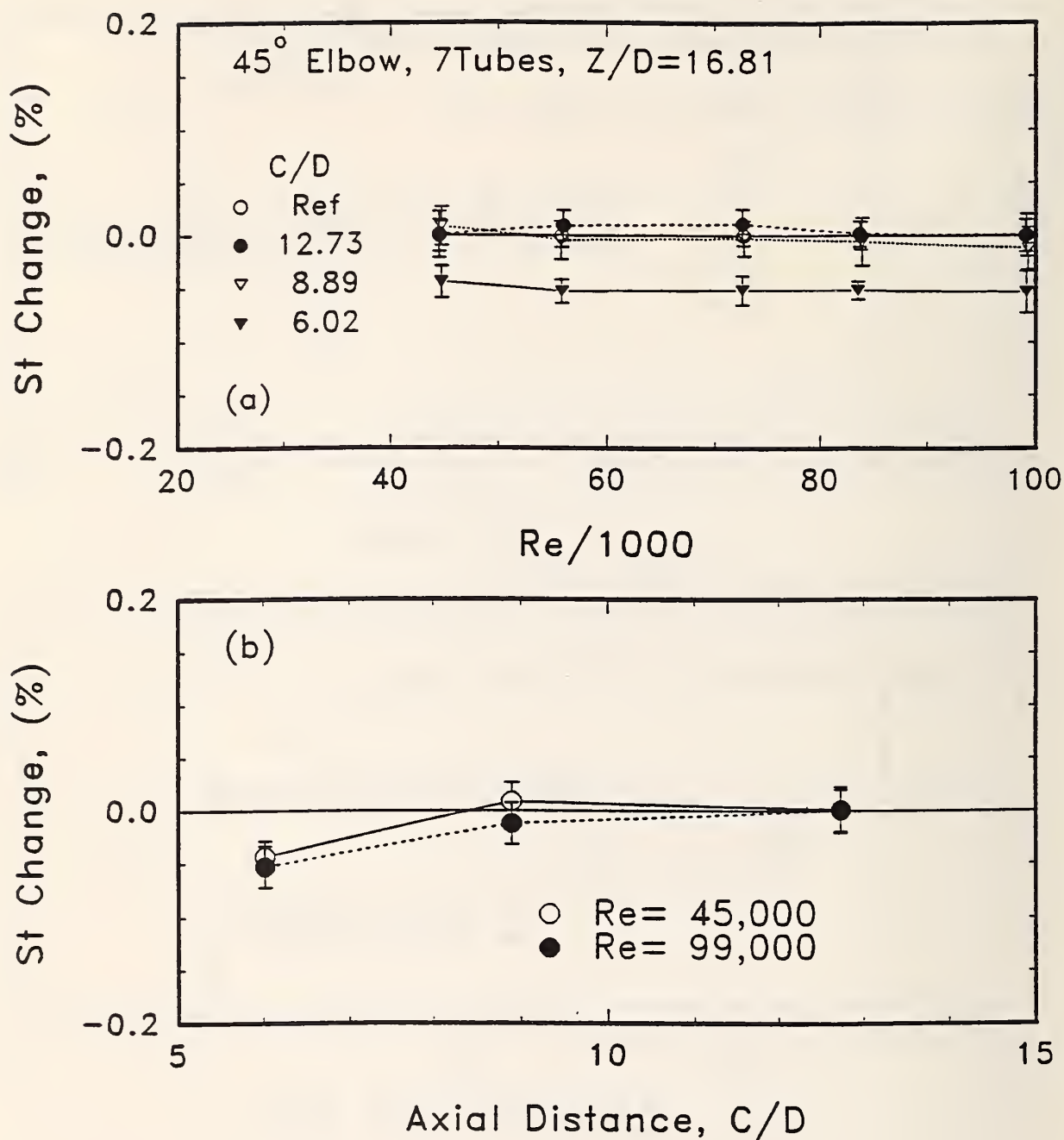


**Figure 55** Percentage Change in Strouhal Number for a Turbine Meter Located 16.81D Downstream of a 45° Elbow with a 7-Tube Tube Bundle Located at Different C Positions.







# NIST Technical Publications

## Periodical

---

**Journal of Research of the National Institute of Standards and Technology**—Reports NIST research and development in those disciplines of the physical and engineering sciences in which the Institute is active. These include physics, chemistry, engineering, mathematics, and computer sciences. Papers cover a broad range of subjects, with major emphasis on measurement methodology and the basic technology underlying standardization. Also included from time to time are survey articles on topics closely related to the Institute's technical and scientific programs. Issued six times a year.

## Nonperiodicals

---

**Monographs**—Major contributions to the technical literature on various subjects related to the Institute's scientific and technical activities.

**Handbooks**—Recommended codes of engineering and industrial practice (including safety codes) developed in cooperation with interested industries, professional organizations, and regulatory bodies.

**Special Publications**—Include proceedings of conferences sponsored by NIST, NIST annual reports, and other special publications appropriate to this grouping such as wall charts, pocket cards, and bibliographies.

**Applied Mathematics Series**—Mathematical tables, manuals, and studies of special interest to physicists, engineers, chemists, biologists, mathematicians, computer programmers, and others engaged in scientific and technical work.

**National Standard Reference Data Series**—Provides quantitative data on the physical and chemical properties of materials, compiled from the world's literature and critically evaluated. Developed under a worldwide program coordinated by NIST under the authority of the National Standard Data Act (Public Law 90-396). NOTE: The Journal of Physical and Chemical Reference Data (JPCRD) is published bi-monthly for NIST by the American Chemical Society (ACS) and the American Institute of Physics (AIP). Subscriptions, reprints, and supplements are available from ACS, 1155 Sixteenth St., NW, Washington, DC 20056.

**Building Science Series**—Disseminates technical information developed at the Institute on building materials, components, systems, and whole structures. The series presents research results, test methods, and performance criteria related to the structural and environmental functions and the durability and safety characteristics of building elements and systems.

**Technical Notes**—Studies or reports which are complete in themselves but restrictive in their treatment of a subject. Analogous to monographs but not so comprehensive in scope or definitive in treatment of the subject area. Often serve as a vehicle for final reports of work performed at NIST under the sponsorship of other government agencies.

**Voluntary Product Standards**—Developed under procedures published by the Department of Commerce in Part 10, Title 15, of the Code of Federal Regulations. The standards establish nationally recognized requirements for products, and provide all concerned interests with a basis for common understanding of the characteristics of the products. NIST administers this program in support of the efforts of private-sector standardizing organizations.

**Consumer Information Series**—Practical information, based on NIST research and experience, covering areas of interest to the consumer. Easily understandable language and illustrations provide useful background knowledge for shopping in today's technological marketplace.

Order the **above** NIST publications from: Superintendent of Documents, Government Printing Office, Washington, DC 20402.

Order the **following** NIST publications—FIPS and NISTIRs—from the National Technical Information Service, Springfield, VA 22161.

**Federal Information Processing Standards Publications (FIPS PUB)**—Publications in this series collectively constitute the Federal Information Processing Standards Register. The Register serves as the official source of information in the Federal Government regarding standards issued by NIST pursuant to the Federal Property and Administrative Services Act of 1949 as amended, Public Law 89-306 (79 Stat. 1127), and as implemented by Executive Order 11717 (38 FR 12315, dated May 11, 1973) and Part 6 of Title 15 CFR (Code of Federal Regulations).

**NIST Interagency Reports (NISTIR)**—A special series of interim or final reports on work performed by NIST for outside sponsors (both government and non-government). In general, initial distribution is handled by the sponsor; public distribution is by the National Technical Information Service, Springfield, VA 22161, in paper copy or microfiche form.

**U.S. Department of Commerce**  
National Institute of Standards and Technology  
Gaithersburg, MD 20899

Official Business  
Penalty for Private Use \$300